Analysis of Vehicle Rollover Using a High Fidelity Multi-Body Model and Statistical Methods

By
Maciej Paweł Czechowicz

Doctoral Thesis

Submitted in partial fulfilment of the requirements for the award of Doctor of Philosophy of Loughborough University

30th September 2014

To Rebecca,

Abstract

The work presented in this thesis is dedicated to the study of vehicle rollover and the tyre and suspension characteristics influencing it. Recent data shows that 35.4% of recorded fatal crashes in Sports Utility Vehicles (SUVs) included vehicle rollover. The effect of rollover on an SUV tends to be more severe than for other types of passenger vehicle. Additionally, the number of SUVs on the roads is rising. Therefore, a thorough understanding of factors affecting the rollover resistance of SUVs is needed.

The majority of previous research work on rollover dynamics has been based on low fidelity models. However, vehicle rollover is a highly non-linear event due to the large angles in vehicle body motion, extreme suspension travel, tyre non-linearities and large forces acting on the wheel, resulting in suspension spring-aids, rebound stops and bushings operating in the non-linear region. This work investigates vehicle rollover using a complex and highly non-linear multi-body validated model with 165 degrees of freedom. The vehicle model is complemented by a Magic Formula tyre model.

Design of experiment methodology is used to identify tyre properties affecting vehicle rollover. A novel, statistical approach is used to systematically identify the sensitivity of rollover propensity to suspension kinematic and compliance characteristics. In this process, several rollover metrics are examined together with stability considerations and an appropriate rollover metric is devised. Research so far reveals that the tyre properties having the greatest influence on vehicle rollover are friction coefficient, friction variation with load, camber stiffness, and tyre vertical stiffness. Key kinematic and compliance characteristics affecting rollover propensity are front and rear suspension rate, front roll stiffness, front camber gain, front and rear camber compliance and rear jacking force.

The study of suspension and tyre parameters affecting rollover is supplemented by an investigation of a novel anti-rollover control scheme based on a reaction wheel actuator. The simulations performed so far show promising results. Even with a very simple and conservative control scheme the reaction wheel, with actuator torque limited to 100Nm, power limited to 5kW and total energy consumption of less than 3kJ, increases the critical manoeuvre velocity by over 9%. The main advantage of the proposed control scheme, as opposed to other known anti-rollover control schemes, is that it prevents rollover whilst allowing the driver to maintain the desired vehicle path.

Keywords: vehicle rollover, stability, design of experiment, multi-body simulation, tyre, suspension

Acknowledgements

I want to first and foremost thank my supervisor Dr. George Mavros for the patience, enthusiasm, invaluable advice and encouragement he showed during this project.

My thanks also go to my current and past employers for allowing me to undertake this reasearch and supporting me throughout its duration. Especially I would like to thank Dr. Suresh Gupta, from SIMPACK UK, for initiating the study, and my managers from Jaguar Land Rover, Nick Fussey, Steve Robinson and Peter Davis, for their continuous assistance.

Finally, I would like to thank my lovely wife, Rebecca, for the enormous support, encouragement and tolerance through my academic journey. Without her help this thesis would never exist.

Contents:

List of Figures

List of Tables

Notation

Note: Equations from literature have symbols explained at the time of introduction

Chapter 3

$F_{dr}(s)$	Driveline controller transfer function
$F_{st}(s)$	Steering controller transfer function
Kp_{dr}	Driveline controller's proportional gain
Kp_{st}	Steering controller's proportional gain
Md	Driving torque at each wheel
SWA	Steering wheel angle
$T1_{dr}$	Driveline controller's time delay constant 1
$T1_{st}$	Steering controller's time delay constant 1
$T2_{dr}$	Driveline controller's time delay constant 2
$T2_{st}$	Steering controller's time delay constant 2
Td_{dr}	Driveline controller's derivative constant
Td_{st}	Steering controller's derivative constant
Ti_{dr}	Driveline controller's integration constant
Ti_{st}	Steering controller's integration constant
V	Tyre forward velocity
dy	Lateral track deviation
dv	Vehicle longitudinal velocity deviation
f	Tyre cross-over frequency from frequency response test
h_{dr}	Driveline controller's output scale factor
h_{st}	Steering controller's output scale factor
k, k_{joint}	Number of DOF in the system and number of DOF given by joint elements
n_{eq}	Total number of equations in the system
σ	Tyre relaxation length

Chapter 4

F_e	External moment stabilising pendulum
c	Rotational damping of pendulum

$f, f_{undamped}$	Damped and undamped frequency of pendulum
g	Gravity
k	Rotational stiffness of pendulum
l	Pendulum length
m	Pendulum mass
α	Pendulum angle, 0 corresponds to pendulum in hanging condition
β	Pendulum angle, 0 corresponds to inverted pendulum
λ	Eigenvalue of pendulum

Chapter 5

A	DoE code for scale factor of cornering stiffness
B	DoE code for scale factor of overturning moment
C	DoE code for scale factor of long. peak friction coefficient
D	DoE code for scale factor of lat. peak friction coefficient
E	DoE code for scale factor of camber stiffness
F	DoE code for tyre vertical stiffness
G	DoE code for variation of lat. friction μ_y with load
K_R	Wheel rate in roll
K_{V2r}	Suspension rate in second half of rebound travel
K_{V1r}	Suspension rate in first half of rebound travel
K_{V1b}	Suspension rate in first half of bump travel
K_{V2b}	Suspension rate in second half of bump travel
K_z	Tyre vertical stiffness
$V_{Critical}$	Critical rollover velocity
k	Number of investigated factors
n	Number of repetitions
p	Size of fraction
p_{Dy2}	Variation of lateral friction μ_y with load
α_L	Linear dependency of toe angle α on lateral force at contact patch
α_V	Linear dependency of toe angle α on wheel travel
α_{V^2}	Quadratic dependency of toe angle α on wheel travel

γ_L	Linear dependency of camber angle γ on lateral force at contact patch
γ_V	Linear dependency of camber angle γ on wheel travel
γ_{V^2}	Quadratic dependency of camber angle γ on wheel travel
ζ_R	Anti-roll bar contribution to wheel rate
$\lambda_{Ky\alpha}$	Scale factor of cornering stiffness
λ_{Mx}	Scale factor of overturning moment
$\lambda_{y\gamma}$	Scale factor of camber stiffness
$\lambda_{\mu x}$	Scale factor of long. peak friction coefficient
$\lambda_{\mu y}$	Scale factor of lat. peak friction coefficient
ρ_V	Kinematic roll centre height
ρ_{V2}	Rate of change of kinematic roll centre height due to wheel travel
ψ_V	Linear dependency of wheel centre lateral position on wheel travel
ψ_{V^2}	Quadratic dependency of wheel centre lateral position on wheel travel
φ_L	Normalised jacking force due to lateral force at contact patch
ψ_L	Linear dependency of wheel centre lateral position on lateral force at contact patch

Chapter 6

$\mathbf{A}$	State space matrix of pendulum controller
$\mathbf{B}$	State space input matrix of pendulum controller
E_{kin}	Total kinetic energy
E_{total}	Total energy consumption of reaction wheel
$F_{clamping}$	Flywheel brake clamping force
I	Total vehicle roll inertia
I_{RW}	Inertia of reaction wheel
$I_{flywheel}$	KERS flywheel inertia
$\mathbf{K}$	State space pendulum controller gain vector
$\boldsymbol{K_1}, \boldsymbol{K_2}$	Pendulum controller position and velocity gains
P, P_{max}, P_{limit}	Instantaneous power, maximum power and power limit of reaction wheel
T	Torque at the reaction wheel

$T_{flywheel}$	Torque at the flywheel
a_y	Vehicle lateral acceleration at CoG
g	Gravity
g_{eff}	Effective gravity
l	Length of the pendulum
m	Total vehicle mass
r	Moment arm of wheel brake
t_{start}, t_{end}	Controller activation and deactivation time
$t_{operation}$	Total time a KERS flywheel deceleration
tr_{av}	Average track at contact patch
tr_{fr}	Front track at contact patch
tr_{re}	Rear track at contact patch
x	State vector consisting of pendulum position and velocity
u	Controller input
z_{CoG}	Vehicle CoG above the ground
α	Difference between actual pendulum angle and pendulum angle corresponding to vehicle in static condition
β	Reaction wheel angle
λ	Eigenvalue
μ	Friction coefficient of KERS flywheel brake
φ	Pendulum angle
φ_{stat}	Pendulum angle corresponding to vehicle in static condition
ω	Pendulum angular velocity

Glossary Terms

ABS	Anti-Lock Braking System
ARB	Anti-Roll Bar
ARS	Active Rear Steer
CoG	Centre of Gravity
DBC	Dynamic Body Control
DoF	Degree of Freedom
DLR	German Aerospace Centre (Deutsches Zentrum für Luft- und Raumfahrt)
DRT	Dynamic Rollover Threshold
DSF	Dynamic Stability Factor
ESP	Electronic Stability Program
FE	Finite Element
HiL	Hardware in the Loop
HVE	Human Vehicle Environment
K&C	Kinematic and Compliance (test rig)
KERS	Kinetic Energy Recovery System
LTR	Load Transfer Ratio
LTR_D	Dynamic Load Transfer Ratio
MBS	Multi-Body Simulation
MF	Magic Formula
NHSTA	National Highway Traffic Safety Administration
NVH	Noise Vibration and Harshness
PID	Proportional Integral Differential (controller)
PPT	Phase Plane Trajectory
RCF	Rollover Critical Factor
RI	Rollover Index
ROI	Rollover Potentiality Index
RW	Reaction Wheel
SSF	Static Stability Factor
SSRT	Steady State Rollover Threshold
SUV	Sports Utility Vehicle
TCS	Traction Control System
TMPT	Tyre Model Performance Test
VSE	Vehicle Stability Enhancement

1. Introduction

1.1. Introduction

The work presented in this thesis aims to improve understanding of vehicle rollover dynamics. The review of the current state of the art suggests that although many low fidelity models have been developed and studied in the past, a high fidelity model has not been used for extensive rollover investigation. Here a high fidelity, correlated vehicle model is used in conjunction with statistical methods to determine the influence of tyre properties and suspension characteristics on rollover propensity. A newly-developed rollover propensity metric is employed in this study. The results of this work can be used as a guide for engineers during tyre and chassis development.

The work also provides insight into how the roll stability of a high fidelity model changes with the roll angle. Finally an innovative rollover control scheme is suggested which prevents vehicle rollover without compromising the path set by the driver. The influence of actuator limitations on vehicle rollover propensity is also explored.

1.2. Context of work

As early as 1965 Ralf Nader's book "Unsafe At Any Speed" [1] featured the Chevrolet Corvair, claiming that the vehicle was unsafe partly due to its propensity to rollover. Even though a later National Highway Traffic Safety Administration (NHSTA) investigation [2] announced the Chevrolet Corvair to be no worse than its competitors, the episode grabbed public attention and influenced later vehicle design as well as public interest in vehicle safety.

More recent examples of vehicles which have high rollover propensity [3, 4, 5, 6], show that the problem of vehicle rollover has not been fully dealt with. Although vehicle rollover is not a common type of accident, it is one of the most dangerous. A type of vehicle that is particularly prone to rollover is the increasingly popular Sports Utility Vehicle (SUV). NHTSA data [7] for 2005 shows 35.4% of fatal crashes in SUVs included vehicle rollover. For comparison only 16.4% of fatal crashes in passenger vehicles included rollover. Once an SUV rolls, the effects tend to be more severe than for other types of passenger vehicles. Altman et al. [8] stated that the number of rolls for SUVs is higher than for other pick-up trucks or passenger vehicles, which may lead to

more severe injuries. As one of the reasons for this the authors cite higher vehicle velocities at initiation of rollover. Due to the increasing number of SUVs on the road, a thorough understanding of factors affecting the rollover resistance of SUVs is greatly needed, as it has the potential to save lives. At the same time experimental testing to improve safety is expensive and dangerous, therefore simulation remains the main tool in improving understanding of rollover dynamics.

There exist different classifications of vehicle rollover in the available literature. One of the most common is presented by Solmaz et al. [9]. The authors distinguish between two types of vehicle rollover; tripped and un-tripped. The former is induced by a vehicle hitting an obstacle. The latter is a driver-induced type of rollover and can occur during fast cornering, lane change manoeuvres or avoidance of an obstacle etc.

Although this thesis focuses mostly on the untripped type of rollover, for completeness, it is worth mentioning the other types of rollover that can occur. A detailed classification of rollover was presented by Parenteau et al. [10]. In this paper eight different types of rollover are distinguished:

- trip-over – vehicle rolls over, when during lateral motion it hits a curb, pothole etc.
- fall-over – when vehicle rollover is caused by the lateral slope of the surface e.g. vehicle leaving the road and falling down a mountain
- flip-over – rollover induced by ramp or ramp-shaped down-turned object e.g. vehicle falling into a ditch
- turn-over – vehicle rollover initiated by lateral friction forces (this is referred to as driver-induced rollover by Solmaz et al. [9])
- bounce-over – vehicle rollover caused by the rebound after driving onto an object
- climb-over – vehicle climbs over the object e.g. barrier, lifts off the ground and rolls on the side of an object opposite to the side from which it was approached
- end-over-end – vehicle rolls about its lateral axis
- collision with other vehicle – collision impact causes vehicle to rollover.

In heavy vehicles, extra attention is drawn to vehicles carrying liquid cargo, as they are especially prone to rollover initiated by slosh forces. If the tank of such a vehicle is only partially full, slosh forces can reduce the lateral acceleration at which rollover can occur to as low as 0.3g - 0.4g. (Acarman et al. [11]). During steady state manoeuvres, movement of the liquid cargo results in the lateral and vertical shift of the centre of gravity. Similarly, during the transient part of a manoeuvre,

dynamics of liquid cargo generate a dynamic slosh force potentially increasing the rollover propensity even further.

1.3. Structure of thesis

This thesis consists of seven chapters. Chapter 1 provides a brief introduction and context of the problem, together with the overall thesis layout. Chapter 2 considers the current state of the art in modelling and understanding vehicle rollover. Based on a critical review of current knowledge, the selection of modelling and analysis tools is presented and briefly discussed. At the end of the literature review, research objectives are presented. Modelling and analysis methodology are discussed in detail in Chapter 3 and Chapter 4 respectively. The former covers tyre and vehicle modelling aspects, the latter presents the stability analysis and design of experiment tools used in the research. Following the methodology is Chapter 5, beginning with a description of measurement of vehicle propensity to rollover, next moving to the analysis of results from tyre and vehicle design of experiments and ending with stability investigations. Chapter 6 describes an innovative controller based around a torque reaction wheel. In the last chapter, the final conclusions and recommendations for further work are summarised.

2. Literature review

2.1. Rollover sources

Untripped rollover requires a number of specific conditions to occur in the time leading up to the accident. Baumann et al. [12] investigated critical steering strategies inducing vehicle rollover. The authors found that the main conditions causing rollover are maximum side forces occurring simultaneously at both front and rear axles combined with high roll-rates, which correspond to high kinetic energy of the roll motion. These conditions can appear when the vehicle is oversteering, as this is necessary for achieving a high rear axle slip angle, and heavy side-to-side vehicle body excitations. The dynamic load transfer leads to increased vertical loads on the outer tyres, allowing even higher lateral forces. These conditions indicate that the fishhook or double lane change could be the most severe manoeuvres inducing rollover. Additionally when high rear slip angle combines with road departure it is likely to result in tripped rollover.

The results presented by Baumann et al. [12] showed that the steering frequencies critical for vehicle rollover are in the region of 0.3Hz to 0.8Hz, which is lower than the natural roll frequency of the vehicle; for the analysed vehicle this was 1.3Hz. This range corresponds to the steering frequency during a double lane change manoeuvre (ISO 3888-2). At these frequencies the vehicle has a tendency to oversteer, which is a necessary condition to achieve high lateral forces at the rear axle. The exact reason for critical rollover frequency being so low was not given, but possibly this could be related to the natural yaw frequency of the vehicle. However Bauman noted that, in isolation, high lateral forces are not a good indicator of rollover.

Baumann et al. [12] also analysed the steering inputs from different drivers during a double lane change manoeuvre (ISO 3888-2). The results showed that to induce rollover of a small passenger vehicle during the above-mentioned test with an entrance speed of 72km/h, steering velocities of over 1000º/s together with steering amplitudes of 450º were needed. For the experimental vehicle built to investigate rollover, these values were respectively 800º/s and 400º.

Dahlberg [13] stated that a vehicle's rollover may be triggered by side winds or road unevenness if its rollover margin is too small in a certain situation. Also Hac et al. [14] noted that rollover may be partially induced by road irregularities. There exists a limited knowledge on the road vertical input triggering vehicle rollover during limit handling manoeuvres. However it is reasonable to expect that roll centre heights and the resultant jacking forces may play a crucial role in this type of rollover as they are a direct link between the roll, lateral and vertical dynamics of the vehicle.

Knowledge of pure vertical vehicle dynamics exists and has been thoroughly described. Simple dynamic models showing the response due to vertical road input have been described by Jazar [15].

The aim of this research is to push forward the understanding of vehicle and tyre properties affecting vehicular rollover, and develop an effective way of controlling rollover. In order to contain the scope of the rollover study, the research work concentrates on untripped rollover on an even surface.

2.2. Current state of the art in vehicle rollover

In this section the current state of the art in vehicle rollover is reviewed. The main focus is on vehicle rollover modelling; however physical studies are also quoted.

2.2.1. Modelling approach

The investigation of vehicle rollover based on real world experiments can be very dangerous and expensive. Therefore simulation is the most suitable method for studying rollover. The main areas of application for vehicle rollover models are:

- rollover dynamics studies
- development of rollover prediction algorithms
- development of control algorithms
- validation of rollover prediction and control algorithms
- studies of driver-controller interactions

A different compromise between accuracy and computational effort is required for different models, e.g. models for testing rollover control algorithms have to include non-linearities and be more accurate than models for derivation of control algorithms. Models used for the design of a control scheme require simplicity to enable the analytical derivation of control algorithms. The main prerequisite for a model designed for hardware in the loop testing is to be able to run in real time, but at the same time it has to be as accurate as possible.

As different modelling areas force different modelling priorities they also determine the modelling approach. An example of this can be seen in the work presented by Hyun et al. [16]. The authors

used a simple roll-plane model to predict the load transfer ratio which can be used as a rollover threat index, and then checked the accuracy of this prediction using a more complex 12 Degrees of Freedom (DoF) model.

One of the possible modelling approaches is to develop a set of mathematical equations by hand. They can be later solved in software such as Matlab/Simulink. This approach is popular in control applications, as it enables the analytical derivation of e.g. a rollover control scheme or stability criteria. Usually the models cannot be computationally demanding, especially when they are to be used for controller scheme testing or implemented as estimators of vehicle states, which often means that they have to be run faster than real time. At the same time the model has to replicate reality accurately; therefore a good balance between accuracy and simplicity is always essential. Models capable of running in real time are useful tools in testing hardware e.g. actuators or performing the analysis of driver-controller interaction. An example of such a simulation was presented by Kim et al. [17]. The authors used the real time model of a vehicle for hardware in the loop (HiL) simulation in which the anti-roll bar connected with an electric actuator was used for active roll control.

Another means of modelling vehicle rollover is to use specialised Multi-Body Simulation (MBS) software. The concept of multi-body dynamics has been described by Rahnejat [18] and Shabana [19]. The field of MBS software has made great progress over the last 30 years, although it is still not as popular as, for example, finite element codes. Wallrapp [20] provided an overview of the development of MBS software in recent years.

The greatest advantage of using MBS software is that it enables the user to rapidly develop models of complex systems in almost any possible scenario. Often models created in MBS software provide a benchmark for simpler analytical models. An example of this can be seen in work completed by Shim et al. [21] and Ghike et al.[22] whereby the authors used vehicle models built in CARSIM and ADAMS for studying the limitations of the mathematical models. The results obtained from the multi-body simulation software were compared with 14 and 8 DoF models. The 14 DoF model gave a fairly good correlation with the full MBS model, whereas the 8 DoF model was able to produce accurate results only up to wheel lift off.

Eger et al. [23] employed multi-body formulation in a Matlab/Simulink environment for modelling of vehicle rollover. Dahlberg [13] used a full vehicle model in ADAMS to test the Dynamic Rollover Threshold (DRT). The author included the flexibility of the trailer in the MBS simulation. This flexibility can have an effect on the rollover propensity of heavy vehicles; however for passenger cars this would presumably not have a great influence, as the body stiffness of passenger vehicles is great compared to that of heavy vehicles. Hussain et al. [24] used the multi-body

simulation software ADAMS for studying the phenomenon of rollover in articulated vehicles. The authors noted that MBS software enables the user to account not only for the suspension kinematics but also for all sources of compliance. Other authors using the MBS software ADAMS were Jones [25], Durali et al. [26], and Wielenga et al. [27, 28] who tested Anti-Rollover Braking using ADAMS models of a Ford Bronco and a Chevrolet Astrovan.

Generally MBS codes simplify the analysis of complex mechanical systems as the equations of motion are generated automatically by the software while the user is building the model using predefined elements. Mathematical models are useful for analysing simple models but for more complex ones analysis might be time consuming or even beyond human capabilities.

MBS software can be linked with control engineering tools. Vaculin et al. [29] provided a complete overview of different possible approaches of coupling two simulation tools; the MBS software SIMPACK and the control tool Matlab/Simulink. The coupling between such tools provides a great opportunity for developing and testing various control algorithms without the need for building prototypes. It also gives development engineers and researchers a chance to try unconventional approaches which otherwise could not be tested due to the associated cost and potential safety risk.

2.2.2. Rollover dynamics

The literature review of existing rollover studies is presented in this section. The analysis of rollover findings will start from simple models based on static force balance. The complexity of the presented models will gradually increase eventually reaching full MBS models.

The simplest models are usually used in rollover prediction algorithms due to the low computational effort required to solve them. These models can be divided into the following distinct groups:

- simple static rollover thresholds
- extension of static threshold by inclusion of some dynamic properties
- energy based considerations
- phase-plane derived models

Consideration of the influence of vehicle parameters on rollover based on static analysis has been presented by many authors [30, 13, 31, 16, 32, 33].

The simplest method of analysing vehicle rollover is by performing static analysis of a rigid vehicle as presented by Gillespie [34]. Based on such a model one can determine that rollover will occur if lateral accelerations exceed the rollover threshold:

$$a_{y\lim} = g \cdot \frac{T}{2H} \tag{2.1}$$

where: T – track, H – height of CoG, $a_{y\lim}$ – lateral acceleration rollover threshold

The term $\frac{T}{2H}$ is often referred to as the Static Stability Factor (SSF). Many authors refer to this metric in their studies either as a simple rollover propensity measure or as a start point for further investigations [35, 23, 36, 37, 38, 39]. Assuming that lateral acceleration is a function of road curvature, driver input and available friction, one can conclude that, using this simplest model, the vehicle properties influencing rollover propensity are track and centre of gravity height.

If an additional roll degree of freedom φ is added to the model, the static rollover threshold is reduced due to the lateral shift of the centre of gravity. The formula (2.1) takes the form of [34]:

$$a_{y\lim} = g \cdot \frac{\frac{T}{2} + \varphi \cdot H}{H} \tag{2.2}$$

The concept can be taken further by assuming roll of vehicle sprung mass around the roll centre [34]:

$$a_{y\lim} = \frac{g \cdot T}{2 \cdot H} \cdot \frac{1}{1 + R_{\varphi} \cdot \left(1 - \frac{H_r}{H}\right)} \tag{2.3}$$

where: R_{ϕ} - rate of roll angle change with lateral acceleration, H_r - roll centre height

Many variations of this equation exist in the literature e.g. Takano et al. [33], and the underlying conclusion is that low roll rate and therefore small roll angles as well as high roll centre height increase the rollover threshold. Another interesting conclusion is that, in general, the more complex is the model used to assess the rollover threshold, the lower the threshold itself. The fact that increasing model complexity reduces steady state rollover stability has been shown in a paper presented by Gertsch et al. [40]. The authors analysed and compared the stability criteria derived from three different roll plane models; a rigid model, a suspended model and a compliant tyre model. It was shown that both the suspended model and the compliant tyre model have a lower roll stability limit than the rigid model.

Sometimes equations similar to (2.1) are expressed in a form representing Load Transfer Ratio (LTR) [16, 41, 31]:

$$LTR = \frac{F_{zr} - F_{zl}}{F_{zr} + F_{zl}} \tag{2.4}$$

where F_{zr} - vertical force on right tyres F_{zl} - vertical force on left tyres

Values of $|LTR| \geq 1$ indicate wheel lift off and impending rollover. As Solmaz at al. [31] noted, for a static condition this gives:

$$LTR = \frac{2 \cdot a_y \cdot H}{g \cdot T} \tag{2.5}$$

Therefore the LTR can be expressed as:

$$LTR = \frac{a_y}{g \cdot SSF} \tag{2.6}$$

This shows that LTR is closely related to SSF.

The rollover thresholds derived from static force balance assume that the vehicle is travelling in a steady state manner which is not usually the case. Cole [39] stated that if the roll eigenfrequency is similar to the frequency of the emergency manoeuvres, then these manoeuvres can cause resonance and in effect vehicle rollover. Therefore, rollover can occur even if the static rollover threshold has not been reached. The use of the oversimplified Static Stability Factor was also negated by a study by Barak et al. [42]. Tammy [43] noted that simple peak lateral acceleration is not an appropriate metric to predict rollover as during transient states this can achieve large values for a very short time without inducing rollover. Also Baumann [12] has stated that high lateral accelerations do not necessarily lead to rollover if they appear for a short period of time. To avoid an early intervention based on the lateral acceleration threshold, Hecker et al. [44] developed a controller which is able to confirm if a high lateral acceleration is actually indicating rollover. For lateral accelerations higher than the threshold value, the controller checks if the inner wheels have lifted off the ground by applying braking torque to them and monitoring their velocity. Rapid deceleration of the wheel indicates wheel lift off which triggers further control actions.

The static rollover threshold can be enhanced by inclusion of dynamic parameters. Solmaz et al. [9, 31, 45] developed the dynamic load transfer ratio (LTR_D), which, in contrast to the more traditional static load transfer ratio, takes into account roll stiffness and damping, but does not account for the lateral shift of the centre of gravity:

$$LTR_D = \frac{2 \cdot (c \cdot \dot{\phi} + k \cdot \phi)}{g \cdot T} \tag{2.7}$$

where k - roll stiffness c - roll damping

As with static LTR, values of $|LTR_D| \geq 1$ indicate impending rollover.

A different approach was presented by Zhang et al. [37]. The Rollover Critical Factor developed by the authors compares the available restoring moment normalised for mass – the equation's (2.8) first square brackets – with moments due to lateral and roll acceleration. The authors developed Rollover Critical Factor RCF as follows:

$$RCF = g \cdot \left[\frac{(t_f + t_r)}{2} - h_s \cdot |\phi| \right] - |a_y| \cdot [(h_s + h_{ra}) - z_s] - (I_{xx})_s \frac{|\ddot{\phi}|}{m_s} \tag{2.8}$$

The RCF accounts for roll angle ϕ, roll acceleration $\ddot{\phi}$, vertical displacement of sprung mass z, as well as roll centre height h_{ra}. Feeding this equation with the vehicle's lateral acceleration and roll acceleration provides a measure of instantaneous rollover margin. Values of RCF close to 0 indicate wheel lift off.

A more sophisticated variation of the rollover threshold was presented by Jin et al. [35]. The authors used the 3 DoF vehicle model for analysing vehicle roll stability. The paper describes the use of the Dynamic Stability Factor (DSF) instead of Static Stability Factor (SSF). Jin proposed the following definition of DSF:

$$DSF = \frac{T}{2H} - \frac{U^2 \cdot m_s \cdot h^2 \cdot \delta}{L \cdot H \cdot (k_\phi - m_s \cdot h \cdot g) \cdot \left\{ 1 - \left(\frac{m \cdot U^2}{L^2} \right) \cdot \left[\frac{a}{2k_r} - \frac{b}{2k_f \cdot \cos\delta} \right] - \frac{U^2 \cdot m_s \cdot h \cdot (c_f - c_r)}{L \cdot (k_\phi - m_s \cdot g \cdot h)} \right\}} \tag{2.9}$$

so that the rollover threshold is:

$$a_{y\lim} = g \cdot DSF \tag{2.10}$$

DSF takes into account such properties as height of the CoG measured from the road (H), height of the CoG measured from the roll centre (h), forward speed of the vehicle (U), tyre cornering stiffness (k_f, k_r), roll stiffness (k_ϕ), steering coefficients induced by roll (c_f, c_r), sprung mass (m_s), total mass (m), steering angle of front wheels (δ), wheelbase of the vehicle (L), longitudinal position of the CoG (a, b).

The analysis they performed showed that use of the SSF results in an "excessively optimistic" rollover threshold and DSF "predicts the rollover more conservatively", a fact which clearly indicates that neglecting the dynamics in rollover modelling is an oversimplification. Even though the DSF is much more advanced than SSF, the authors suggested that the model used in the paper is relatively simple and further research needs to be done to predict rollover more accurately by including the influence of tyre deformation, suspension displacement, non-linear tyre characteristics and time delay of the driver.

From the analysis of the DSF, Jin et al. [35] concluded that:

- decreasing the height of the vehicle's centre of gravity gives greater improvement of vehicle roll stability than increasing the track
- moving the centre of the sprung mass towards the front axle improves the stability of vehicle rollover
- rollover stability improves if the vehicle is moving at a low speed or with a small steering angle
- higher roll stiffness of the vehicle results in a higher value of DSF
- decreasing the ratio between front tyre cornering stiffness to rear tyre cornering stiffness k_f / k_r increases the DSF
- decreasing the roll induced steering coefficient at the front c_f or increasing at the rear c_r increases DSF.

An alternative approach to static or dynamic force balance is to predict impending rollover based on the conservation of energy theorem. Choi [46] proposed the use of a Rollover Potentiality Index (ϕ_0) for predicting rollover.

$$\phi_0 = \frac{1}{2} \cdot \left| V_x \cdot \beta \right|^2 - \sqrt{g^2 - a_{ym}^2} \cdot \sqrt{d^2 + h^2} + d \cdot a_{ym} + h \cdot g \qquad \textbf{(2.11)}$$

where: V_x - vehicle longitudinal velocity, β - slip angle, a_{ym} - measured vehicle lateral acceleration, d - half of vehicle track width, h - nominal CoG height

The Rollover Potentiality Index (ROI) estimates the lateral kinetic energy of the vehicle and compares it with the energy needed for the vehicle to rollover. The authors assume that vehicle rollover is most likely to occur when the vehicle travels with a large slip angle.

Johansson et al. [47] presented a different energy based formulation for preventing wheel lift off which therefore prevents vehicle rollover. The authors based their algorithm on an estimation of the sum of kinetic roll energy, $\frac{1}{2}\cdot\varphi^2\cdot c_\varphi - m\cdot g\cdot h'\cdot(1-\cos(\varphi))$, and potential roll energy, $\frac{1}{2}\cdot(I_{xx}+m\cdot h')\cdot\dot{\varphi}^2$, and compared it with the critical energy needed for wheel lift off. The roll energy takes the form:

$$E_{roll}=\frac{1}{2}\cdot\varphi^2\cdot c_\varphi - m\cdot g\cdot h'\cdot(1-\cos(\varphi))+\frac{1}{2}\cdot(I_{xx}+m\cdot h')\cdot\dot{\varphi}^2 \qquad \textbf{(2.12)}$$

The critical energy formula is based on the moment equation about the roll axis and is the minimum energy that can cause wheel lift off:

$$E_{crit}=F_z\cdot l - F_y\cdot h=(l-\mu\cdot h)\cdot m\cdot g=\varphi\cdot c_\varphi+\dot{\varphi}\cdot k_\varphi \qquad \textbf{(2.13)}$$

where: φ- roll angle, c_φ - roll stiffness, k_φ - roll damping, m - mass, I_{xx} - roll inertia, h' - distance from roll axis to CoG, l - half of vehicle track width, μ - friction coefficient, h - distance from ground to roll axis

Chen et al. [32] employed the energy based rollover detection developed by Johansson et al. [47] for controller investigations with driver in the loop. According to Eger et al. [23] the energy based method is not accurate as it ignores energy dissipation e.g. through damping or friction. Eger et al. [23] developed a rollover stability boundary based on the momentum conservation method, as the authors regard it as being more accurate. The stability boundary derived from phase plane analysis takes the form:

$$\omega_x \le \sqrt{\frac{2\cdot m\cdot g\cdot r\cdot[1-\cos(\kappa-\varphi_x)]}{\theta_x+m\cdot r^2\cdot\sin^2(\kappa-\varphi_x)}} \qquad \textbf{(2.14)}$$

$$|\varphi_x|\le\kappa \qquad \textbf{(2.15)}$$

where: ω_x - roll velocity, m - mass, r - distance from pivot point to CoG, φ_x - roll angle, $\kappa=\text{atan}\left(\frac{\text{z}}{\text{h}}\right)$ - tip angle, θ_x -roll inertia

Dahlberg [13] also proved that the Steady State Rollover Threshold (SSRT), which in its simplest form is represented by equation (2.1), is a very conservative indicator of rollover. The SSRT is the maximum lateral acceleration which does not lead to rollover in a steady state condition. A more complex version of SSRT, incorporating roll stiffness, has also been presented. Using an energy approach Dahlberg developed the dynamic rollover threshold (DRT). The DRT is the minimum

absolute peak of lateral acceleration of all manoeuvres leading to rollover. The DRT presented in the paper can over- or under-estimate the required acceleration but provides a simple tool for measuring vehicle resistance to rollover. Dahlberg [13] noted that although two vehicles may have the same SSRT they may have very different DRTs. The author showed that DRT can be increased by using high damping ratios. However after wheel lift off the roll motion cannot be counteracted by dampers as most of the motion appears between the tyre and the ground and not between the suspension and the vehicle body. Therefore the predicted DRT is higher than the DRT obtained from simulation for damping ratios above 15%. The author notes that for certain situations, e.g. exit from a roundabout, increased damping reduces the rollover thresholds; unfortunately the author does not explain this mechanism.

Yoon et al. [48] developed the rollover index (RI) which is based on the roll angle and roll rate phase plane analysis and wheel lift threshold:

$$\begin{cases} RI = C_1 \cdot \left(\dfrac{|\phi(t)| \cdot \dot{\phi}_{th} + |\dot{\phi}(t)| \cdot \phi_{th}}{\phi_{th} \cdot \dot{\phi}_{th}} \right) + C_2 \cdot \left(\dfrac{|a_y|}{a_{y,c}} \right) \\ + (1 - C_1 - C_2) \cdot \left(\dfrac{|\phi(t)|}{\sqrt{(\phi(t))^2 + (\dot{\phi}(t))^2}} \right), & \phi \cdot (\dot{\phi} - k_1 \cdot \phi) > 0 \\ RI = 0 & \phi \cdot (\dot{\phi} - k_1 \cdot \phi) \le 0 \end{cases} \quad \textbf{(2.16)}$$

where: C_1, C_2 and k_1 are positive constants and $0 < C_1 < 1$, $0 < C_2 < 1$.

The higher the value of RI the higher the danger of rollover, with $RI = 1$ indicating wheel lift off. The RI shows that even for a small roll angle the potentiality of rollover can be high, provided that the roll velocity is high enough.

As it is expensive to measure the roll angle and roll velocity directly, Yoon et al. [48] proposed that it could be estimated from other signals that are easier to measure; i.e. lateral acceleration, yaw rate, steering angle, vehicle velocity and the vehicle's constant parameters. The authors used a 3 DoF model to develop the estimator which uses the above-mentioned inputs for determining the roll angle and roll rate. The estimator, modelled in MATLAB/Simulink, was connected to the vehicle, modelled in CARSIM. The estimator showed good correlation with the CARSIM model in terms of roll angle and roll rate only up to the point of wheel lift off. Tseng et al. [49] showed a method of estimating the roll angle based on lateral acceleration, yaw rate and vehicle speed which gives a good estimate in a low frequency range. For improving high frequency estimation a kinematics model based observer was employed. Hac et al. [14] investigated several approaches to

estimating the roll angle. The most promising results were achieved using a closed loop roll angle adaptive observer with input from lateral acceleration and a roll rate sensor. This approach gave the best results for all types of roll angle excitations. The observer adapts its gains depending on the roll motion before and after two-wheel lift off.

Based on these relatively simple models, a list of crucial vehicle parameters influencing vehicle rollover propensity can be formulated:

- track width – wider track decrease rollover propensity
- CoG height from the ground – lower height decreases rollover propensity
- Roll centre height from the ground – greater height decreases rollover propensity
- Roll stiffness and damping – higher roll stiffness reduces steady state roll angle, high roll damping reduces transient roll peak angle and roll velocity, hence both decrease rollover propensity
- Roll inertia – low roll inertia reduces the potential roll energy and reduces rollover propensity

Hamblin et al. [50] undertook a comparison of dynamic roll models with different levels of detail. The authors compared four vehicle models found in the literature with results obtained from the experiment. The low-order models were originally developed for designing controllers, hence their relative simplicity. The comparison of the lateral velocity, yaw rate and roll angle was performed in both time and frequency domains. The first three models had 3 DoF - lateral velocity, yaw angle and roll angle. The fourth model was a simple bicycle model (2 DoF) which was used only to find or fit, by comparison with the experiment, the chassis parameters which are used in the other three models.

To enable comparison the models were given a common form of:

$$M \cdot \ddot{q} + D \cdot \dot{q} + K \cdot q = F \cdot u_f \qquad \textbf{(2.17)}$$

The first model was based on the model presented by Mammar et al. [51]. It assumed sprung and unsprung mass asymmetry about the XZ plane (Ixz is not 0). The second model was based on the model presented by Kim et al. [17] and assumed separate sprung and unsprung mass but did not include the asymmetry. The third model was based on the model presented by Carlson et al. [52]. It did not use the unsprung mass and the whole vehicle mass was treated as a sprung mass.

The overall correlation of the models with experimental results was described as good. The results obtained by the use of different models were close to each other and the differences between them

were smaller than the errors in parameter fitting. Although this paper investigated only roll dynamics and did not cover vehicle rollover, the authors concluded that non-linear models are necessary for the modelling of on-limit vehicle behaviour.

Drawing further conclusions regarding the factors affecting rollover requires the development of more sophisticated models. Lozia [36] compared rollover threshold acceleration obtained from models with different levels of detail ranging from simple static equilibrium of a single body to a 14 DoF model with step input steering wheel excitation. He concluded that the more sophisticated the model, the lower the rollover threshold, with the differences in the results being up to 38%. Lozia [36] listed the aspects that are important for the realistic modelling of rollover:

- lateral displacements of tyre footprints
- vertical motion of body CoG
- non-linear suspension characteristics
- tyre model including influence of camber angle and traction forces
- roll steer
- steering system flexibilities

The results presented by Shim et al. [21] and Ghike et al. [22] exposed the limitations of the 14 DoF model when compared to a complex multi-body model developed in ADAMS. The 14 DoF model lacked some accuracy at extreme roll angles and after wheel lift off because it did not account for the changes in the suspension geometries and therefore the changes in the roll centre height.

Shim et al. [21] and Ghike et al. [22] also described the influence of various simplifications in the 14 DoF model on the accuracy of roll behaviour:

- linearising the trigonometric terms narrowed the range of roll angles at which the model is correct only up to wheel lift off. For large roll angles (8-10º) this assumption is no longer valid - therefore this approach can be used only for studies before wheel lift off
- ignoring the unsprung mass lateral and longitudinal inertial force increased the roll moment acting on the vehicle, whereas dropping the vertical inertial forces counteracted this effect
- ignoring the terms multiplied by roll and pitch angle in the formulation of the forces acting on the sprung and unsprung mass reduced the roll moment acting on the sprung mass, which lead to increased error at high roll angles

- assuming that the longitudinal and lateral velocities of the tyre are the same as the corresponding sprung mass, corner velocities changed the roll frequency significantly
- not considering the roll centre in the model changed the roll response of the model across the whole range of roll angles
- dropping the tyre inclination angle changed the response only at high roll angles

Shim et al. [21] and Ghike [22] also investigated the use of the 8 DoF model for modelling rollover. They noted that this model can be used only when longitudinal accelerations are not significant, as the model does not account for the pitch of the vehicle.

Marimuthu [30] studied the sensitivity of rollover propensity to vehicle parameters using an 8 DoF non-linear model. He concluded that CoG height and track width are the primary factors defining rollover propensity. Moreover increasing the wheelbase gave better roll stability. The author suggested that there are many other parameters to which rollover is sensitive, and to investigate their influence on rollover propensity further work using multi-body simulation software is required.

One of the crucial aspects of vehicle rollover which needs careful consideration is researchers' approach to roll centres. The majority of researchers using mathematical models assume that there exists a longitudinal axis in a vehicle around which the sprung mass rolls. This assumption is highly inaccurate as an "instantaneous roll centre" is not a geometrical place. Blundell and Harty [54] and Dixon [53] note that the term "roll centre" is itself misleading, as it refers to the point on the vehicle body at which applied lateral force would not cause the vehicle to roll, although it could cause lateral as well as vertical displacement of the vehicle. Dixon suggests using the term "shear centre" instead of "roll centre" and Blundell and Harty suggests the use of "lateral load path". Both authors note that, especially for large lateral accelerations and large roll angles, defining a roll centre based on kinematics is inappropriate. Jones [25] also stated that using kinematic roll centres can be misleading and that analysis of the forces applied to the body is the best approach. This can be seen especially when a tyre on one side of the vehicle loses contact with the road. The simplest way to incorporate this in the model is to give one wheel, or one side of the vehicle when using a two-dimensional model, a vertical degree of freedom.

It is interesting that the majority of researchers do not take into account vehicle pitch motion. This aspect may be necessary to accurately model non-simultaneous wheel lift off at the front and rear axle.

Ghike et al. [22] assumed that roll centre height is constant with respect to unsprung mass. The authors defined the roll centre as the point at which forces are transmitted to the sprung mass and not as a kinematic constraint. This approach accounts for the jacking forces which were proved to be important during rollover; however, no variation of the roll centre height due to suspension geometry was included. The authors state that roll centre is also the instantaneous centre of rotation of the vehicle's sprung mass in relation to the ground. However the study performed by Jones [25] using a vehicle model built in ADAMS showed that the two instantaneous centres of roll, kinematic roll axis and body roll axis, are different, therefore the assumption that these coincide is invalid. These differences are due to load transfer, track change and tyre deflection.

Knowing that the force approach to the vehicle roll centre is correct, it can be seen that jacking forces are not only dependent on the kinematic roll centre. These forces can be generated also by suspension non-linearities. Hac [55] wrote that reducing roll centre heights and suspension non-linearities, such as non-linear springs, decreased jacking forces during cornering. Non-linear spring stiffness causes the inner wheel to have more rebound than bump of the outer wheel, which in effect increases the height of CoG. A similar conclusion was drawn by the same author in [56] - jacking forces tend to increase the vehicle's CoG during hard cornering, increasing the tendency to rollover. Hac [55] also found that jacking forces are the main coupling between vehicle roll, heave and subsequent yaw motions. This author also notes that if jacking forces during cornering differ between front and rear they can contribute also to the pitch motion; however, this effect has not been investigated.

If jacking forces can be affected by spring characteristics, then dampers must also affect them when the vehicle's roll rate is high enough. Potentially the increased rebound damping and decreased bump damping could partially counteract the effect of non-linear springs.

Similarly to non-linear springs, bump stops also play an important role in vehicle rollover. Baumann et al. [12] noted that when the suspension travel is suddenly limited by a bump stop, the body's roll motion decelerates, which increases the dynamic load on the outer tyres and leads to higher lateral forces being produced by these tyres.

There exist a limited number of studies focused on the effect of suspension kinematics, compliance and their non-linearities. Hussain et al. [24] identified the fact that rollover resistance can be improved by limitation of the CoG lateral shift and roll steer effects. The authors also noted that stiffness of the chassis, progressive spring stiffness and the existence of anti-roll bars could have an effect on rollover propensity. Malcher et al. [59] developed two simple, two-dimensional models which were validated against a multi degree of freedom, three-dimensional model built in Human Vehicle Environment (HVE) software. The first two-dimensional, 4 DoF model assumed no lateral

transfer of the CoG and rotation of only the sprung mass. The second model used a single rod connecting the unsprung masses of the suspensions to the sprung mass. This enabled the model to account, in a simplified manner, for the suspension's kinematics e.g. track change. Moreover this model accounted for the lateral shift of the CoG and assumed large roll angles. Both mathematical models used the lateral acceleration generated by the HVE software as an input to compute the roll angle, roll velocity and tyre forces. The results from the fishhook manoeuvre showed that the second model correlated better with the HVE simulation. This suggests that it is important to account for the lateral CoG shift as well as for the change in the track due to suspension kinematics.

Choi [46] stated that roll angle estimation based on the roll rate and dynamic vehicle model loses accuracy at high roll angles if the model does not capture suspension non-linearities. Cole [39] noted that compliance in the suspension reduces the rollover threshold by increasing the lateral shift of the centre of mass towards the outer wheels. Ghike et al. [22] did not include suspension compliance due to bushing but acknowledged that this is a limitation of the model they developed.

Few researchers have investigated the rollover phenomenon after the point of wheel lift off. Yoon et al. [48] suggested that rollover mitigation control after wheel lift off is very difficult, therefore the authors regard wheel lift off as an indication that rollover will occur. Choi [46] stated that vehicle rollover has to be predicted before wheel lift off happens as the combined delay and lag of a typical brake actuator used for the Electronic Stability Program (ESP) is over 0.5s, and the same actuators could be used for mitigation of vehicle rollover. On the other hand Eger et al. [23] performed a simulation of a tripped rollover using a two bodies, two degrees of freedom model. The results showed that the time from impact initiating the rollover to the actual rollover can vary between 0.5s and 3.0s. This result indicates that there can be enough time for the anti-rollover control scheme to bring the vehicle back into the stable region after one side of the vehicle has already lifted off. Simulation results presented by Ghike et al. [22] indicated that from rear wheel lift off it takes about 1.5 seconds, out of which the vehicle is travelling on 2 wheels for close to 1.0s, before the vehicle roll angle reaches 15º.

Tammy [43] showed that the time between lift off and launch, where outer tyres lose contact with the surface, is several times greater than typical vehicle collision contact time. Simulations showed that time between lift off and launch can be as great as 1.5s. This time is dependent on the friction coefficient and it decreases in a strongly non-linear manner for high friction coefficients.

Most rollover models are designed to be accurate up to the point when one of the wheels lifts off – after this point most models become invalid, while the models that are designed to work with wheels off the ground often require a switch between different sets of equations. This is because

the dynamics of the roll after wheel lift off become highly non-linear, e.g. bump stops come into action, and linear assumptions such as linear spring stiffness, are no longer valid. Eger et al. [23] suggested that for accurate rollover modelling, a complex state machine, switching between different models, accurate for the current situation, is needed.

To incorporate wheel lift off in simple mathematical models, Malcher et al. [59] proposed changing the system matrices by introducing factor ζ which takes values of either 0 or 1 and multiplies the expression for the force between the tyre and the ground. This enables the model to avoid having negative tyre forces; i.e. forces which would be pulling the wheel down after tyre lift off. Shim et al. [21] and Ghike et al. [22] accounted for tyre lift off in 14 DoF by switching the tyre force to zero when the tyre radial compression is less than 0, whereas the 8 DoF model presented does not include this non-linearity. Yoon et al. [48] use two different sets of equations describing roll dynamics, depending on whether the tyres have contact with the ground or not. For the non-lift-off situation, the vehicle body is assumed to roll around the roll centre, whereas for the wheel lift off situation it is assumed that the vehicle body rolls around the contact patch.

One modelling aspect which is often missed by researchers is the potential asymmetry of the vehicle, which can be significant especially for asymmetrically loaded vehicles. Lozia [36] performed a simulation of a 14 DoF model with the centre of gravity of the vehicle positioned asymmetrically; i.e. 31mm from the longitudinal plane crossing the centre of the vehicle and being perpendicular to the ground. The results showed that the maximum velocity leading to rollover differed between left and right turns by up to 20%.

An in-depth rollover analysis could not be performed without the consideration of tyre properties. Many authors use simple tyre models to investigate vehicle rollover. As these tyre models are usually developed for handling or ride applications they may not operate properly in such extreme conditions as those seen during rollover. For example Ghike et al. [22] used the Magic Formula model and assumed no lateral shift of the contact patch. Hac [56] used Duggoff's parametric tyre model for rollover modelling. This model includes the effects of longitudinal and lateral stiffness coefficients, surface adhesion coefficient on a normal load and camber influence on tyre forces.

Takahashi et al. [60] developed an improved tyre model formulation to represent the tyre overturning moment. The overturning moment is generated by lateral shift of the contact patch. The proposed simple model assumes that the lateral shift of the contact patch, in other words pneumatic scrub, is proportional to the difference of lateral stiffness divided by lateral force and displacement caused by camber angle.

$$P_{s,s} = F_y / K_L + R_L \cdot \tan \gamma \qquad \textbf{(2.18)}$$

where: $P_{s,s}$ - pneumatic scrub; F_y - lateral force; K_L - lateral stiffness; R_L - tyre static radius; γ - camber angle;

This simple model gave a fairly good correlation with the measurement when the camber and slip angle had opposite signs; i.e. when the lateral force generated by the camber angle had the same direction as the force generated by the slip angle. For improved accuracy Takahashi et al. [60] employed the same formula as used in Magic Formula. This model gave good agreement with measurements for a wide range of camber and slip angles. The authors also investigated the influence of the overturning moment on vehicle rollover behaviour in a fishhook type manoeuvre. The results showed that the more sophisticated the overturning moment model, the lower the maximum lateral acceleration not inducing rollover, and the better the agreement with the experiment. From the diagrams published in the paper one can conclude that not including the overturning moment in a rollover simulation can lead to a rollover threshold 0.3m/s^2 higher than the experiment.

Wielenga [38] used experimental tyre data from sixteen different tyres to analyse their properties influencing rollover using a simple mathematical model based on a static stability margin. The key findings are worth quoting here:

- friction coefficient is the biggest factor influencing rollover propensity; the higher the friction the more likely the vehicle is to rollover
- more advanced and expensive tyres improve traction, braking and handling but at the same time they increase the danger of rollover due to higher friction
- the greater the drop of the friction coefficient with increased load, the more likely that high roll stiffness at the front will mitigate rollover as the vehicle will have more understeering characteristic for on-limit handling
- the greater the load, the more slowly the lateral force versus slip angle builds up; the presented diagrams suggest that to achieve maximum lateral force at high load, a slip angle of 30º could be necessary. As this has to appear simultaneously at both front and rear axle, it would mean that vehicle slip angle would have to be around 30º
- positive camber reduces the lateral forces – which itself mitigates rollover danger – but at high slip angles and high loads this effect reverses and a tyre at a positive angle can produce higher lateral force than a tyre at 0º camber - no explanation of this is given in the paper

- tyre wear – on dry roads a worn tyre can achieve higher friction coefficients – tyre wear was also investigated by Gilbert [61] and the results of the test performed showed that tyre shoulder wear did not affect the vehicle lateral accelerations or yaw rates – however this study was performed on a tyre with relatively high profile i.e. 235/75R15
- pressure – there is no clear outcome; some cases suggested increased friction at load pressure, some decreased friction
- overturning moment due to shift of the contact patch – reduces the half track of the vehicle and therefore reduces the stability margin – the half track change increases more than proportionally with vertical load increase, and it also increases with high friction tyres as well as with low pressure
- positive camber angle – it can increase the half track of the vehicle as the contact patch centre moves outboard – but the effect is small at high loads which appear during rollover

Therefore increasing sensitivity to load, stiffening the sidewall and using wider tyres reduces rollover danger but the most effective way to mitigate rollover is by using tyres with low lateral friction.

In pre-rollover manoeuvres the steering wheel can be subject to sudden changes of driver input leading to transient vehicle dynamics. Therefore an appropriate tyre model which can capture these effects may be necessary. Pacejka [57, 58] discussed tyre transient behaviour under step slip angle, turn slip and camber angle input. The measured response showed that for all these inputs the lateral force builds up for about 1.5m travelled distance. An interesting fact is that there exists an initial non-lagging lateral force for step camber input, which has an opposite direction to the force seen in steady state straight line rolling. Even though the distance of tyre response seems relatively small compared to the distance travelled during a typical untripped rollover, the tyre transient behaviour may have an effect on vehicle stability during rollover.

2.2.3. Rollover control

In this section a review of rollover control schemes is presented. Each control algorithm requires a number of inputs. Due to the prohibitive cost vehicles only have a limited number of sensors, hence it is often the case that states required for roll control have to be estimated based on information from available sensors. The most popular inputs required by rollover control algorithms are:

- lateral acceleration

- yaw rate
- forward velocity
- steering wheel angle

A good example of a rollover control scheme using a limited number of measured signals has been presented by Choi [46]. The author developed a rollover control algorithm based on the same sensors and actuators as an ESP; i.e. it used lateral acceleration and forward velocity as an input and brakes as actuators. As part of the algorithm Choi [46] proposed a method for the dynamic estimation of the CoG height and roll angle by using the measured roll rate and dynamic model.

As with sensors, the number of actuators available to control rollover is also limited. The majority of researchers suggest using one or a combination of the following actuators: differential braking, active steering and active anti-roll bars. Occasionally the use of semi-active damping is also proposed as part of a hybrid control scheme.

Cole [39] discussed different approaches to rollover prevention systems for heavy vehicles. He noted that the use of electronic brake systems enables the prevention of rollover by locking the wheels to cause the loss of adhesion, but such systems, which modify the path of the vehicle, may lead to other undesirable situations. Cole noted that another way to increase the rollover threshold is the use of controllable suspensions which can reduce the roll of the vehicle or even roll the vehicle into the bend. Cole also suggested that fully active suspensions consume too much energy and therefore switchable air springs and semi-active dampers are better for controlling the roll of the vehicle.

Brakes are the most common actuator used in rollover controllers. Johansson et al. [47] proposed the use of brakes for preventing rollover. The proposed control allocator calculates the available tyre friction forces and applies braking forces to prevent wheel lift off. A similar approach was taken by Schofield et al. [62], who described the control allocation which uses actual controls, in this case brakes, to achieve the desired levels of virtual controls. To ensure low computational effort of the allocation algorithm (which obtains actual control levels to meet the correct levels of virtual control), the friction circle of the tyre maximum forces is replaced by the friction square with linear relationship between lateral and longitudinal tyre forces. The limit of the lateral force is determined based on the limit roll angle. Yoon et al. [48] applied differential braking control law to mitigate rollover by direct influence on the yaw moment. Chen et al. [32] also used differential braking to avoid rollover. Holler et al. [63] proposed using the standard Anti-Lock Braking System (ABS) of the trailer to prevent rollover of an articulated vehicle. It was concluded that the system can prevent rollover in most common situations but rollover is still possible. To implement a

rollover prevention system the ABS would require only minor changes. Wielenga et al. [27, 28] proposed Anti-Rollover Braking to prevent rollover. The system limits the lateral acceleration and lateral tyre forces when the vehicle is close to rollover. The brakes are applied on the front outer wheel which reduces the yaw rate, reduces available lateral forces at the wheel and reduces vehicle speed. Anti-Rollover Braking changes the curvature of the vehicle path by initially making it wider – reduced lateral acceleration, and later tighter – due to reduced speed. This altered vehicle trajectory in the first part can lead to other potentially dangerous situations, although the authors claim that the path is altered by a very small amount (0.3m). The authors proposed sensing the impending rollover by monitoring lateral acceleration or alternatively by sensing the contact with rebound bumpers. The simulation showed that to prevent rollover the brakes had to be fully applied at a lateral acceleration of 0.7g for the Ford Bronco model and 0.6g for the Chevrolet Astrovan. The lateral acceleration thresholds used in this paper seem to be very low for the type of vehicles investigated.

Active steering is an alternative method of altering vehicle path to prevent rollover. The active steering proposed by Solmaz et al. [9] was of a mechatronic-angle superposition type; i.e. the controller action is super-positioned with the driver input. The reason for using this kind of active steering was that it maintains the physical connection of the steering wheel with the steered front wheels. This is not the case when full steer-by-wire steering is employed. Using the superposition type of steering system forces the controller to regard the driver's input as a disturbance.

As mentioned earlier, active roll control can also be used for rollover prevention. Miege et al. [64] and Samson [65] presented and tested through simulation a heavy vehicle control strategy consisting of rolling the vehicle into the bend by using active anti-roll bars. The results presented by Miege et al. [64] proved that the method is successful for heavy vehicles as it reduced peak normalised load transfer by 20% compared to the passive vehicle. However this method of improving rollover stability would be difficult to implement in passenger vehicles, as it reduces the feedback given to the driver during cornering. Everett et al. [66] and Hac [56] wrote that the use of active roll control can be very beneficial for off-road vehicles, as it allows the vehicle to have good off-road capabilities when anti-roll bars are disconnected, but at the same time enhances vehicle handling during on-road manoeuvres. This demonstrates why active anti-roll bars are becoming even more popular in current SUVs. However, active anti-roll bars have a very limited effect in quick, transient manoeuvres as they act with a significant delay due to the nature of the hardware. Cimba et al. [67] noted that improvement of the hardware setup, namely use of servo-valves instead of solenoid valves, could result in a quicker response. This property of active anti-roll bars reduces their suitability for rollover control in transient manoeuvres (Everett et al. [66]). Hac [56]

showed that active roll bars may even cause an overshoot of the roll angle during a sudden change of cornering direction as the speed of response of the active roll bars, called Dynamic Body Control (DBC), is limited by the power of the pump. For large steering angles this overshoot may cause a rollover. The author found that for a fishhook manoeuvre, which includes a rapid change of steering angle, an active roll bar increases the vehicle resistance to rollover only slightly compared to an uncontrolled vehicle. Results from the fishhook and double lane change manoeuvres showed that brake based Vehicle Stability Enhancement (VSE) improved the rollover resistance much more than Active Rear Steer (ARS) and active roll control, which performed poorly. It is worth noting that both ARS and brake based vehicle stability control reduce the vehicle's ability to corner. Hac [56] also showed that combinations of VSE and ARS or VSE and DBC out-perform the systems working alone. Kim et al. [17] presented a hybrid control system of the motion of the vehicle which used a variable damper together with active roll control using an electric actuator acting on the anti-roll bar. The performance of this actuator was tested in Hardware in the Loop (HIL) simulation. The use of a variable damper smoothes the response in the transient state as the active roll control acts with a delay. Baumann et al. [12] suggested that to prevent rollover the following measures could be taken:

- limit high steering rates at high lateral accelerations
- avoid high slip angles at the rear axle
- reduce high roll rates and dynamic tyre loads through damping and limitation of roll motion, e.g. active roll control

Actuator limitations influence how successful the proposed control scheme is. Therefore they need to be carefully taken into consideration when working on the rollover control. For example Everett at al. [66] modelled a hydraulic actuation system of active roll control. Thanks to this, the authors were able to show that during rapid transient manoeuvres actuator delay can reduce the effectiveness of active roll control.

Other authors also modelled the actuators to capture their limitations. Holler et al. [63] modelled the pneumatic system of brakes used as actuators to prevent rollover. Durali et al. [26] modelled the hydraulic anti roll system in detail using Matlab/Simulink which was co-simulated with an MBS model in ADAMS. Hac [56] has included a simple brake system model including hydraulics and control systems; ABS and TCS (Traction Control System). Moreover the author modelled in detail the following active chassis control systems, and investigated their effectiveness in preventing rollover was:

- brake based Vehicle Stability System

- Active Rear Steer
- Dynamic Body Control

Understanding the limitations of actuators is important as it puts significant constraints on the effectiveness of the control systems. By combining different actuators to control the rollover the weak points of one actuator can be corrected by another. As shown above [66], active roll bars are good for steady state but perform poorly in transient manoeuvres. Switchable dampers have an effect only during transient manoeuvres. Differential braking reduces the velocity but at the same time alters the vehicle trajectory. Combining all three types of actuators could produce good rollover prevention, however the exact efficiency of such a system is unknown, and so are the interactions between these three actuators. Coordinated control management would be necessary for the efficient operation of a hybrid system. There are various ways in which the control system could be coordinated; a good overview of different approaches was given by Gordon et al. [68]. The authors described different architectures of the integrated control system, such as centralised control, supervisory control and decentralised and hierarchical control. The application of optimal control to active suspension was shown by Gordon [69].

The results of experimental work performed by Jurecki et al. [70] show that during avoidance manoeuvres, actions undertaken can be dramatically different for different drivers. The authors have managed to describe driver behaviour using a mathematical model by dividing the drivers into different groups. If a driver has to interact not only with the dynamics of the vehicle but also with the controller, the spectrum of possible behaviours may be even wider.

Cole [39] argued that the interaction between the driver and the vehicle with controllable suspension needs to be understood to predict the response of the vehicle. Smid et al. [71] described a 24 DoF driving simulator which could be used for development of a rollover detection and warning system. Also Chen et al. [32] investigated the use of a PC-based driving simulator and scaled vehicle testing system for studying the interaction between the driver and the rollover prevention controller. The model presented in the paper had 4 DoF including longitudinal, lateral, yaw and roll motion. The model assumed small roll angles, constant vertical tyre forces dependant on the static load distribution between vehicle front and rear, and elliptical friction envelope. The only input from the driver was the steering angle. The authors noted that the vehicle model becomes invalid when it operates in a near-rollover situation. In a different paper Chen et al. [72] analysed the effectiveness of the proposed roll strategy using Driver in the Loop simulation. The results showed that in one of the test scenarios a vehicle with a control system gave worse results than a vehicle without it. The reason for this was that a human driver compared to a driver model gave much noisier steering input which degraded the effectiveness of the control algorithm. This

example confirms that human in the loop testing is an effective tool for confirming if the control system performs as expected.

2.3. Critical assessment of current knowledge

The literature review presented in the previous section outlines the important aspects of rollover modelling. To summarise, for the accurate modelling of rollover, a model should:

- be valid after wheel lift off; i.e. switch off the tyre forces after wheel lift off, account for the change in instantaneous roll centre
- account for jacking forces
- account for the lateral shift of the CoG
- account for the roll stiffness from the anti-roll bars
- include progressive spring characteristics and bump stops
- account for vertical tyre deflection
- account for unsprung masses
- use a tyre model including: influence of camber angle, load and traction/braking forces on the lateral force and overturning moment (include lateral displacements of tyre footprints)
- not assume small angles and therefore should not linearise trigonometric terms
- be a 3D model as the wheelbase has an effect on rollover propensity
- include asymmetry of sprung and unsprung mass about the XZ plane
- account for track change, camber angle, roll steer by introducing suspension kinematics, e.g. by simplifying the suspension of each wheel by single arm
- account for asymmetry of vehicle loading
- not be computationally demanding

Moreover the model should enable the user to implement the inputs for control actuators such as brakes, active steering, active roll control, switchable air springs or semi-active dampers.

Even though the available literature covers many aspects of rollover modelling, the significance of some parameters is not known. Some of the modelling uncertainties are:

- pitch motion and resulting longitudinal load changes – it has been shown that positioning the centre of gravity closer to the front of the vehicle improves rollover stability but the influence of dynamic shift of the longitudinal centre of gravity on rollover has not been investigated
- the influence of transient tyre effects on rollover
- kinematic and compliance characteristics of the suspension – the lateral compliance could potentially increase the lateral centre of gravity shift but the magnitude of this effect is not known
- the influence of vertical road irregularities on roll dynamics

Moreover the majority of previous research work has been based on low fidelity models [36, 30, 35, 50, 40 etc]. However, vehicle rollover is a highly non-linear event due to the large angles seen in vehicle body motion, extreme suspension travel, tyre non-linearities and large forces acting on the wheel, resulting in suspension spring-aids, rebound stops and bushings operating in the non-linear region.

Moreover suspension compliance effects such as compliance steer can also play a significant role as they affect understeer gradients. Taking into account the above findings, one can conclude that a high fidelity, non-linear model is necessary to accurately simulate vehicle rollover.

The use of such a model could help to establish how significant each vehicle property is for rollover propensity, which has not been done so far. The significance of large numbers of parameters can be studied by employing design of experiment methodology. Such a study could give insights not only into the relevant modelling aspects but also could present the chassis engineers with data on the sensitivity of a vehicle to key factors affecting rollover.

The literature review of rollover prevention schemes shows that the use of differential braking, active steer and active anti-roll bars as rollover prevention actuators has been well researched. However, all of these actuators have significant disadvantages. The first two of these reduce the lateral force through correction of the trajectory of the vehicle. This may prevent the rollover but could potentially lead to other unforeseen outcomes. The latter actuator prevents rollover in steady state but the actuator delays are too great to prevent rollover in highly dynamic manoeuvres. This can be partly mitigated by simultaneous use of semi-active damping. However, both active anti-roll bars and semi-active dampers lose their effectiveness after wheel lift off. Therefore there is a need for the development of a rollover control algorithm which could prevent rollover even after wheel lift off without affecting the vehicle trajectory. Mavros [73] proposed a novel approach to the roll

stability of a motorcycle. The author described the application of a torque reaction wheel to stabilise a motorcycle subjected to lateral acceleration input. This type of actuator has the potential to fulfil the outlined requirements. Moreover there exists a strong similarity between motorcycle dynamics and vehicle dynamics after two wheels lift off. An investigation into a torque reaction wheel as part of rollover prevention control has not been yet performed.

2.4. Research objectives

The extended literature study revealed that a detailed study concentrating on suspension characteristics affecting vehicle rollover has not been yet performed. Moreover only a few authors have attempted to study the influence of tyre properties on rollover, therefore the existing knowledge is still fairly limited.

The proposed approach is to use a vehicle model with a high level of detail, set up using MBS software and use statistical methods, such as design of experiment, to draw robust conclusions about factors influencing rollover. The output of such an experiment would provide in-depth knowledge about the main suspension and tyre properties affecting rollover dynamics, which could be used as guidance for a rollover control algorithm. At the end of the research a simple control algorithm will be developed. The main objective of the controller is to be able to prevent vehicle rollover without affecting vehicle trajectory and be effective also after wheel lift off.

The research objectives can be listed in the following points:

- Build a non-linear MBS vehicle model
- Correlate the model to the measurement data
- Develop a rollover propensity measurement suitable for assessing vehicle properties' influence on rollover using a full MBS model
- Determine tyre properties influencing rollover using DoE technique
- Determine kinematic and compliance suspension properties affecting rollover
- Propose a roll control scheme based on a reaction wheel actuator and confirm if it is able to prevent vehicle rollover without affecting the vehicle trajectory

2.5. Modelling and analysis tools used in research

In order to accomplish the above-mentioned research objectives a number of modelling and analysis tools will be necessary. The choice of the tools was dictated mostly by their suitability to perform the given task; however, the availability of relevant data and commercial software also introduced some constraints. A brief outline of the tools starts with MBS software used to build the vehicle model. As discussed in more detail in Chapter 3, SIMPACK uses relative kinematics formulation, which together with an efficient solver and flexible scripting language made it a suitable choice for this tool. A more in depth justification for the choice of software is provided in Chapter 3. The Magic Formula (MF) tyre model has been employed; chosen for the familiarity of the equations, ease of modification and the available tyre data. An example of vehicle rollover simulation using an MBS model coupled with MF tyre model is shown in Figure 2.1. In order to generate a statistical experiment a combination of design of experiment methodology and statistical data analysis techniques have been used. Finally, Lyapunov's indirect method was employed to analyse vehicle stability, and develop the controller.

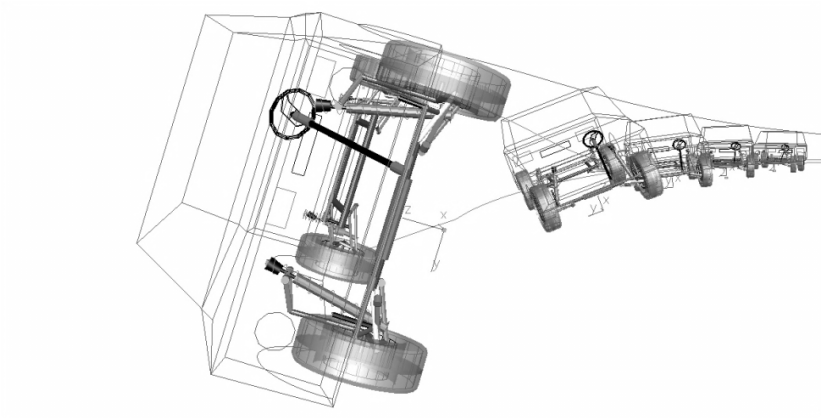

Figure 2.1 Example of vehicle rollover simulation.

3. Modelling methodology and model development

This chapter is divided into four parts. The first covers modelling in the MBS environment and aims to provide an introduction into available MBS formulations as well as a description of the chosen technique followed by the justification. The second section describes the modelling details of the vehicle model. The third section is related to tyre modelling and provides a brief overview of available tyre model formulations, as well as a characterisation of the tyre used in this study. Finally in the fourth section a full vehicle model is characterised in road manoeuvres.

3.1. Modelling using multi-body formulation

In order to generate a high fidelity vehicle model able to capture complex, elastokinematic suspension characteristics, a multi-body approach is necessary. The multi-body approach to modelling of physical systems consists of dividing the analysed system into separate parts which can be represented by elements such as rigid or flexible bodies, joints, force elements (passive and active), gravity etc. All these elements joined together create a multi-body model of a physical system. As the complexity of the analysed system increases, and with it the number of elements in multi-body model, a specialised Multi-Body Simulation (MBS) software becomes necessary. There exist a number of commercial MBS tools, which differ in the formulations of equations of motion employed, solver efficiency and user-friendliness.

Equations of motion are the heart of multi-body models. They describe the dynamic behaviour of the model. Over the years different approaches to deriving equations of motion have been developed. The three main solutions used in multi-body models are based on:

- Constrained Lagrange
- Kane
- Newton-Euler

The above-mentioned solutions will be briefly introduced in this chapter.

3.1.1. Lagrange equations

Probably the most popular approach to formulating equations of motion is based on the D'Alembert-Lagrange equation [19]:

$$\sum_j \left[\frac{d}{dt}\left(\frac{\partial T}{\partial \dot{q}_j} \right) - \frac{\partial T}{\partial q_j} - Q_j \right] \delta q_j = 0 \qquad \textbf{(3.1)}$$

Where:

q_j - generalised coordinate with $j = 1,2,...,n$

T - total kinetic energy in the system:

$$T = \sum_{i=0}^{n_p} T^i = \sum_{i=0}^{n_p} \frac{1}{2} m^i \dot{\mathbf{r}}^{i\mathrm{T}} \dot{\mathbf{r}}^i \qquad \textbf{(3.2)}$$

Q_j - component of the generalised force along coordinate q_j

$$Q_j = \sum_{i=1}^{n_p} \mathbf{F}^{i\mathrm{T}} \frac{\partial \mathbf{r}^i}{\partial q_j} \qquad \textbf{(3.3)}$$

In complex multi-body systems the bodies are connected using joints which constrain motion. Therefore the generalised coordinates are dependent on each other and the equation (3.1) cannot be employed directly. Hence the main difficulty in formulating the equations of motion is capturing the constraints. These can be incorporated into the equations of motion in two different ways.

The first approach, called the embedding technique [19,74], is to find a set of independent coordinates which satisfy the constraints. This approach results in a minimum number of differential equations without the need for additional algebraic constraints. In practice this technique is rarely used in multi-body codes as it is computationally demanding.

The second approach, referred to as augmented formulation [19,74], is to apply a method of Lagrange multipliers, which results in equations of motion referring to both dependent and independent coordinates and a vector of multipliers. Equations of motion derived using this formulation take the shape of [19]:

$$\mathbf{M}\ddot{\mathbf{q}} - \mathbf{Q} + \mathbf{C}_\mathbf{q}^\mathrm{T}\boldsymbol{\lambda} = \mathbf{0} \qquad \textbf{(3.4)}$$

Where:

$\mathbf{M}$ - system mass matrix

$\ddot{\mathbf{q}}$ - generalised accelerations

$\mathbf{Q}$ - sum of centrifugal and Coriolis inertia forces, and externally applied forces

$\mathbf{C}_\mathbf{q}$ - constraint Jacobian matrix

$\boldsymbol{\lambda}$ - vector of Lagrange multipliers

This approach is much more common in application to general multi-body dynamics software than the embedding technique. The main disadvantage is the large number of differential equations, supplemented by non-linear algebraic equations for constraints.

3.1.2. Kane equations and virtual power

Using the Lagrange equations and the D'Alembert method for embedding dependent coordinates, the equations of motion can only be written for systems with geometric (holonomic) constraints. However for some dynamic problems it is easier to define the constraints in terms of velocities rather than geometry. The principle of virtual power enables the formulation of equations of motion satisfying both holonomic and non-holonomic constrains. Kane's equations based on this principle result in the minimum set of generalised coordinates equal to the number of degrees of freedom in the system. Kane equations for the system of *N* particles are briefly introduced below [75].

Q_k is defined as the generalised active force and Q_k^* as generalised inertia force:

$$Q_k = \sum_{i=1}^{N} \mathbf{F}_i^a \cdot \boldsymbol{\beta}_{ik} \tag{3.5}$$

$$Q_k^* = -\sum_{i=1}^{N} m_i \dot{\mathbf{v}}_i \cdot \boldsymbol{\beta}_{ik} \tag{3.6}$$

where:

$\mathbf{F}^a$ – active forces

$\boldsymbol{\beta}_{ik}$ - so called partial velocity is expressed as

$$\boldsymbol{\beta}_{ik} = \frac{\partial \mathbf{v}_i}{\partial \dot{\mathbf{q}}_k} \tag{3.7}$$

Then the sum of generalised active force Q_k and generalised inertia force Q_k^* is equal 0:

$$Q_k + Q_k^* = 0 \tag{3.8}$$

The above equation is referred to as Kane's equation. Despite the advantages, Kane equations have not found many applications in commercial MBS codes.

3.1.3. Newton-Euler equations

The Newton-Euler formulation is the last approach presented here to deriving equations of motion of multi-body system. Newton's law written in body coordinates has the following form [76]:

$$m \cdot \dot{\mathbf{v}}^b + \boldsymbol{\omega}^b \times m \cdot \mathbf{v}^b = \mathbf{f}^b \tag{3.9}$$

Where:

m – mass

$\mathbf{v}^b$ – translational velocity in body coordinate frame

$\boldsymbol{\omega}^b$ – angular velocity in body coordinate frame

$\mathbf{f}^b$ – force in body coordinate frame

The Euler equation states that angular momentum is equal to the applied torque [76]:

$$\mathbf{I} \cdot \dot{\boldsymbol{\omega}}^b + \boldsymbol{\omega}^b \times \mathbf{I} \cdot \boldsymbol{\omega}^b = \boldsymbol{\tau}^b \tag{3.10}$$

where

$\mathbf{I}^s$ – instantaneous inertia tensor relative to the inertial frame

$\boldsymbol{\omega}^s$ – spatial angular velocity

$\boldsymbol{\tau}$ – externally applied torque

Combining the above equations results in the Newton-Euler equation described in the body coordinate frame [76]:

$$\begin{bmatrix} m & 0 \\ 0 & \mathbf{I} \end{bmatrix} \cdot \begin{bmatrix} \dot{\mathbf{v}}^b \\ \dot{\boldsymbol{\omega}}^b \end{bmatrix} + \begin{bmatrix} \boldsymbol{\omega}^b \times m \cdot \mathbf{v}^b \\ \dot{\boldsymbol{\omega}}^b \times \mathbf{I} \cdot \boldsymbol{\omega}^b \end{bmatrix} = \mathbf{F}^b \tag{3.11}$$

where:

$\mathbf{I}$ – inertia tensor

$\mathbf{F}^b$ – external wrench applied at centre of mass

The above Newton and Euler equations describe rigid body dynamics due to force and torque applied at the centre of mass of the body.

3.1.4. Relative and absolute coordinates

The position and orientation of bodies in a constrained multi-body system can be described using an absolute or relative set of coordinates. Employing absolute kinematics, the position of each body in space is described using coordinates in the inertial frame of reference. To deal with constraints, the Lagrange or Kane equations can then be employed to embed the constraints in the set of equations of motion using independent coordinates. Alternatively constraints can be taken into account by supplementing the equations of motion with Lagrange multipliers. When using relative kinematics the equations of motion of bodies in kinematic chain are described relative to each other, proceeding down to the base of the kinematic chain. Position and velocity of subsequent bodies are a result of generalised joint coordinates of all preceding bodies. For example for the joint between the "From" marker $M_{i\text{-}1}$ of body i -1 to "To" marker M_i coincident with body reference system R_i following equations can be derived [77]:

- Orientation given by transformation matrix A:

$$\mathbf{A}_{M_{i-1}R_i} = \mathbf{A}_{M_{i-1}R_i}(\mathbf{q}_i, t) \tag{3.12}$$

- Position:

$$\mathbf{r}_{M_{i-1}R_i} = \mathbf{r}_{M_{i-1}R_i}(\mathbf{q}_i, t) \tag{3.13}$$

- Angular velocity:

$$\boldsymbol{\omega}_{M_{i-1}R_i} = J_{\varpi_i}(\mathbf{q}_i, t)\cdot\dot{\mathbf{q}}_i + \overline{\boldsymbol{\omega}}_{M_{i-1}R_i}(\mathbf{q}_i, t) \tag{3.14}$$

- Translational velocity:

$${}^{M_{i-1}}\dot{\mathbf{r}}_{M_{i-1}R_i} = J_{v_i}(\mathbf{q}_i, t)\cdot\dot{\mathbf{q}}_i + {}^{M_{i-1}}\dot{\overline{\mathbf{r}}}_{M_{i-1}R_i}(\mathbf{q}_i, t) \tag{3.15}$$

- Angular acceleration:

$${}^{M_{i-1}}\dot{\boldsymbol{\omega}}_{M_{i-1}R_i} = J_{\varpi_i}(\mathbf{q}_i, t)\cdot\ddot{\mathbf{q}}_i + {}^{M_{i-1}}\dot{\overline{\boldsymbol{\omega}}}_{M_{i-1}R_i}(\mathbf{q}_i, \dot{\mathbf{q}}_i, t) \tag{3.16}$$

  Where: ${}^{M_{i-1}}\dot{\overline{\boldsymbol{\omega}}}_{M_{i-1}R_i}$ is the part of relative angular acceleration ${}^{M_{i-1}}\dot{\boldsymbol{\omega}}_{M_{i-1}R_i}$ which is only dependent on the generalised joint states $\mathbf{q}_i, \dot{\mathbf{q}}_i, t$

- Translational acceleration:

$${}^{M_{i-1}}\ddot{\mathbf{r}}_{M_{i-1}R_i} = J_{v_i}(\mathbf{q}_i, t)\cdot\ddot{\mathbf{q}}_i + {}^{M_{i-1}}\ddot{\overline{\mathbf{r}}}_{M_{i-1}R_i}(\mathbf{q}_i, \dot{\mathbf{q}}_i, t) \tag{3.17}$$

  Where: ${}^{M_{i-1}}\ddot{\overline{\mathbf{r}}}_{M_{i-1}R_i}$ is the part of relative translational acceleration ${}^{M_{i-1}}\ddot{\mathbf{r}}_{M_{i-1}R_i}$ which is only dependent on the generalised joint states $\mathbf{q}_i, \dot{\mathbf{q}}_i, t$

The main advantage of using relative kinematics is the fact that equations of motions are dependent on a reduced number of generalised coordinates. For open kinematic chains the number of generalised coordinates equals the number of degrees of freedom in the system. If closed kinematic chains are to be analysed additional constraint equations become necessary.

3.1.5. Summary of formulation of equations of motion

Currently most MBS codes employ one of two routes to identify a set of differential equations describing the motion of rigid bodies in the model. The first approach is to describe the position and orientation of each body using a Cartesian set of coordinates. Each body's position and orientation is therefore described by 6 coordinates. The equations of motions can be formed in a straightforward manner. The relative motion between bodies or bodies and ground is constrained by the application of algebraic equations describing the constraints. These constraints can then be either integrated into the set of equations of motion by finding a set of independent coordinates satisfying the constraints (embedding technique), or can be integrated into the equations using Lagrange multipliers (augmented formulation). The second route is to use relative coordinates, in which the position and orientation of each body is described with relation to the preceding body in the kinematic chain, or if the body is at the base of the chain, with relation to the ground. This approach results in the minimum set of differential equations necessary to describe the motion of the system. This recursive approach is often used in conjunction with the Newton-Euler formulation. The disadvantage of this approach is that the formulation of forces acting between the bodies is somewhat more complex than in a system based on a Cartesian set of coordinates. However as the set of differential equations is greatly reduced, this gives a good basis for fast and accurate simulation. The commercially available MBS software SIMPACK is a good example of the implementation of such an approach [77]. SIMPACK uses recursive algorithms for solving the equations of motion. The computation effort increases in a linear manner with the number of bodies. This makes SIMPACK well suited to solving complex mechanical systems with many degrees of freedom.

SIMPACK modelling formalism is based on bodies connected together with joint elements creating open kinematic chains. For the motion of reference frame *R* of the body *i* with respect to the inertial reference frame *I* Newton-Euler equations describing the motion of rigid bodies take the shape of [77]:

$$ {}^{R_i}\mathbf{I}_i \cdot \dot{\boldsymbol{\omega}}_{IR_i} + m_i \cdot \mathbf{r}_{R_iG_i} \times \ddot{\mathbf{r}}_{IR_i} + \boldsymbol{\omega}_{IR_i} \times \left({}^{R_i}\mathbf{I}_i \cdot \boldsymbol{\omega}_{IR_i} \right) = \sum_e \mathbf{T}_e + \sum_f \mathbf{r}_{R_iF_f} \times \mathbf{F}_f \qquad \textbf{(3.18)} $$

$$m_i \cdot \left[\ddot{\mathbf{r}}_{IR_i} + \mathbf{r}_{R_iG_i} \times \dot{\boldsymbol{\omega}}_{IR_i} + \boldsymbol{\omega}_{IR_i} \times \left(\boldsymbol{\omega}_{IR_i} \times \mathbf{r}_{R_iG_i}\right)\right] = \sum_f \mathbf{F}_f \qquad \textbf{(3.19)}$$

Closed kinematic loops are achieved by application of constraint elements. Jourdain's Principle of Virtual Power cancels out joint constraint forces [77]:

$$0 = \delta P_{J_i} = \mathbf{T}_{J_i} \cdot \delta\omega_{M_{i-1}R_i} + \mathbf{F}_{J_i} \cdot \delta^{M_{i-1}}\dot{\mathbf{r}}_{M_{i-1}R_i} \qquad \textbf{(3.20)}$$

Where: P_{J_i} - power from joint constraint forces $\mathbf{F}_{J_i}$ and torques $\mathbf{T}_{J_i}$

Additionally forces applied to the bodies are generated by force elements.

3.1.6. SIMPACK overview

The development of MBS software was prompted by kinematic and dynamic problems in the mechanical systems of satellites, spacecraft and aeroplanes. The history of MBS software developed by DLR (Deutsches Zentrum für Luft- und Raumfahrt), the German Aerospace Centre, dates from the early 1970s when FADYNA software was developed. SIMPACK is a direct successor to FADYNA (1977) and MEDYNA (1984). In 1993 INTEC GmbH (now SIMPACK AG) was founded to develop SIMPACK for commercial use. From that time an increased emphasis was laid on the development of user-friendly interfaces and adapting the program to new fields of engineering. The first add-on modules were launched in 1996 when Railway and Automotive+ were released. This opened doors to the rail and automotive industries. Today SIMPACK is used by many leading automotive companies.

As mentioned before, global reference frame (inertial), rigid (or flexible) bodies, joints, constraints and force elements are the main components of a multi-body system. The majority of modelled mechanical systems consist of rigid instead of flexible bodies, because deflections of flexible bodies are relatively small in comparison with the translations or rotations of joints. Constantly increasing computing power, however, means that the use of flexible bodies is becoming more and more common.

The heart of SIMPACK is its Kinematics and Dynamics module. It consists of three parts: Model Set-up, Solver, and Post-Processor. Model Set-Up with its 3D graphical representation allows the user to build a model consisting of bodies, joints, constraints, force elements etc. Solver automatically generates equations of motion and performs time integration. The solution can be viewed in Postprocessor both in the form of an animation and plots of various signals. Additionally

SIMPACK software can be extended with modules that adapt the program for solving problems in specific fields of engineering. Amongst the most common add-on modules are: Automotive+, Engine, Wheel/Rail and Noise Vibration and Harshness (NVH). These extra modules consist of pre-defined substructures, special kinds of joints, constrains, force elements or control loops. The models developed for use in this work were based on heavily modified elements from the Automotive+ module. This module offers a number of predefined, fully parameterised substructures for automotive components. A brief description of major modelling elements available in SIMPACK is given below.

Bodies are basic elements when constructing a model. There are two different kinds of bodies:

- Rigid Bodies – most commonly used in MBS simulations; they have only mass and inertia properties
- Elastic Bodies – possess not only mass and inertia but also modal stiffness and damping

Each body can have several markers (a minimum of one), which are additional local coordinates systems used for connections, measurements, graphics etc. Graphical elements representing bodies are only visualisation elements and they do not have any physical meaning. In order to create a body, several inputs are required; name, mass, position of centre of mass described relative to Body Fixed Reference System or any predefined marker, inertia tensor described with respect to centre of mass, body fixed reference system or any predefined marker. For setting up the connections between bodies, joints and constraints can be used. Each body contains one and only one joint.

Joints are the connections between two bodies or body and reference frame which give degrees of freedom to the body. There can be one and only one joint per one body to which it is strictly associated. They describe the relative motion between bodies. A joint can give from 0 to 6 degrees of freedom to the body they refer to. Each joint is attached to the body it belongs to with a “To” marker and connected to another body or reference frame by a “From” marker. Joints take their names from the bodies they are associated to. There are a few dozen different kinds of joints available in SIMPACK, from simple revolute joints to complicated ones like the Automotive Track Joint. A joint does not have any mass or inertia matrix. To define a joint the following input is required: “To” and “From” markers, type of joint, initial state of the joint including its position and velocity, specific joint parameters such as initial displacement or gear ratio.

Constraints are the connections between two bodies or body and reference frame that remove extra degrees of freedom from the system. Because each body can have only one joint, constraints are required to define kinematically closed loops. In a real mechanical system joints and constrains would not be distinguished but because of the way equations are created in SIMPACK, the

definition of constraints is necessary to close the kinematic tree. There are a few dozen predefined kinds of constrains but there is also the capability for the user to define new ones. To define constraints the following inputs are required: name, “To” and “From” markers, type of constraint, specific constraint parameters.

Force elements are massless connections between two bodies or body and reference frame that apply forces or torques or a combination of forces and torques to connected bodies. To connect two bodies with a force element two markers on these bodies must be chosen. The forces and torques applied on the markers are calculated according to the defined types of force elements. The input data for force elements can depend on the measurement of distance between the markers on connected bodies but it can also be a function of time. Other kinds of input are also allowed. There are two different kinds of force elements:

- Point-to-point force elements where force is applied to both bodies along the line between “From” and “To” markers. This means that the direction of generated force does not depend on which marker coordinate system is used.
- Component force elements where the forces are calculated with respect to the “From” marker coordinate system. These tend to cover more sophisticated force laws.

In order to define a force element the following is needed: name, “From” and “To” markers between which connected forces are applied, type of force element, specific force elements parameters e.g. stiffness in a given direction.

There are also other elements and tools that can be used during the modelling of a mechanical system. They allow the user to apply different kinds of action to the model. Some of these actions are: sensors – for extra measurements, control loops, substructures – sub-models imported into the main model, time excitations – for assigning a time function to the actuator, input functions – for defining non-linear functions used by other modelling elements, polynomials – for defining polynomials used in stochastic elements, substitution variables – to parameterise models, expression – for defining expressions that can be attached to a force element, generate a result channel etc.

Before modelling a mechanical system in SIMPACK it is important to first design its topology. Careful planning of the way model is going to be built helps to avoid mistakes and may reduce simulation time. To ease model topology planning, a set of specific symbols is used to describe the system (Figure 3.1). An example of a crank and slider mechanism is shown in Figure 3.2.

As mentioned before, SIMPACK’s formulation is based on relative kinematics and Newton-Euler equations of motion. This approach has its implications in the model building process. By choosing

specific joints which give specific DOF to the bodies, the user indicates which coordinates should be used by the software to create equations. This way a system of equations describing an open kinematic chain can be created. In order to create a mechanism and close the kinematic chain, extra algebraic constraints have to be applied. The user indicates which motions should be constrained by the use of constraint modelling elements. As the user has direct control over the set of coordinates used to formulate equations of motion, model efficiency can be greatly influenced by model topology. The number of degrees of freedom of a mechanical system can be calculated as:

$$k = \sum k_{joint} - \sum constraint \tag{3.21}$$

Where:

k – number of DOF in the system

k_{joint} – number of DOF given by joint elements

Whereas the total number of equations n_{eq} in the system is defined as:

$$n_{eq} = 2 \cdot \sum k_{joint} + \sum constraint \tag{3.22}$$

To illustrate how the same system can be modelled in two ways leading to a difference in efficiency, let us consider the slider crank mechanism shown in Figure 3.2. Two modelling approaches are shown in Figure 3.3.

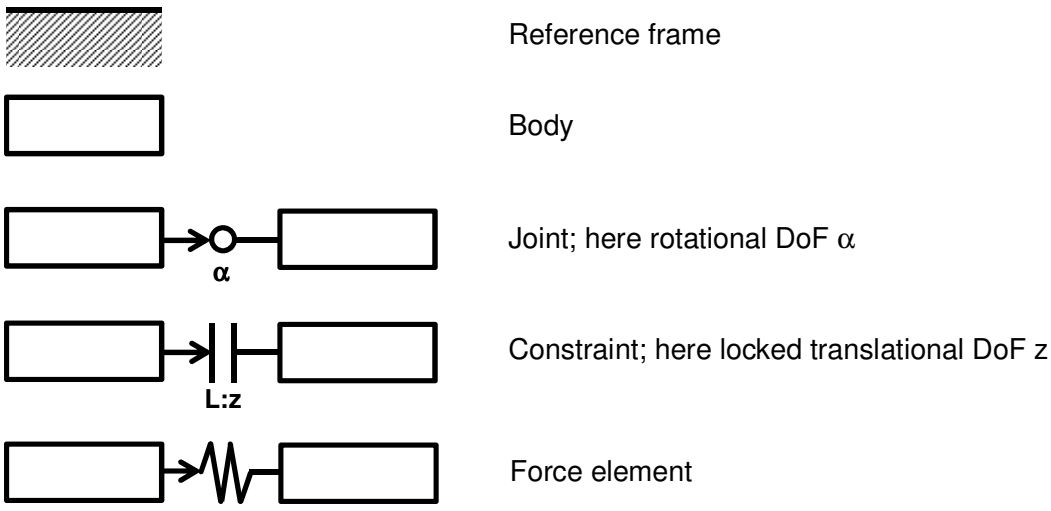

Figure 3.1 Topology symbols

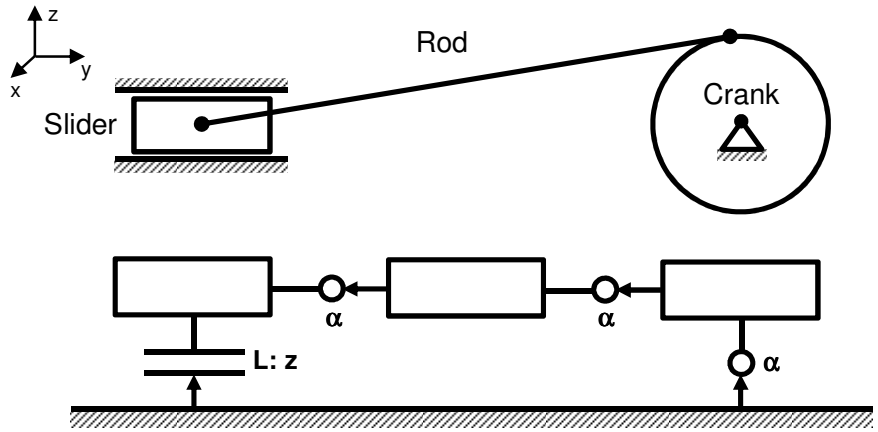

Figure 3.2 Topology of crank and slider mechanism

Using equation (3.22) it is easy to show that the model defined using relative kinematics results in only 6 differential and 2 algebraic equations whereas the same model set up using global kinematics results in 36 differential and 17 algebraic equations.

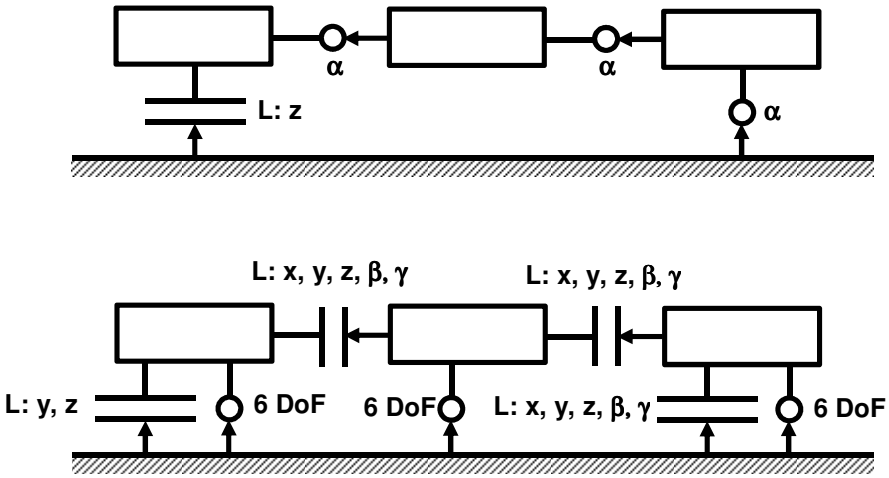

Figure 3.3 Different description of the same mechanical system: top - local coordinates, bottom – global coordinates

3.2. Vehicle model description

The vehicle model (Figure 3.4) set up for this research contains 165 degrees of freedom. Most of the suspension members have 6 degrees of freedom in order to accurately replicate suspension compliances. In addition, 2 rotational degrees of freedom are given to each hub, to account for the

conical stiffness of the wheel bearing. The number of degrees of freedom for model subsystems is given in Table 3.1. Importantly, the model contains non-linear elements for spring aids, rebound stops and dampers. The vehicle uses TNO's Magic Formula tyre model version 6.1. [78]. This model contains 15 internal states used to predict the dynamics of the tyre including relaxation lengths**.** The aim behind creating such a complex vehicle model is to replicate real vehicle behaviour in as much detail as possible and then treat that model as the subject of experiments. For completeness, the model's sub-systems are briefly described below.

Subsystem	No. Degrees of Freedom:
Vehicle body	6
Front axle suspension	78
Rear axle suspension	76
Steering system	1
Wheels	4
Total:	**165**

Table 3.1 Degrees of freedom in each subsystem.

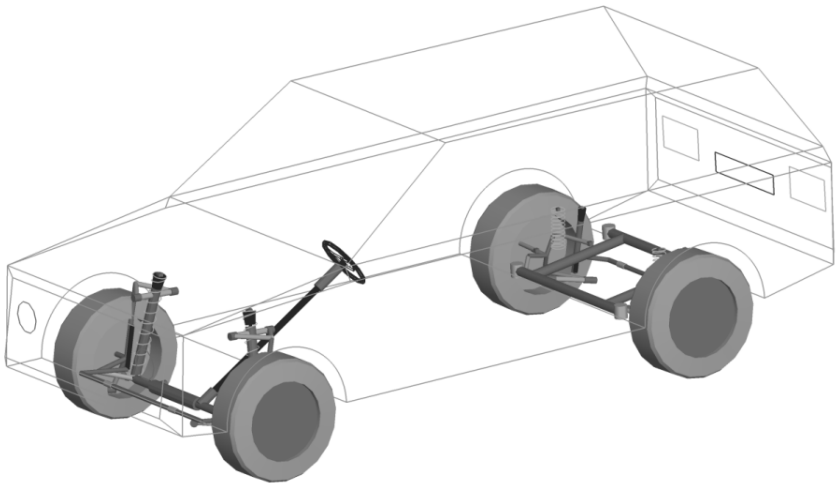

Figure 3.4 Vehicle image

3.2.1. Front suspension

The vehicle uses double wishbone suspension architecture at the front axle (Figure 3.5). The model of the front suspension consists of the following bodies for each side of the vehicle:

- Two lower arm links
- Upper arm
- Damper housing
- Damper rod
- Track rod
- Knuckle
- Wheel
- Wheel help body

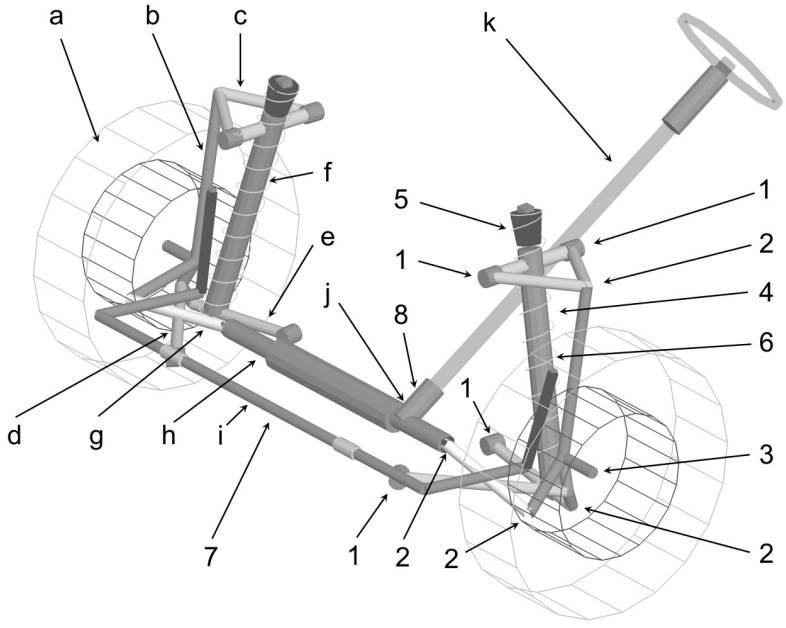

Figure 3.5 Suspension components and source of suspension compliances based on front axle model; a – wheel and tyre, b – upright, c – upper control arm, d – front lower control link, e – rear lower control link, f – damper housing and damper rod, g – track rod, h – rack bar, i – anti-roll bar, j – pinion, k – steering column with steering wheel; 1 – bush, 2 – ball joint, 3 – hub compliance, 4 – spring, 5 – spring aid, 6 – rebound spring, 7 – anti-roll bar, 8 – torsion bar.

All bodies apart from the wheel, wheel help body and damper rod were given 6 DoF. The wheel help body is necessary in the model to implement the hub compliance force element. The wheel help body is connected to the knuckle using a joint with two rotational DoF; around the global x-axis and the z-axis. The wheel is connected to the wheel help body using a revolute joint with a degree of freedom around the y-axis in the local coordinate system. The damper rod is connected to the damper housing using a prismatic joint with a degree of freedom in the z-axis of the local coordinate system along the centreline of the damper rod. Additionally two dummy interface bodies with 0 DoF joint and negligible mass are included in the model in order to be able to connect the suspension substructure with other substructures in the full vehicle model. When using substructures in the main model, the 0 DoF joints from the ground are reconnected to appropriate bodies. The front suspension substructure uses several force elements for each side:

- Bushes
- Ball joints
- Hub compliance
- Spring
- Spring aid
- Rebound spring
- Damper

The road spring force element is acting between the vehicle body and damper housing. The road spring has a linear rate with a specified preload at a nominal length. The damper is acting between the damper rod and damper housing. The damper's force is a non-linear function of velocity. Suspension bushes act between the vehicle body interface and suspension arm, links, or damper rod. All translational and rotational bush stiffnesses and damping coefficients are defined as linear. The suspension ball joints have only linear translational stiffness and damping, and act between the knuckle and other suspension components and also between the damper housing and rear lower link. The spring aid force element acts between the vehicle body and damper housing and enables the suspension to achieve a highly non-linear wheel rate. The non-linear characteristic of the spring aid ensures that force is generated only after initial compression travel of two connected parts. The rebound spring force element acts between the damper rod and damper housing. Its function is to increase the suspension rate in rebound. Similarly to the spring aid the rebound spring force is only generated once displacement between the "From" and "To" markers becomes positive.

The spring aid, bump stop and rebound stop together with the damper provide highly non-linear suspension characteristics for vertical travel of the suspension. This enables the user to model a rising wheel rate with bump or rebound travel of the suspension which contributes to jacking effects. The non-linear damper characteristic ensures asymmetric characteristics for bump and rebound velocities which allow for accurate modelling of the transient response of the vehicle to the steering input. The kinematic tree together with location of force elements is given in Figure 3.6.

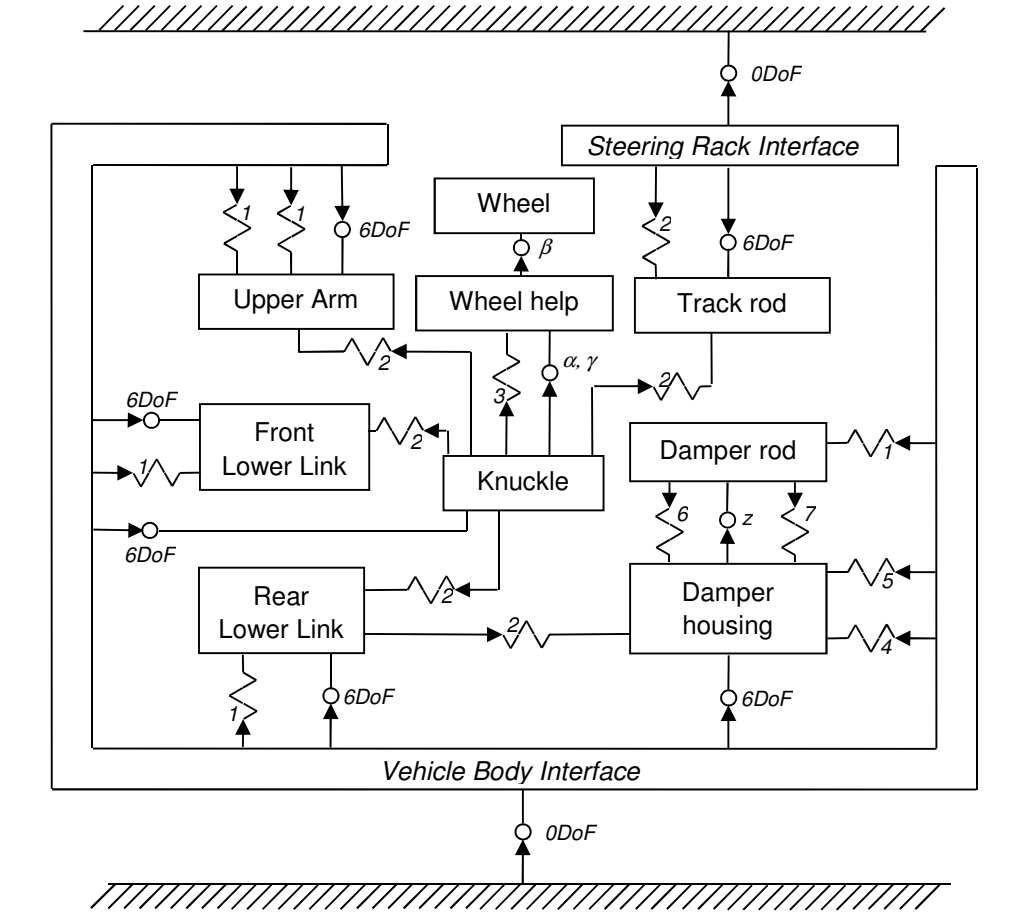

Figure 3.6 Front suspension force elements; 1 – bush, 2 – ball joint, 3 – hub compliance, 4 – spring, 5 – spring aid, 6 – rebound spring, 7 – damper.

3.2.2. Rear suspension

The vehicle uses multi-link suspension architecture attached to an isolated subframe at the rear axle (Figure 3.7). The model of the rear suspension consists of the following bodies for each side of the vehicle:

- Three links
- Lower arm
- Damper housing
- Damper rod
- Knuckle
- Wheel
- Wheel help body

The above bodies are complemented by a single subframe body.

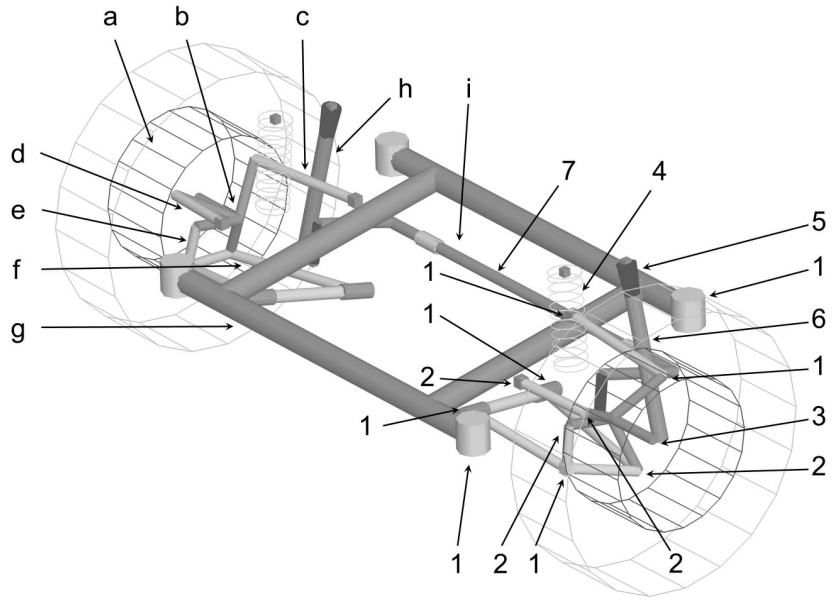

Figure 3.7 Suspension components and source of rear suspension compliances; a – wheel, b – upright, c – upper lateral link, d – front lateral link, e – front vertical link, f – lower control arm, g – subframe, h – damper housing and damper rod, i – anti-roll bar; 1 – bush, 2 – ball joint, 3 – hub compliance, 4 – spring, 5 – spring aid, 6 – rebound spring, 7 – anti-roll bar.

All bodies apart from the wheel, wheel help body and damper bodies were given 6 DoF. The function of the wheel help body is identical to the same body in the front suspension. Similarly the kinematic connection of the wheel, wheel help body and damper rod is as described in the front suspension. The rear suspension contains only one dummy interface body with a 0 DoF joint and negligible mass. It ensures that the suspension substructure can be connected to the vehicle body

when loaded into the full vehicle model. The rear suspension substructure uses several force elements for each side:

- Bushes
- Ball joints
- Hub compliance
- Spring
- Spring aid
- Damper
- Subframe mounts

The road spring force element acts between the vehicle body and the knuckle. The road spring has a linear rate with a specified preload at nominal length. The damper acts between the damper rod and damper housing. The damper's force is a non-linear function of velocity. Suspension bushes act between the subframe and lower arm and upper link, between the integral link and lower arm, between the upper link and knuckle, and between the vehicle body interface and damper rod. All translational and rotational bush stiffnesses and damping coefficients are defined as linear. The suspension ball joints have only linear translational stiffness and damping and act between the knuckle and the remaining suspension components, and also between the lower link and subframe. Subframe mounts act between the subframe and vehicle body interface. The spring aid force element acts between the vehicle body and damper housing and enables the suspension to achieve a non-linear wheel rate in bump. The non-linear characteristic of the spring aid ensures that force is generated only after initial compression travel of two connected parts. The rebound spring force elements act between the damper rod and damper housing. Their function is to increase the suspension rate in rebound. Similarly to the spring aid, the rebound spring force is only generated once the displacement between "From" and "To" markers becomes positive. The kinematic tree together with location of force elements is given in Figure 3.8.

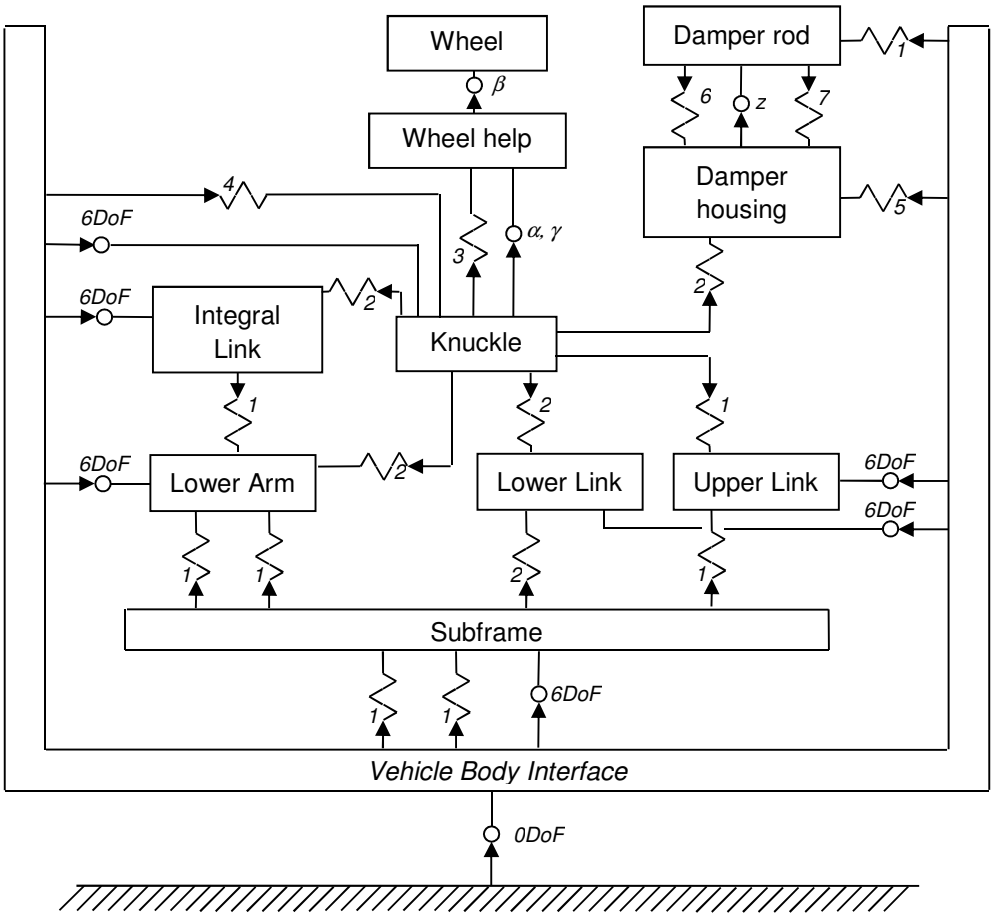

Figure 3.8 Rear suspension force elements; 1 – bush, 2 – ball joint, 3 – hub compliance, 4 – spring, 5 – spring aid, 6 – rebound spring, 7 – damper, 8 – subframe mount

3.2.3. Steering system

The vehicle model uses a simplified steering model. The steering column does not include any universal joints, so their effect on steering ratio linearity has not been captured. The steering system consists of the following bodies:

- steering wheel with upper column
- rack

The steering rack housing is not modelled as a separate body and is incorporated into a massless vehicle body interface. The steering rack has one translational degree of freedom with respect to the vehicle body interface. The steering wheel with upper column has one rotational degree of

freedom with respect to the vehicle body interface. The rotation of the steering wheel is linked with translation of the steering rack through a compliant rack and pinion force element with a specified ratio. The kinematic tree together with location of force elements is given in Figure 3.9. Depending on the type of simulation required, steering should operate in an open or closed loop. Therefore two derivatives of the steering system were developed. The first one uses an explicitly defined steering angle as a function of time to impose the rotation of the steering wheel joint. To account for this the steering wheel joint has been changed from revolute with 1 DoF to a rheonomic joint with no degrees of freedom. The second derivative uses a simple PID steering controller to decide on the steering wheel angle. The controller follows the road by reducing lateral path deviation at the front axle by controlling the steering wheel angle. The controller's transfer function is given below:

$$F_{st}(s) = \frac{SWA(s)}{dy(s)} = h_{st} \cdot \frac{Kp_{st} + \frac{Kp_{st}}{Ti_{st} \cdot s} + Kp_{st} \cdot Td_{st} \cdot s}{s \cdot \left((1 + T1_{st} \cdot s) \cdot (1 + T2_{st} \cdot s)\right)} \tag{3.23}$$

where:

SWA – steering wheel angle [rad]

dy – lateral track deviation [m]

As in the case of the driveline controller, the gains have been kept at default levels as the controller response proved to be adequate. Gains are given below:

$Kp_{st} = 0.01 \cdot steering\_ratio = 1.0740487705$ – proportional gain

$Ti_{st} = 5$ – integration constant

$Td_{st} = 1$ – derivative constant

$T1_{st} = 0.125$ – time delay constant 1

$T2_{st} = 0.1$ – time delay constant 2

$h_{st} = 1$ – output scaling factor

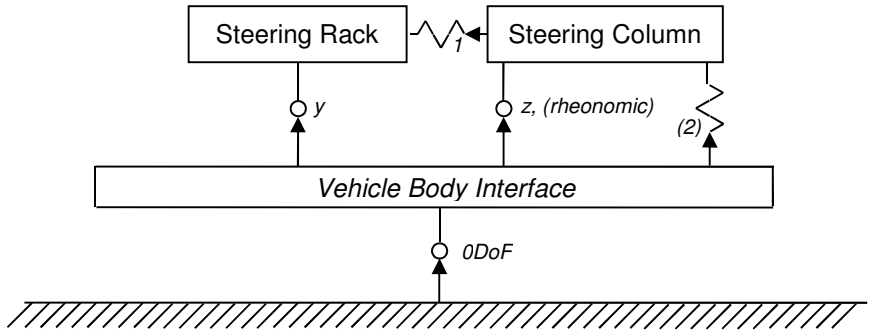

Figure 3.9 Steering system topology; 1 – compliance rack and pinion force element, 2 – optional control system with actuator

3.2.4. Anti-roll bars

The anti-roll bar (ARB) model consists of two rigid bodies representing the left and right hand sides of the anti-roll bar. Both rigid bodies are connected to the vehicle interface body with revolute joints. The stiffness of the anti-roll bar is represented by a rotational force element acting between the left and right parts of the anti-roll bar. Drop links are modelled using massless, constant distance algebraic constraints. The topology of the anti-roll bar system is presented in Figure 3.10. Suspension interfaces from the anti-roll bar substructure are in the full vehicle model connected to knuckles if the anti-roll bar is used on the front, and the lower arm if it is used at the rear.

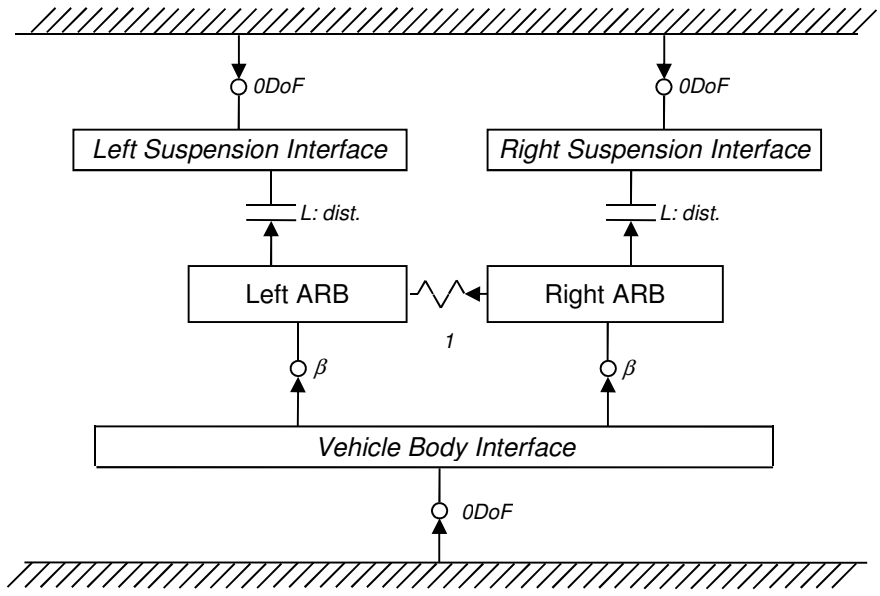

Figure 3.10 Topology of anti-roll bar model; 1 – torsional stiffness of ARB

3.2.5. Driveline

Sometimes it is necessary to apply driving or braking torque to the wheels during a simulation. To account for this requirement a driveline substructure was developed. The substructure consists of 6 interface bodies with negligible mass which are necessary to connect the driveline substructure to bodies from other substructures. The interface bodies are:

- front left and right wheels
- rear left and right wheels
- front torque reaction body
- rear torque reaction body

The schematic of driveline model is shown in Figure 3.11. The driving and braking actuators apply torques between the wheels and the respective torque reaction body. For example at the rear of the vehicle model, torque applied to the wheels is reacted by the torque reaction body connected rigidly to the subframe. This closely resembles a configuration in which the differential is mounted on the rear subframe. The torque necessary to achieve a given velocity profile is calculated by a PID controller. The controller's transfer function is given below:

$$F_{dr}(s) = \frac{Md(s)}{dv(s)} = h_{dr} \cdot \frac{Kp_{dr} + \frac{Kp_{dr}}{Ti_{dr} \cdot s} + Kp_{dr} \cdot Td_{dr} \cdot s}{s \cdot \left((1 + T1_{dr} \cdot s) \cdot (1 + T2_{dr} \cdot s)\right)} \qquad \textbf{(3.24)}$$

where:

Md – driving torque at each wheel [Nm]

dv – velocity derivation [m/s]

The controller gains have been kept at default levels as the controller response proved to be adequate. Gains are given below:

$Kp_{dr} = 75$ – proportional gain

$Ti_{dr} = 500$ – integration constant

$Td_{dr} = 3$ – derivative constant

$T1_{dr} = 0.15$ – time delay constant 1

$T2_{dr} = 0.1$ – time delay constant 2

$h_{dr} = 1$ – output scaling factor

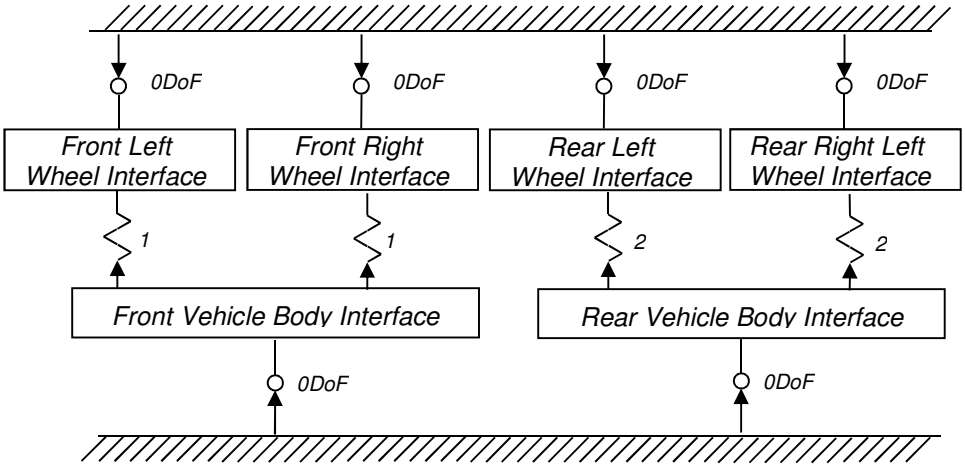

Figure 3.11 Topology of driveline model; 1 – front wheel rotational actuator, 2 – rear wheel rotational actuator

3.2.6. Tyres

The tyre substructure contains 5 interface bodies with negligible mass: 4 interface bodies to the wheels, and one to the main model track joint. The tyre force elements act between the road and the centre of each wheel. More detailed information about the tyre models is provided in the second part of this chapter.

3.2.7. Vehicle body

The vehicle body substructure contains only one body which represents the mass and inertia of the vehicle body, powertrain, occupants and all other systems which are not modelled as separate substructures.

3.2.8. Model validation

For correlation purposes a kinematic and compliance (K&C) test rig was set up in SIMPACK. The test rig consists of a platform and four posts, one at each corner of the vehicle. The platform which connects with 0 DoF to the vehicle body is able to impose vertical, roll and pitch displacement to the vehicle body. All four tyres are meanwhile supported by wheel pads on top of the posts. The posts allow the contact patch to slide freely in the horizontal plane. Additionally, the Knuckle Interface body contains a congruent marker which follows the contact patch maker on the Post Contact Patch body and allows the application of forces directly to the knuckle at the true contact patch. The main modelling difficulty comes from modelling the projection of the contact patch onto the ground plane. The topology of the K&C test rig set up in SIMPACK is shown in Figure 3.12 and explains how the projected contact patch is automatically calculated.

The K&C rig can perform three different virtual tests:

- Vertical
- Lateral Compliance
- Roll

During the vertical test simulation, the optional Platform Pitch and Platform Bounce joint degrees of freedom are removed, and the rheonomic joint of the Platform Bounce Driven body is given a vertical displacement as a function of time. The rheonomic joint of the Platform Roll Driven body is kept inactive. During the simulation of vertical test the vehicle body moves up and down whereas the wheels are resting on fixed Posts. During the simulation of lateral compliance test, the vertical rheonomic joint is deactivated and the remaining kinematics kept unchanged from the vertical simulation. Therefore the vehicle body remains fixed to the platform. The lateral forces are then applied at the contact patch in a twofold manner; in-phase where all forces are acting on the contact patches in same direction, or out-of-phase where left and right hand forces are acting in opposite directions.

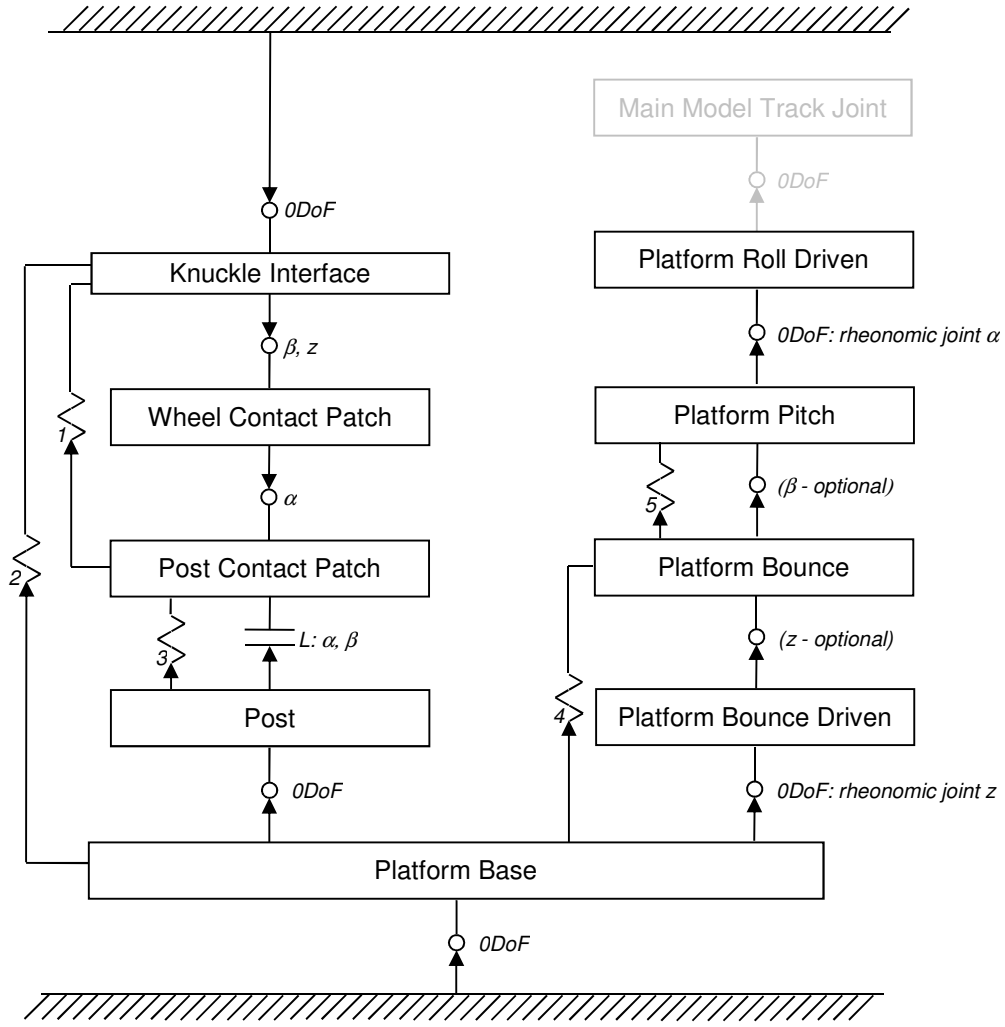

Figure 3.12 Topology of K&C test rig (for simplicity only one post included in the figure); 1 – tyre vertical and overturning stiffness, 2 – lateral force actuator, 3 – stiff, unilateral spring, 4 – optional bounce actuator for closed loop control, 5 – optional pitch actuator for closed loop control.

The roll test is the most complex with regard to the test rig setup. The rheonomic joint of the Platform Roll Driven body is given a roll angle as a function of time, and the optional Platform Bounce and Platform Pitch joints are given their degrees of freedom, respectively z and β. The rheonomic joint of the Platform Bounce Driven body is kept inactive. During the test the vertical forces at all four contact patches are measured and fed back to the closed loop controller which ensures that the fore-aft weight distribution remains constant during the test. To achieve this, the PID controller applies vertical force and pitch torque using two actuators as shown in Figure 3.12. The graphical representation of the vehicle model on the kinematic and compliance test rig is shown in Figure 3.13.

The model parameterisation was based on two main sources of parameters. Some of these parameters involved direct measurement, or prior knowledge. Other parameters were derived from the correlation of a kinematics and compliance test performed on a real vehicle. The physical test data was supplied by Jaguar Land Rover. The vehicle model has been correlated to kinematic and compliance measurements of a real vehicle for the following simulations:

- kinematics – vehicle motion in pure vertical direction
- lateral compliance – lateral forces applied at the contact patch, two separate ~~tests~~ simulations performed for side forces acting in the same or opposite directions
- roll test – vehicle roll motion

For all the above simulations, the measured signals include contact patch forces, position and orientation of the wheel centre, position of wheel pad with respect to the body.

The vehicle body and wheel pads were driven during the simulation by the signals acquired from physical measurements. The model's forces at the contact patch as well as the position and orientation of the wheel centres were therefore the result of suspension geometry, spring and spring aids stiffness, anti-roll bar stiffness and bush compliances. Virtual measurement signals were exported from the model and compared to the corresponding data from the physical test. The discrepancies between the model and physical results were corrected by methodically adjusting the suspension parameters. The process consisted of the following comparisons between data from the model and the physical test:

- compare results from kinematic simulation and if necessary make small changes to the suspension geometry as well as spring, spring aid and rebound stop characteristics
- compare results from lateral compliance simulation with forces acting in the opposite direction and adjust suspension bush compliances
- compare results from lateral compliance simulation with forces acting in the same direction and adjust steering system compliance and rear subframe compliances
- compare results from roll simulation and adjust anti-roll bar stiffnesses

To achieve good correlation several cycles were needed. Examples of the resulting model correlation are show in Figure 3.14 to Figure 3.25. For the purpose of concealing sensitive information the figures present normalised measurements.

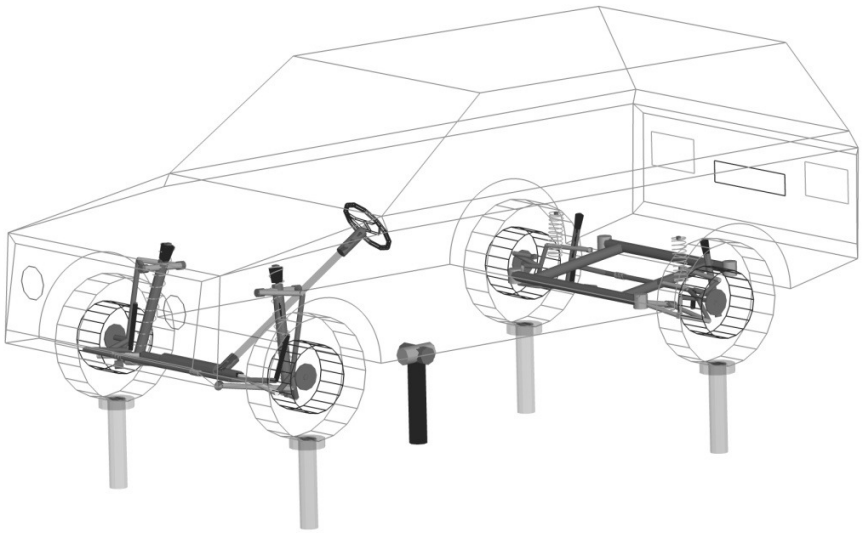

Figure 3.13 Vehicle model on kinematic and compliance test rig in SIMPACK.

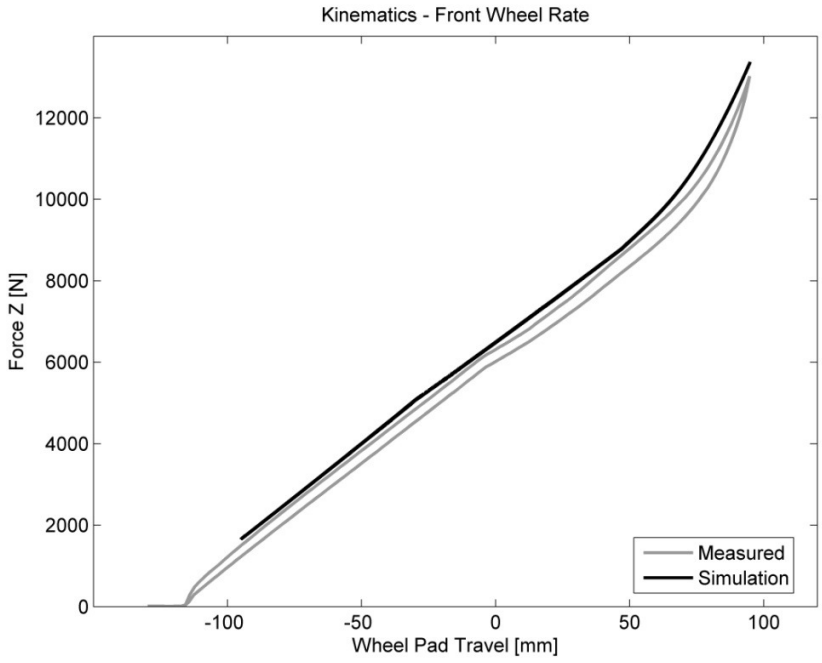

Figure 3.14 Example of model correlation – front wheel rate.

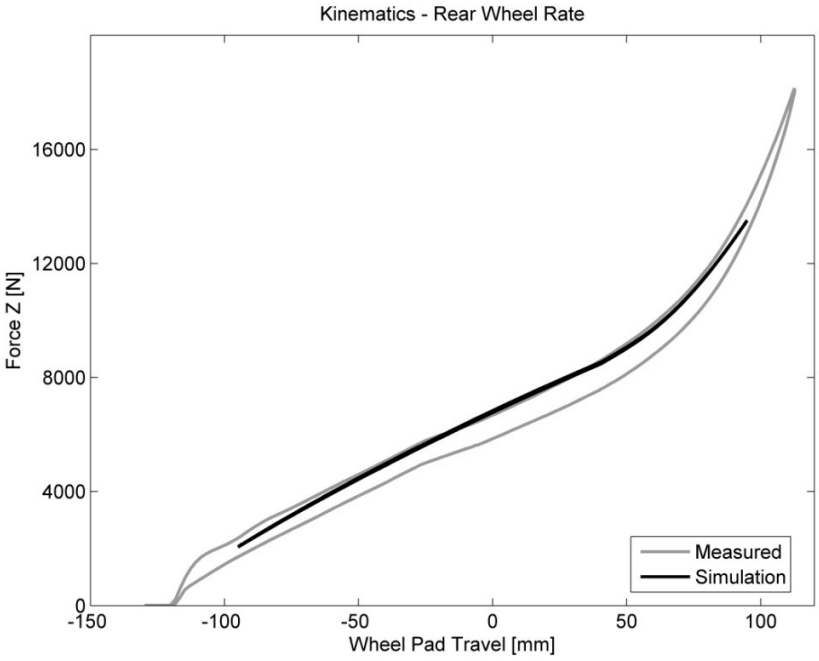

Figure 3.15 Example of model correlation – rear wheel rate.

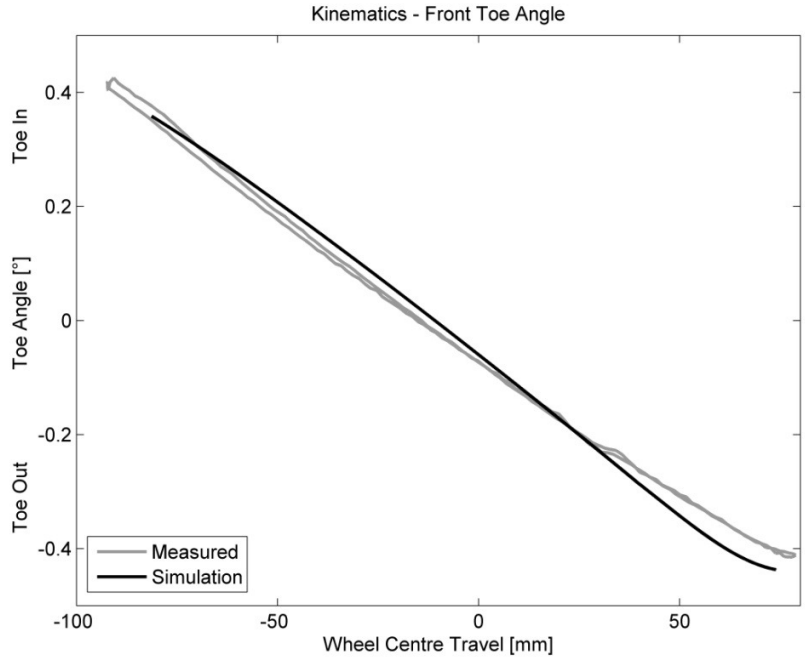

Figure 3.16 Example of model correlation – front toe kinematics.

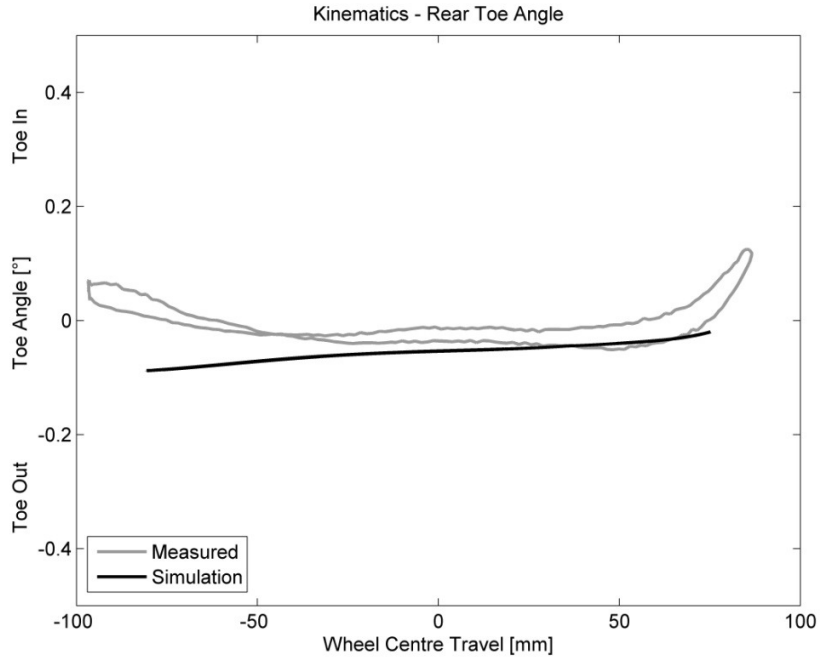

Figure 3.17 Example of model correlation – rear toe kinematics.

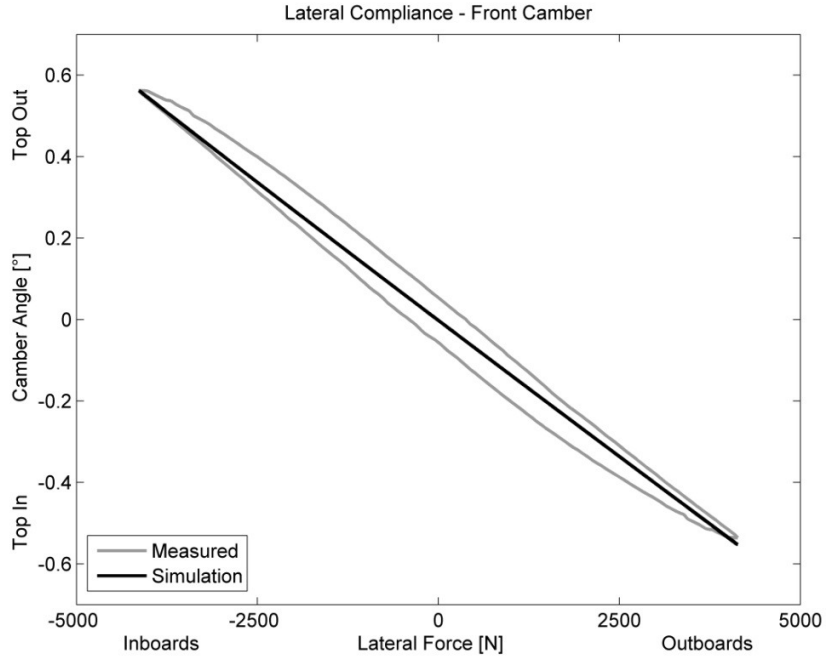

Figure 3.18 Example of model correlation – front camber compliance.

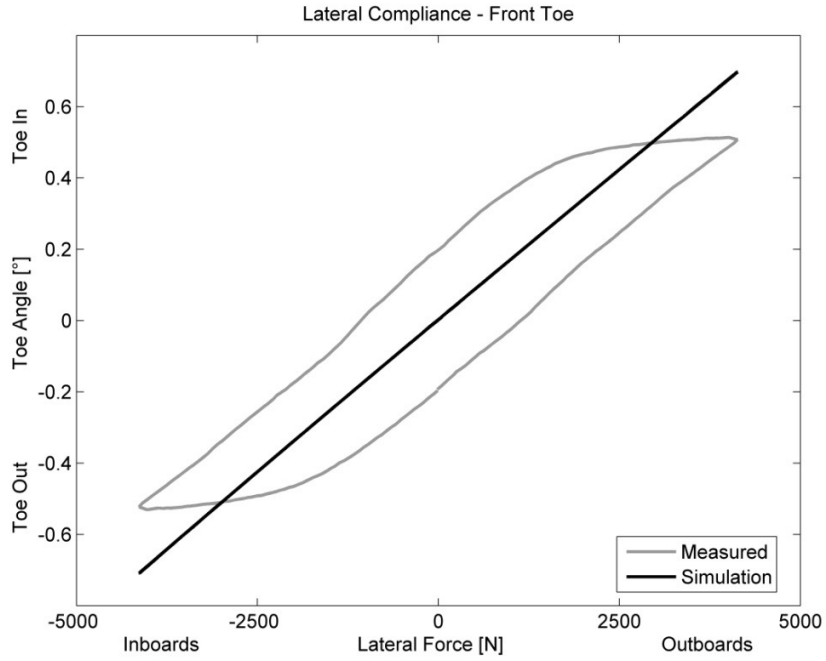

Figure 3.19 Example of model correlation – front toe compliance.

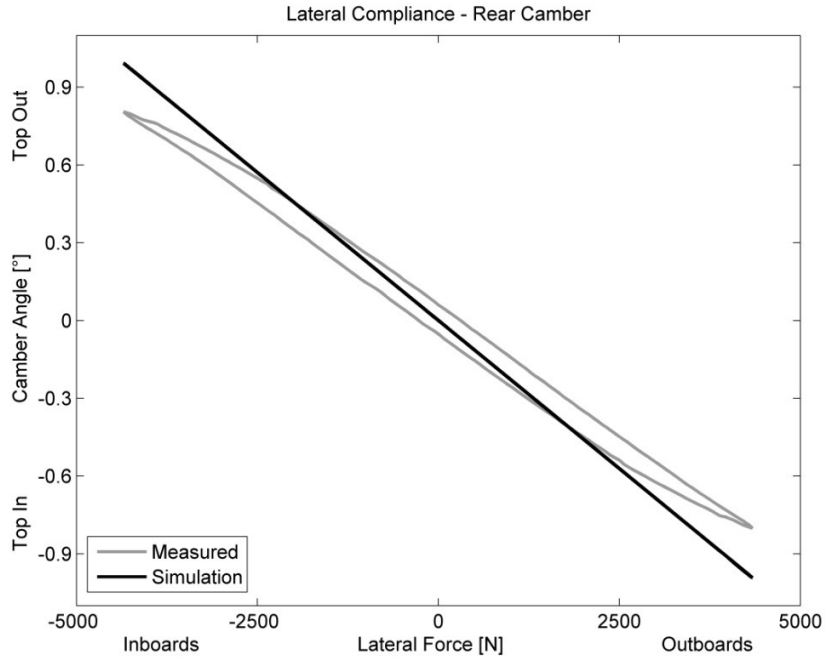

Figure 3.20 Example of model correlation – rear camber compliance.

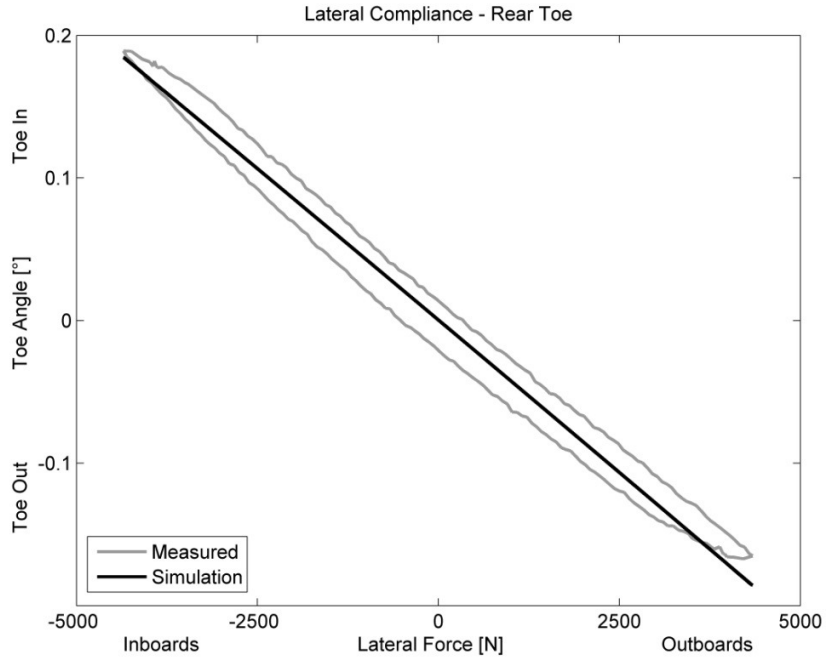

Figure 3.21 Example of model correlation – rear toe compliance.

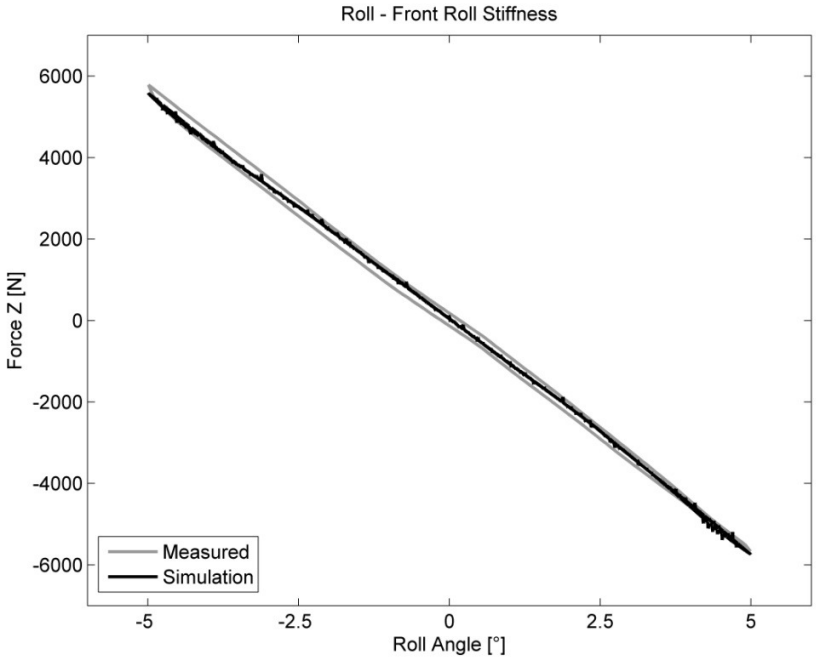

Figure 3.22 Example of model correlation – front roll stiffness.

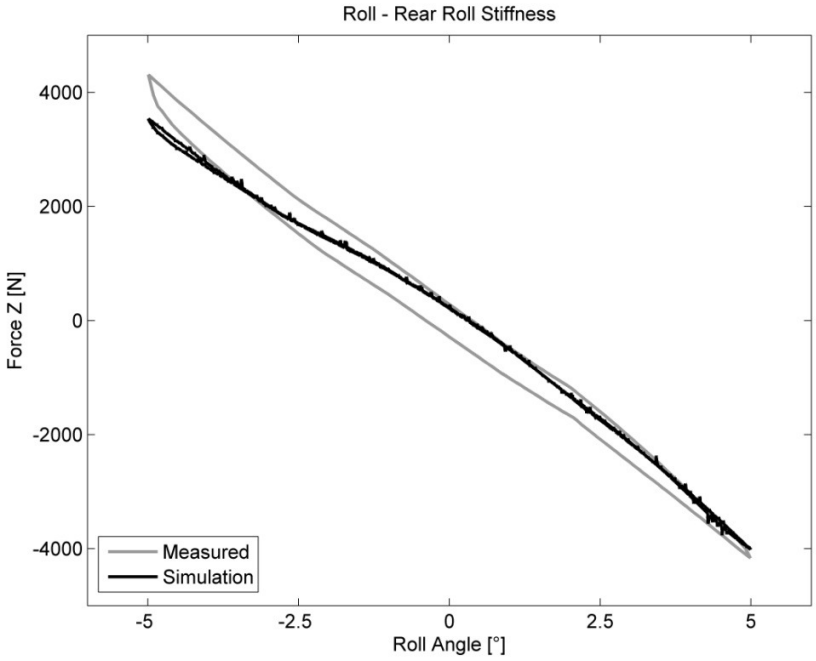

Figure 3.23 Example of model correlation – rear roll stiffness.

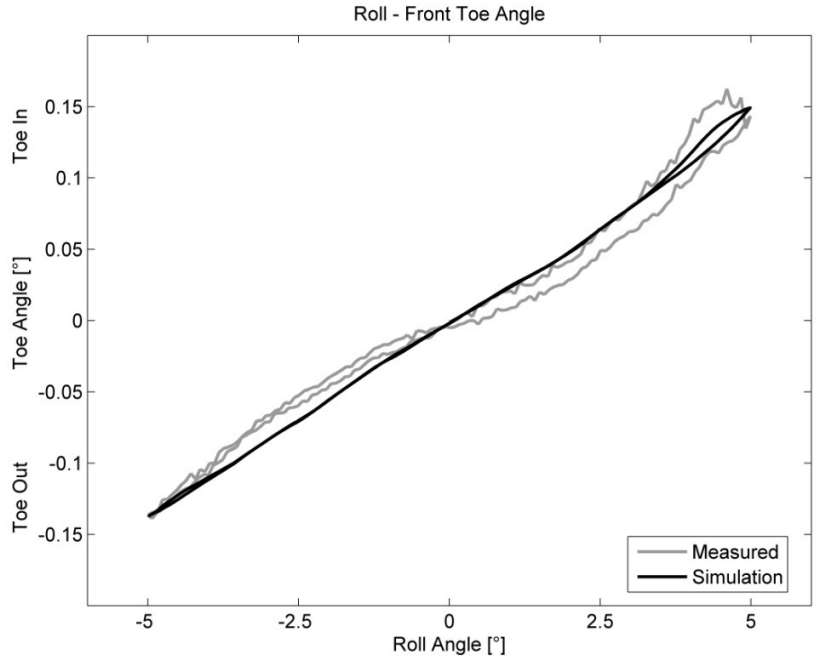

Figure 3.24 Example of model correlation – front roll steer.

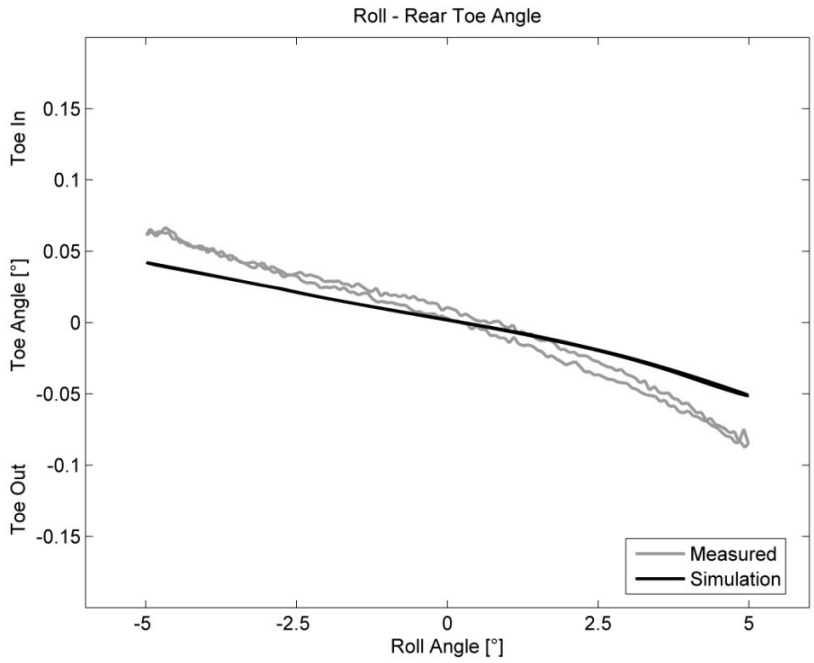

Figure 3.25 Example of model correlation – rear roll steer.

As can be seen, the vehicle model matches real life measurements well. This was achieved by making relatively small changes to the initial suspension geometry and the bush compliances.

3.3. Tyre modelling

There exist a large number of available tyre models and variations of them. In order to present an overview of tyre models in an organised manner a systematic classification is necessary. One method of classifying tyre models is to group them according to the modelling approach used [79]:

- Simple tyre models – The formulation of these types of tyre models usually accounts only for the linear relationship between force and slip. These models do not take into account combined slip conditions. They also do not include any belt dynamics. Due to their simplicity and low computational effort simple tyre models find their application in basic vehicle handling, in control algorithm development and hardware in the loop simulation
- Approximation tyre models – The mathematical formulation of these tyre models is designed to approximate the behaviour of a measured tyre. To achieve good accuracy these models are able to capture the non-linear tyre force characteristics. They usually take into

account combined slip, and are sometimes combined with rigid ring dynamics. The main application of approximation tyre models is handling analysis and low frequency ride analysis.

- Physical or semi-physical models – The formulation of these tyre models is based on the physical model of thread, belt or side walls. These tyre models can accurately describe the kinematic and dynamic behaviour of rubber in the contact patch. An example of such a tyre model is the brush model. The main application area is static and dynamic vehicle handling, ride including secondary ride, durability loads, and prediction of noise vibration and harshness

- Finite-element (FE) tyre models – These are highly detailed FE models of the entire tyre. Thanks to the physical nature of the model they can be used to directly study the effects of physical tyre properties and therefore assist tyre development. The high level of complexity brings high computational effort compared to other tyre models. The main application areas are abuse investigations and high frequency noise analysis

The typical tyre model interface with the MBS has been described by Eichberger et al. [79]. The input information to the tyre model consists of the kinematics of the wheel centre with respect to the inertial frame of reference, and if the tyre model contains internal states, MBS also returns these to the tyre model. On the output from the tyre model, the MBS program receives forces and moments acting between the rim and the road. If the tyre model has internal states, time derivatives of these states are also returned. Due to the large number of tyre models and MBS codes available, a Standard Tyre Interface has been developed to provide a common platform between tyre models and MBS software.

Based on the literature review the most popular type of tyre model in vehicle handling and rollover simulation is the approximation tyre model represented by different dialects of Magic Formula [58]. As noted by Rauh et al. [80] approximation formula tyre models are good for interpolation of measured tyre properties. However extrapolation should be treated with special care as it can lead to unexpected tyre behaviour. Rauh et al. [80] gave examples of incorrect tyre extrapolations including incorrect behaviour under high load and slip angles, a condition which often occurs during rollover simulation. Additionally due to issues arising from coordinate system definitions, slip definitions, and a variety of existing dialects of Magic Formula, it is important that the tyre model is tested in the MBS code to find its limitations and check for potential errors. The authors developed tyre fingerprint diagrams to capture inconsistent behaviour of tyre models. A good starting point for developing the virtual tyre test rig and associated diagrams has been described by Lugner et al. [81], who developed a set of tests for tyre model characterisation called the Tyre

Model Performance Test (TMPT). The test generates a set of predefined characteristics in two major simulation application areas; handling, and high frequency range tests. The set of tests presented in the paper included:

- parking efforts
- cornering
- μ step changes
- combined slip steady-state conditions
- brake cycle with ABS brake
- sinusoidal steering sweep frequency
- cleat tests

The Magic Formula tyre model was chosen to perform the rollover studies in this research. Despite the many shortcomings of this model, the following aspects led to this choice:

- clear and "open source" formulation
- ease of modification
- availability of tyre data
- author's experience in using this type of tyre model in previous work

A detailed description of MF tyre formulation can be found in [58]. However the basic concepts of this tyre model are reproduced in this section. The beginnings of MF tyre can be traced to the cooperative research between TU-Delft and Volvo which resulted in a paper published in 1987 [82]. The model is capable of describing the tyre characteristics using an empirically derived mathematical formulation. The general form of the formula is as follows:

$$y = D \cdot \sin\left[C \cdot \arctan\left\{B \cdot x - E \cdot \left(B \cdot x - \arctan\left(B \cdot x\right)\right)\right\}\right] \quad \textbf{(3.25)}$$

with:

$$Y(X) = y(x) + S_V \quad \textbf{(3.26)}$$

and

$$x = X + S_H \quad \textbf{(3.27)}$$

where: Y - output variable (e.g. F_x, F_y, M_z), X - input variable (e.g. $\tan\alpha$, κ)

and: α - slip angle, κ - longitudinal slip, B - stiffness factor, C - shape factor, D - peak value, E - curvature factor, S_H - horizontal shift, S_V - vertical shift

The function $y(x)$ generates a curve which resembles typical force vs. slip tyre characteristics in that it passes through the origin, reaches maximum value and finally tends to a horizontal asymptote. To allow for tyre asymmetries due to conicity and ply steer, vertical and horizontal shifts are applied. Over the years the formulation has been developed to create a more accurate fit to the tyre measurements; however the basics of this still resemble the equation (3.25) quoted above. A detailed description of the formulation can be found in [58].

As mentioned in the literature review the MF tyre may lose accuracy at high camber angles as experienced during rollover. The formulation presented by Takahashi et al. [60] improves this by accounting for lateral shift of the contact patch. However due to a lack of tyre data measured at these extreme camber angles it is impossible to apply this MF extension in this research. Therefore the existing MF 6.1 tyre model is employed with extra care. To ensure that the tyre is not generating unexpected forces at large camber angles, the model is tested on the TMPT type testrig [81, 83]. The testrig model is shown in Figure 3.26.

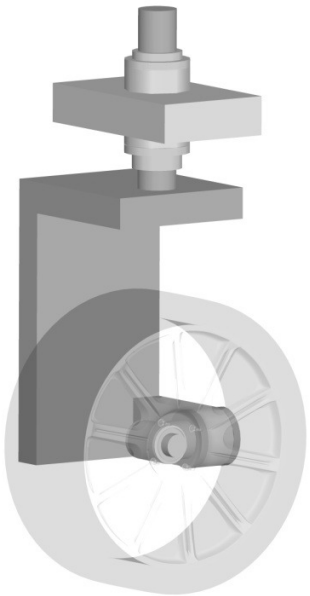

Figure 3.26 Tyre model performance test rig modelled in SIMPACK

A number of quasi-static and dynamic tests were performed on the tyre model using the TMPT rig. The results from these tests are shown in Figure 3.27 to Figure 3.35.

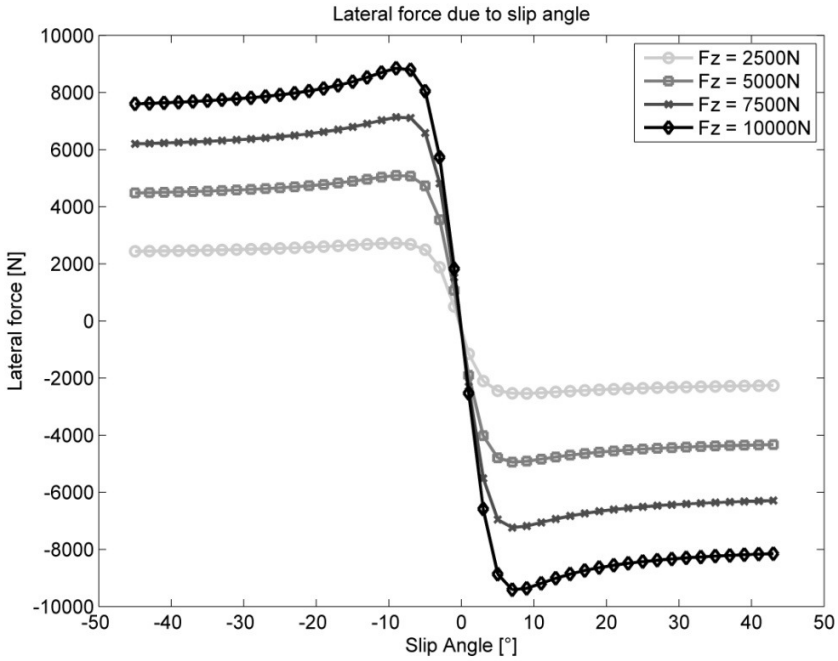

Figure 3.27 Lateral force characteristics due to lateral slip

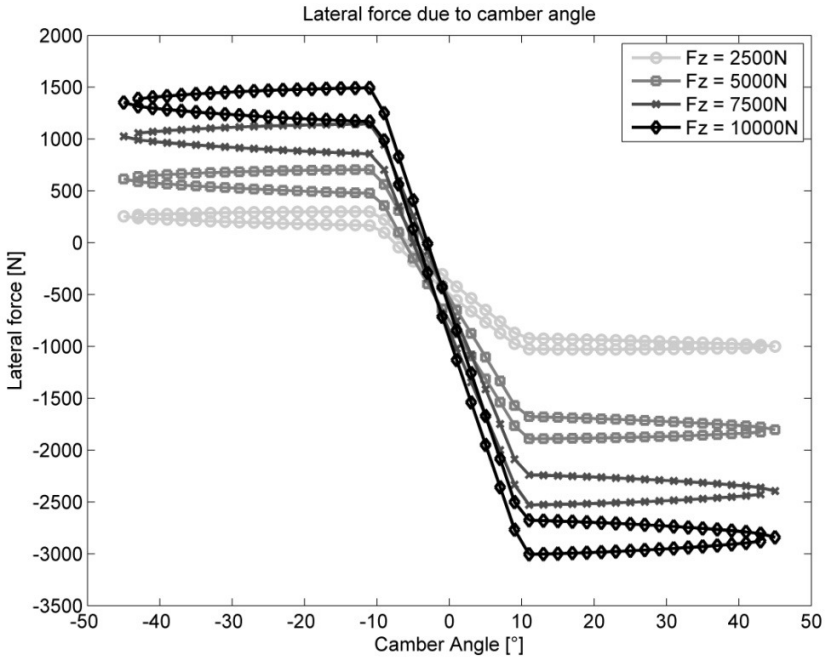

Figure 3.28 Lateral force characteristics due to camber angle

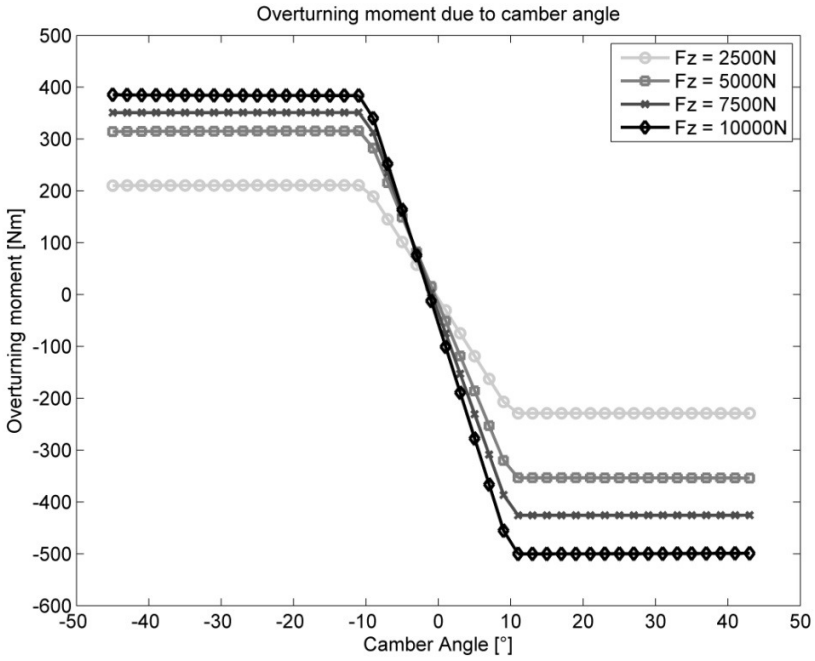

Figure 3.29 Overturning moment characteristics due to camber

The overturning moment characteristic has the potential to affect rollover results, therefore this characteristic is discussed in more detail. It can be clearly seen in Figure 3.29 that once a camber angle greater than 10º is achieved, the overturning moment remains constant. Such characteristics indicate that the tyre model has been correlated up to 10º of camber angle and to avoid erroneous extrapolation a limit camber angle has been introduced. As no tyre measurements for camber angles above 10º were available, the tyre extrapolation settings have not been changed for further full vehicle model testing. A simple calculation indicates that a 500Nm of overturning moment at 10000N vertical force is equal to a lateral displacement of the tyre contact patch centre of pressure of 50mm. Bearing in mind that the tyre width is 255mm, a value of 50mm does not seem excessive. Additionally the results from the TMPT show strong asymmetry in terms of camber angle sensitivity. The source of this asymmetry is unknown, however as the results look plausible, the tyre properties are not artificially altered to make this characteristic symmetrical.

Results of overturning moment as a function of slip and camber angle are presented in Figure 3.31. Large positive slip angles and large positive camber angles are typical conditions in rollover manoeuvres on the outer (loaded) tyres. Positive lateral tyre slip reduces the overturning moment due to positive camber angle. It is worth noting that for a given vertical force and camber angle the minimum overturning moment which stabilises the vehicle occurs at slip angles corresponding to

maximum lateral tyre force. Tyre behaviour at camber angles above 10º remains unchanged due to extrapolation settings.

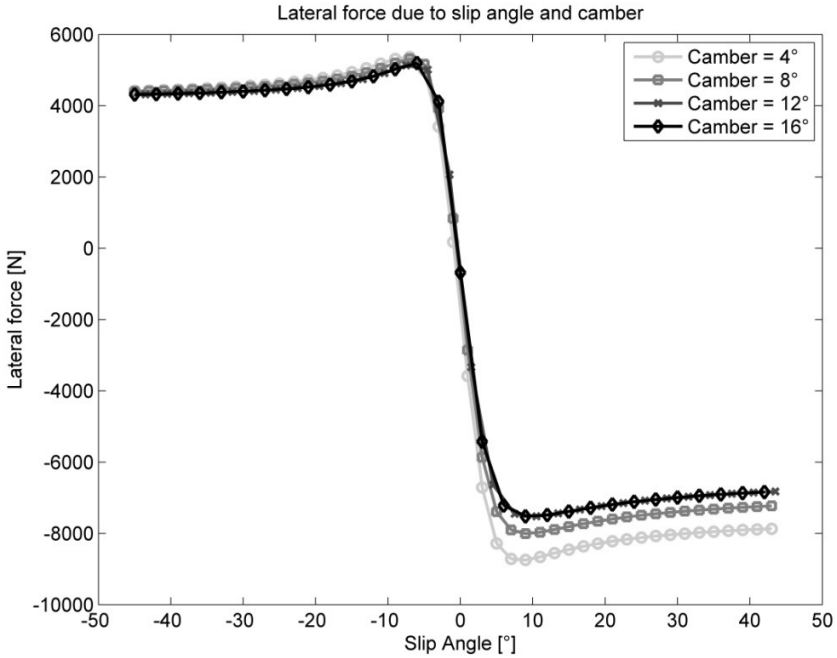

Figure 3.30 Lateral force characteristics due to slip and camber angle for vertical force of 7500N

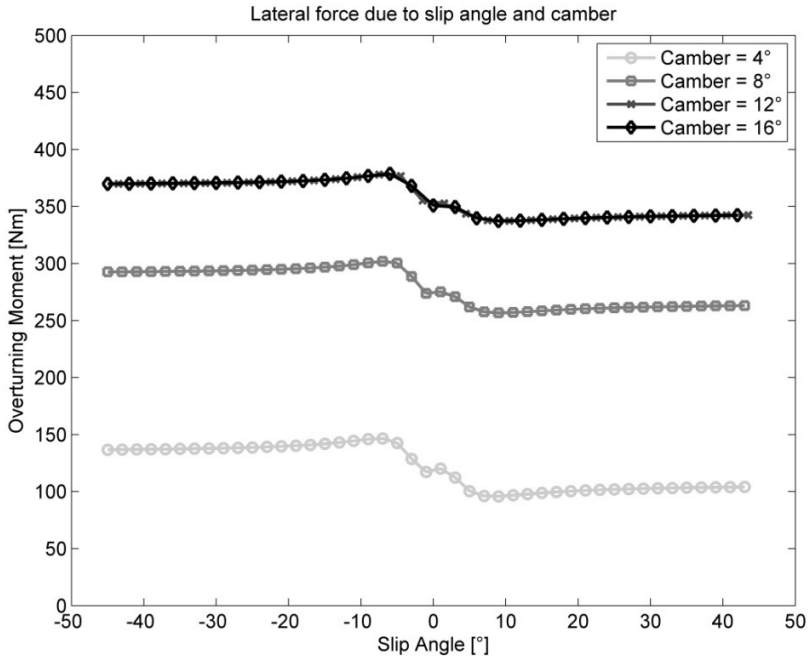

Figure 3.31 Overturning moment characteristics due to slip and camber angle for vertical force of 7500N

Apart from the quasi-static test, a couple of dynamic tests were also performed. Firstly a tyre model was subjected to a steering angle frequency sweep and the lateral force Fy response was measured. In order to keep the tyre operating in the linear region the amplitude of the steering angle was set to 1°. Additionally vertical force was kept constant at 7500N, and vertical forward velocity was set to 1m/s. The result of the test is shown in Figure 3.32. Based on the shape of response magnitude, the tyre lateral relaxation length was found. Low frequency and high frequency asymptotes were plotted and the cross-over frequency was found (Figure 3.33). Based on cross–over frequency, the relaxation length was computed as follows:

$$\sigma = \frac{V}{f \cdot 2 \cdot \pi} \tag{3.28}$$

The results indicate that the cross-over point occurs at 0.2015Hz, hence the relaxation length is 0.7899m. A brief analysis of time history of lateral force and steer angle at very low frequency confirmed this result. Similarly the tyre model lateral force response to 1° camber angle frequency sweep was measured (Figure 3.34). The relaxation length to camber response was also based on cross-over frequency of low and high frequency asymptotes (Figure 3.35). As the cross-over point occurs at 0.1143Hz, the corresponding lateral force relaxation length due to camber is calculated as 1.392m.

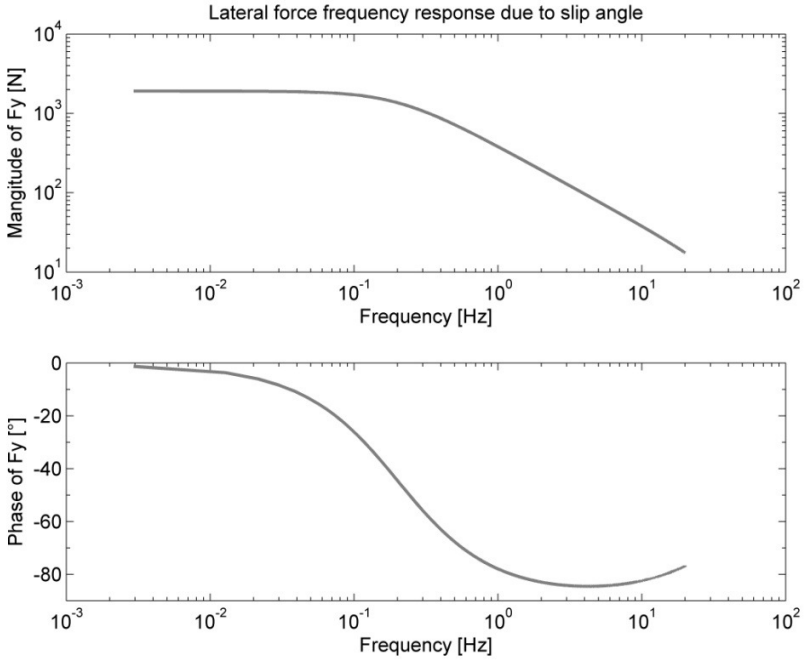

Figure 3.32 Lateral force frequency response due to 1° steer angle

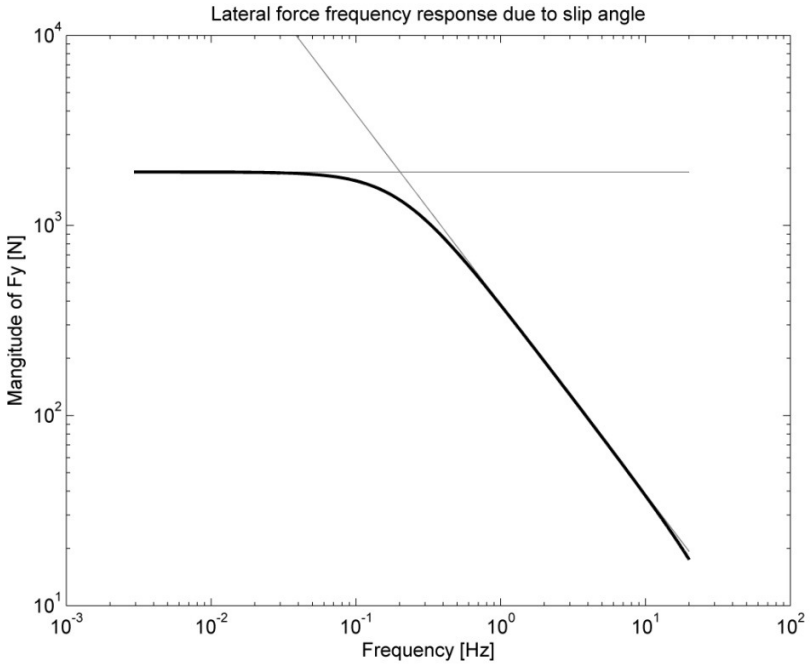

Figure 3.33 Lateral force frequency response due to 1º steer angle – asymptotes indicating relaxation length (see text)

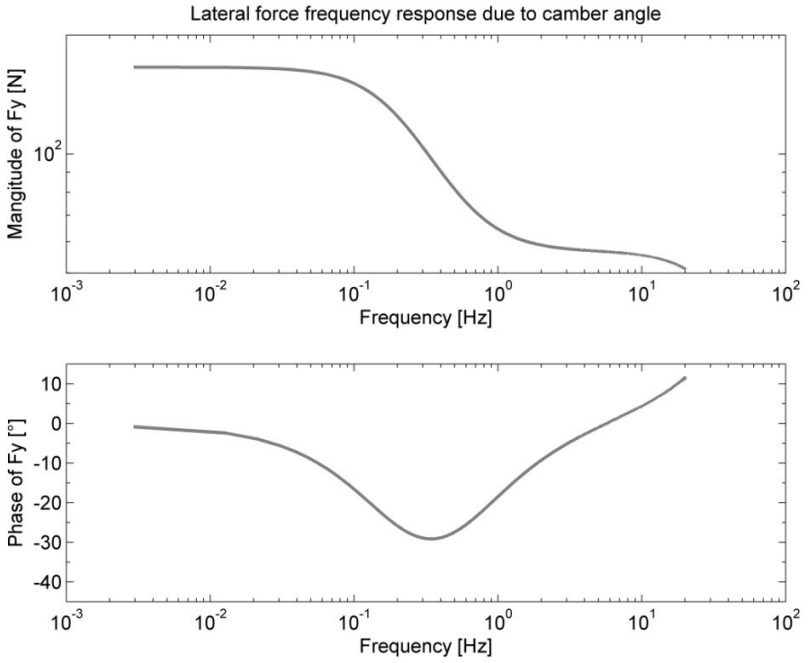

Figure 3.34 Lateral force frequency response due to 1º camber angle

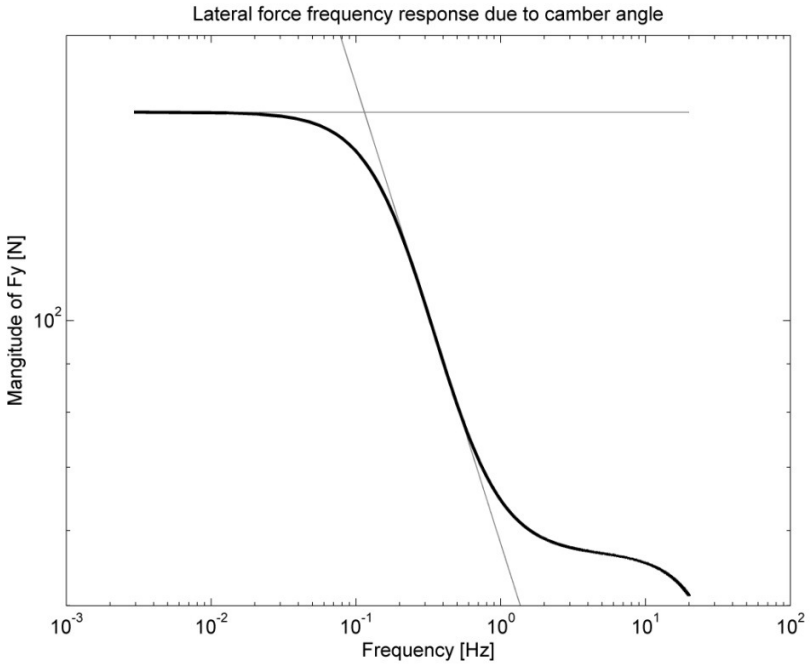

Figure 3.35 Lateral force frequency response due to 1º camber angle – asymptotes indicating relaxation length (see text)

3.4. Vehicle Characterisation

Once the vehicle model had been validated on the K&C rig and the tyre model had been characterised using the TMPT rig, the two could be combined into the full vehicle model. The aim of this section is to characterise this full vehicle model in typical handling manoeuvres on an even surface. However before this could take place a few model improvements had to be implemented. Firstly, the physical vehicle measured on the K&C rig was equipped with airsprings at the rear axle. These are modelled as linear springs. However as the K&C test is performed in a quasi-static manner, the rear airspring's volume changes slowly enough to assume that air inside the airspring is compressed in an isothermal process. However during driving on the road,the airspring thermodynamic processes are closer to being adiabatic. Therefore the spring stiffness derived from the K&C test needs to be appropriately increased.

The following adiabatic indices are assumed:

$\gamma_S = 1$ - adiabatic index for quasi static K&C test – isothermal process

$\gamma_D = 1.38$ - adiabatic index for dynamic road event – near adiabatic process

It is known that:

$$p \cdot V^{\gamma} = const. \tag{3.29}$$

The symbols used in this proof:

A - effective area of an airspring

p - initial airspring pressure

l - initial airspring length

V - initial airspring volume

F - initial airspring force

K_s - airspring static stiffness

K_D - airspring dynamic stiffness

So:

$$p \cdot V^{\gamma} = (p + dp) \cdot (V + dV)^{\gamma} \tag{3.30}$$

Therefore:

$$dp = p \cdot \frac{V^{\gamma}}{(V + dV)^{\gamma}} \tag{3.31}$$

Also:

$$dV = dl \cdot A \tag{3.32}$$

$$F = p \cdot A \tag{3.33}$$

$$K = \frac{dF}{dl} = \frac{dp \cdot A}{dl} = \frac{p \cdot \frac{V^{\gamma}}{(V + dV)^{\gamma}}}{dl} = \frac{p \cdot \left(\frac{V}{V + dl \cdot A}\right)^{\gamma}}{dl} \tag{3.34}$$

So the ratio between the dynamic and static stiffness can be written as:

$$i = \frac{K_D}{K_S} = \frac{p \cdot \left(\frac{V}{V + dl \cdot A}\right)^{\gamma_D}}{dl} \cdot \frac{dl}{p \cdot \left(\frac{V}{V + dl \cdot A}\right)^{\gamma_S}} = \frac{\left(\frac{V}{V + dl \cdot A}\right)^{\gamma_D}}{\left(\frac{V}{V + dl \cdot A}\right)^{\gamma_S}} \tag{3.35}$$

The ratio of both stiffnesses as dl approaches 0 is:

$$\lim_{dl \to 0} i = \lim_{dl \to 0} \frac{K_D}{K_S} = \lim_{dl \to 0} \frac{\left(\frac{V}{V + dl \cdot A}\right)^{\gamma_D}}{\left(\frac{V}{V + dl \cdot A}\right)^{\gamma_S}} \tag{3.36}$$

Using l'Hôpital's rule and remembering that $\gamma_S = 1$ yields:

$$\lim_{dl \to 0} i = \lim_{dl \to 0} \frac{\left(\frac{V}{V + dl \cdot A}\right)^{\gamma_D}}{\left(\frac{V}{V + dl \cdot A}\right)^{\gamma_S}} = \lim_{dl \to 0} \frac{\left[\left(\frac{V}{V + dl \cdot A}\right)^{\gamma_D}\right]'}{\left[\left(\frac{V}{V + dl \cdot A}\right)^{\gamma_S}\right]'} \tag{3.37}$$

$$= \lim_{dl \to 0} \frac{\gamma_D \cdot \left(\frac{V}{V + dl \cdot A}\right)^{\gamma_D - 1}}{\gamma_S \cdot \left(\frac{V}{V + dl \cdot A}\right)^{\gamma_S - 1}} = \frac{\gamma_D \cdot (1)^{\gamma_D - 1}}{1 \cdot (1)^0} = \gamma_D$$

Therefore the increase in airspring stiffness from the value derived from the K&C test to the dynamic value applicable to road manoeuvres is equal to the adiabatic index for dynamic road event $\gamma_D = 1.38$.

The second point requiring attention before performing any road manoeuvres is the setting of the correct ride height. As the physical vehicle is equipped with a self-levelling system, it is able to maintain the same constant steady state ride height for different loading conditions. The same feature had to be replicated in the SIMPACK model. The self-levelling was achieved using a simple controller. The controller's operation is briefly described below. The error between actual and required wheel centre position measured with respect to the body is provided to the controller as an input. The controller calculates the vertical force required to achieve 0 displacement error. The force is applied in the model by an actuator force element acting parallel to the spring. As the controller internal dynamics change the dynamics of the entire system, the preload control is only active between 0.5s and 5.0s of the initial integration time. To ensure effective operation of the ride height controller the vehicle is coasting freely with no steering wheel input during the first 5s of time integration.

Changes to suspension geometry and bush stiffnesses during the study affect not only the suspension kinematics and compliance characteristics but also static camber and toe angles. Therefore a closed loop controller for toe and camber angle is introduced into the model. The difference between the actual and required toe and camber angles of each wheel is measured with

respect to the vehicle body. Based on this error the controller calculates the required changes in the geometry; for the toe angle this is a change in track rod length, for the camber angle this is an orientation of wheel centre marker on the knuckle. Similarly to the ride height controller, the toe and camber control is only active between 0.5s and 5.0s of the initial integration time when the vehicle is coasting on the road with the steering wheel locked in the straight ahead position.

In order to characterise the vehicle dynamic and quasi-steady state handling manoeuvres were performed. Firstly a constant radius simulation with steadily increasing vehicle speed based on [84] was performed. The results of this simulation are shown in Figure 3.36 and Figure 3.37. Based on this simulation the following vehicle characteristics were found:

- understeer gradient
- roll gain

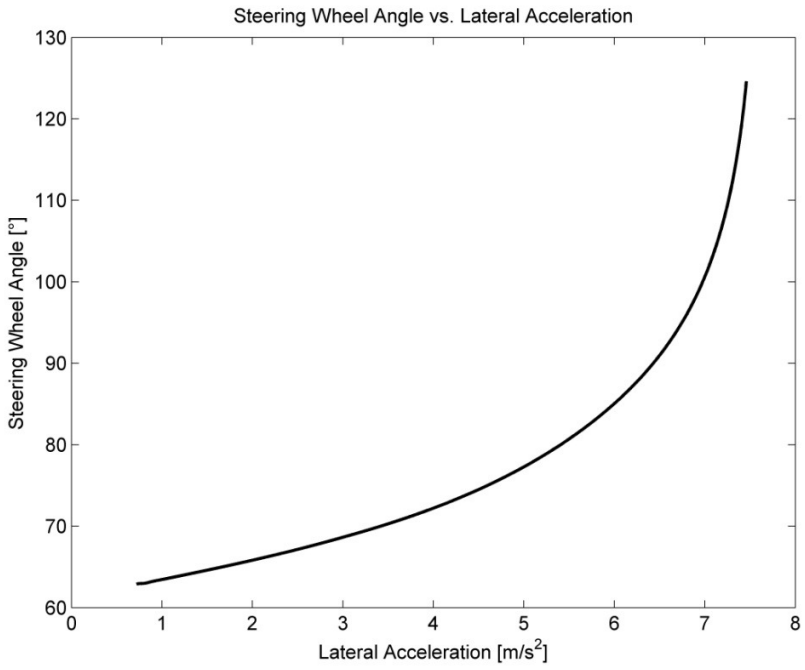

Figure 3.36 Vehicle understeer characteristics

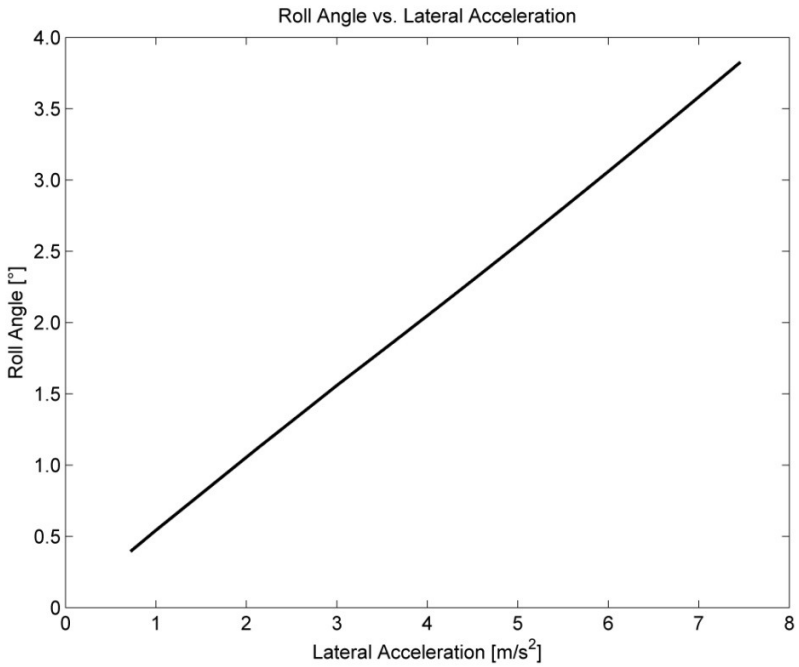

Figure 3.37 Vehicle roll characteristics.

The second simulation consisted of the frequency response to a steering wheel input of fixed amplitude. The results of this simulation are shown in Figure 3.38 to Figure 3.40. Based on this simulation it can be concluded that peak yaw response occurs at 1.1Hz whereas peak roll response occurs in a steady state condition. The transmissibility from steering wheel angle to yaw rate, lateral acceleration and roll rate is shown below.

Finally a step steer manoeuvre was performed; the response of the vehicle to 15°, 45° and 75° step steer input is shown in Figure 3.41, Figure 3.42 and Figure 3.43. It is worth noting that the roll angle overshoot seems to follow the lateral acceleration overshoot.

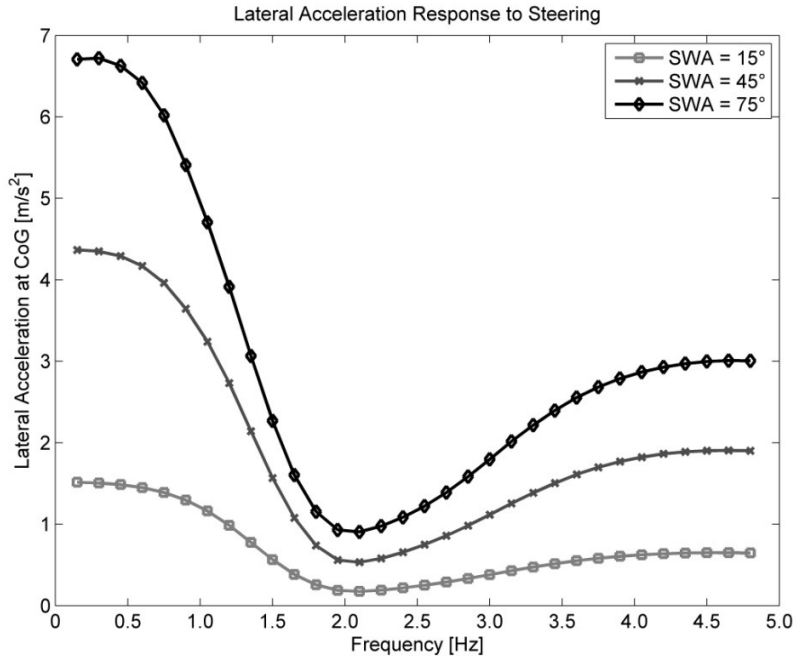

Figure 3.38 Vehicle lateral acceleration as a function of steering input

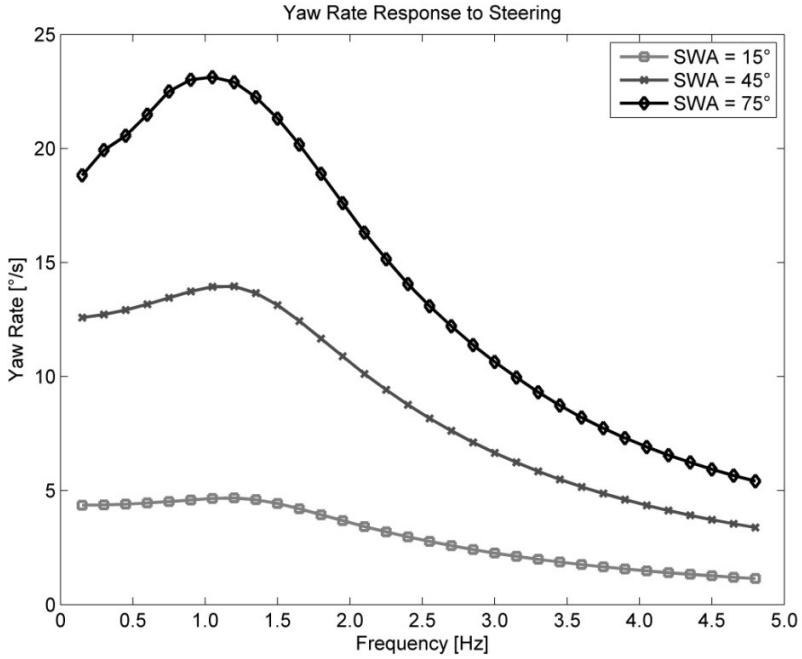

Figure 3.39 Vehicle yaw rate as a function of steering input

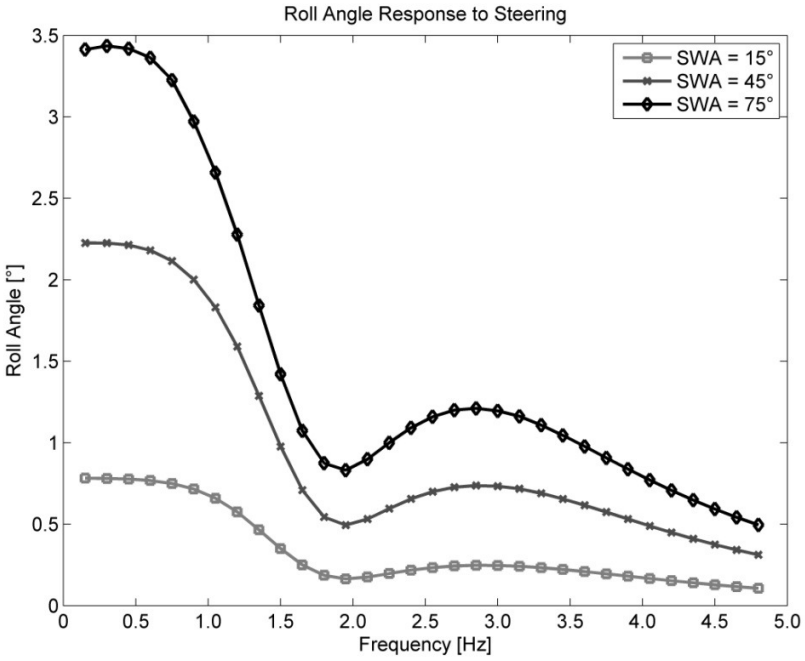

Figure 3.40 Vehicle roll angle as a function of steering input.

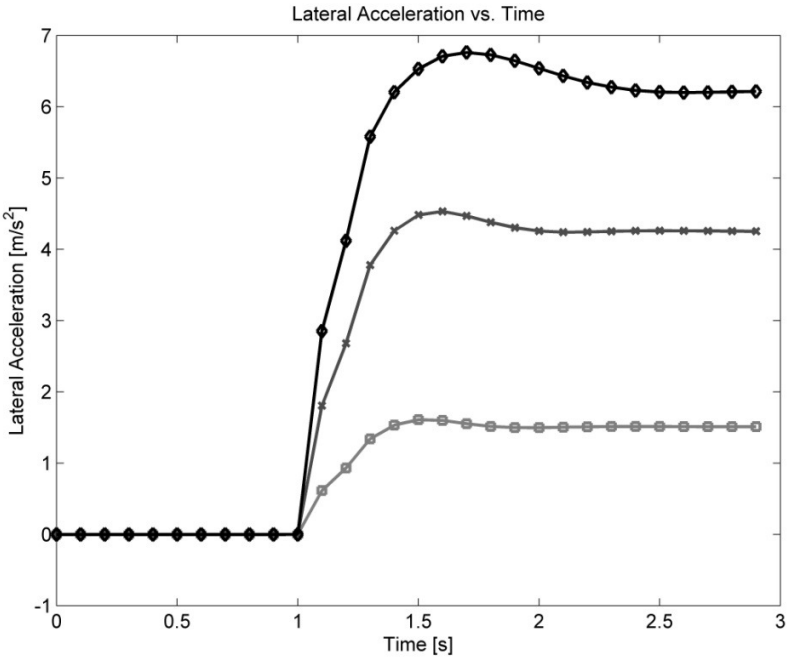

Figure 3.41 Vehicle lateral acceleration response to step steer input

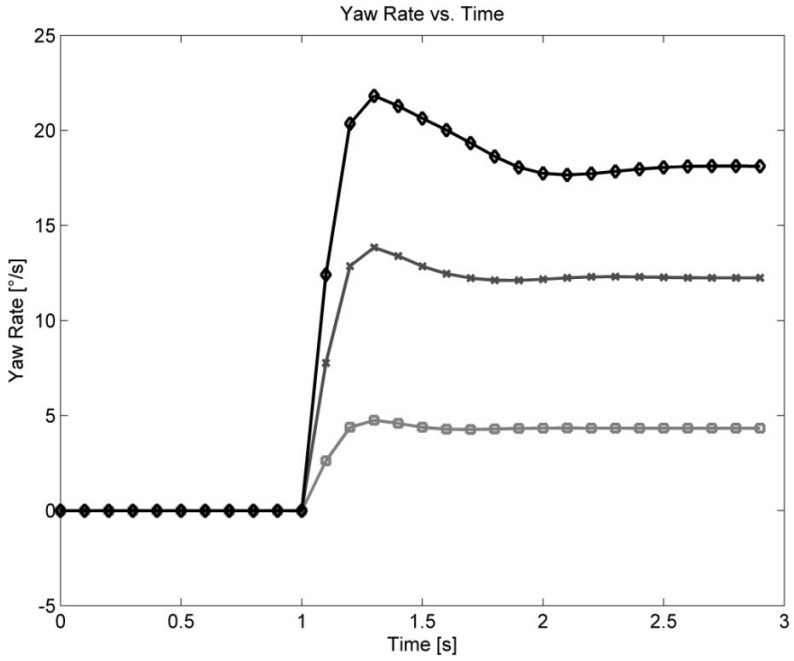

Figure 3.42 Vehicle yaw rate response to step steer input

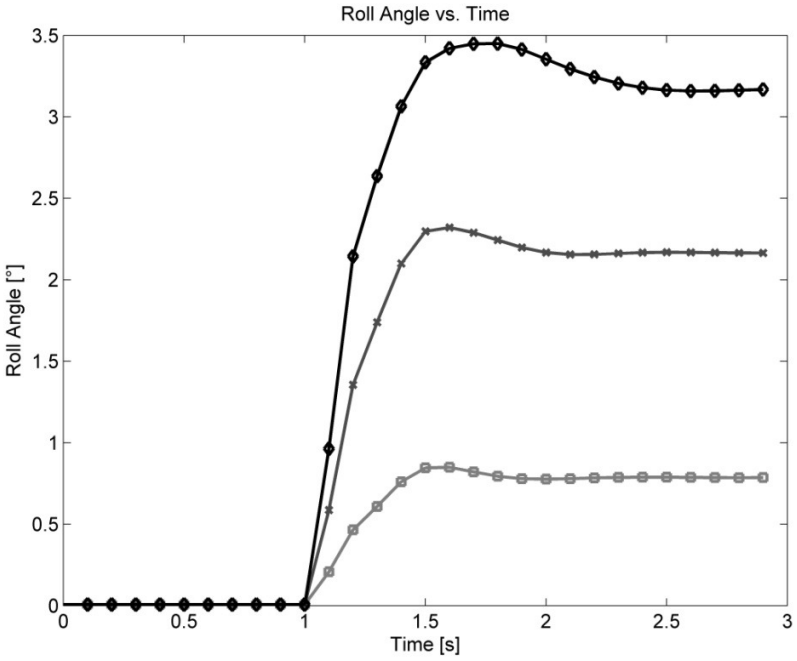

Figure 3.43 Vehicle roll angle response to step steer input

4. Analysis methodology

This chapter is divided into two sections. The first section covers statistical methods used in this thesis; the second provides a background to stability analysis.

4.1. Design and analysis of experiment and data mining methods

Increased modelling accuracy requires higher complexity of vehicle models. Current state of the art MBS vehicle models contain not only over a hundred degrees of freedom (here 165) but also well over a thousand parameters (here 1628). Due to the complexity of the model a fully analytical approach to analysis often becomes very difficult. Distinguishing between cause and effect is also harder in high fidelity models compared to their low fidelity counterparts. In order to improve understanding of model behaviour an alternative approach may be employed. This consists of treating the complex model as a system, the exact behaviour of which is unknown, and seeking the relationship between input and output. A statistical approach becomes very effective when drawing conclusions from such a system. One form of statistical approach is the use of design of experiment (DoE) techniques. DoE provides a very effective methodology for the statistical analysis of systems. The DoE concept has been explained by Antony [85] in a very accessible manner, whereas Montgomery [86] presents a comprehensive description of methods used during design and analysis of experiments. A brief introduction of the techniques used in this thesis is presented in the following sections.

4.1.1. Introduction to experimental design

An experiment is defined as a series of tests performed on a system which is being analysed, and in which some changes are made to the input variables in order to observe changes in output from the system. From analysing the response due to different inputs, conclusions about the performance of the system itself can be drawn. In broader respects learning through experimentation consists of making a judgment based on inconclusive or incomplete evidence, then performing an experiment to confirm the judgment. The data from the experiment leads to another judgement which needs to be confirmed.

The variables influencing the response of a system can be divided into two main groups; variables that are controllable and ones that are not controllable. The experimenter may have different objectives when starting the experiment, for example:

- determine which variables have greatest influence on the response of the system
- determine what values of input give the desired response (low variability or response close to nominal)
- determine how to minimise the influence of uncontrollable variables by choosing correct values of controllable variables

There are different possible approaches to an experiment; best-guess, one-factor-at-a-time, factorial or fractional factorial design being the most common. The best-guess approach consists of achieving the desired response of the system by changing the inputs based on previous knowledge. This approach works well when the experimenter has a good understanding of the system being studied, but if the initial best guess does not give the desired results, it may take a long time to achieve them. Moreover there is no guarantee that this will happen and there is a hidden risk that if the initial best guess gives satisfactory results the experimenter might stop the experiment even though the best solution has not been found. The one-factor-at-a-time approach consists of selecting a start point and changing one factor over its range while other factors remain unchanged. This method does not consider interactions between the factors and when many factors are involved it is less efficient than methods based on a statistical approach to design. Statistical design of experiment is a systematic approach to planning or designing the experiment in such way that the experiment produces a set of results which can be analysed using statistical methods, and therefore valid conclusions about the examined system can be drawn. A correctly designed experiment can reduce the number of trials needed to learn about certain aspects of the system or process. Design of experiment also provides the maximum amount of information about the analysed system in the minimum number of runs.

The simplest type of experimental design is factorial design. In this approach, factors are varied together in all possible combinations, which enables the experimenter to examine the influence of all factors and all their interactions. However as the number of factors increases, the numbers of required runs grows exponentially, e.g. for 8 factors varied at two levels (2^8 factorial design) the number of runs is 256, but for 10 factors the number of runs rises to 1024. Such full factorial design captures all factors and all their interactions. However, as high order interactions are usually likely to be of a lower significance, they can be sacrificed to significantly reduce the number of runs. Such design, called fractional factorial design, allows the experimenter to draw meaningful

conclusions on the main effects of factors and some interactions based on only a subset of the runs of a full factorial design. The factorial and fractional factorial experimental design form the basis of the design approach to experiments. Simple orthogonal designs, with factors varied at two levels, assume a linear influence of factors of response. If a higher order response is expected from the system the factorial designs can be expanded in the later phase of the project, in order to investigate a factor's non-linearities or higher order interactions. Alternatively choosing a relatively low spread between high and low levels of factors can achieve a more linear response of the system, thus making the orthogonal design better suited to the problem.

One of the great advantages of design of experiment is that once the experiments have been performed and results analysed, a response surface can be created to represent the relation between the inputs of the experiment and the response of the system [86]. This simplified model can predict the behaviour of a system to given inputs without performing another run and therefore can be used to quickly find an optimum set of parameters for the operation of the system. As the parameters used to mitigate vehicle rollover also influence other areas such as vehicle handling or ride comfort, these response surfaces can be used for multi-objective optimisation.

In order to achieve the best results when designing and analysing the experiment, Montgomery et al. [86] recommend following the procedure given below:

1. Recognition of and statement of the problem
2. Choice of factors, levels and range
3. Selection of response variable
4. Choice of experimental design
5. Performing the experiment
6. Statistical analysis of data
7. Conclusions and recommendations

Moreover Montgomery et al. [86] recommend using not only statistical but also non-statistical knowledge of the problem when performing the experiment. The experiments often begin with a screening experiment. Such an experiment usually involves studying a large number of factors, which enables the experimenter to estimate which factors and interactions of factors influence the process and which do not. After the screening experiment more in-depth studies can be undertaken.

A large part of statistical design and analysis of experiment focuses on extracting valuable information from the experiment i.e. checking if an effect is significant, eliminating nuisances, etc. The basic principles of experimental design targeted at dealing with errors in an experiment are:

- Replication – helps to find an experimental error and find more precise estimation of effect
- Randomisation – helps to ensure that errors and observations are randomly distributed
- Blocking – helps to reduce variability coming from nuisance factors

The above-mentioned tools help to reduce experimental error to a minimum. However in the ideal world of computer simulation where the influence of uncontrollable factors is minimal, if non-existent, these techniques become less important as:

- Experimenter has full control over which parameters are changed
- Repeating the same simulation over and over again will always result in exactly the same answer
- Changing the order in which different simulations are performed will not have any effect on results
- Finally, one can ensure the same environment for the entire experiment by e.g. performing all the simulations using the same version of the software

4.1.2. Full and fractional factorial designs

In this section an introduction to DoE theory is presented. Firstly the effect of a factor or factors is defined as the change in response due to a change in the level of a factor or factors. The effect of a factor in factorial design with two levels of factors, usually noted as "-1" and "+1", is the difference between the average response at a low level of this factor and at a high level of the factor. Effects are denoted using capital letters and they can be split into different categories:

- main effects - effect in change of response due to single factor. This can be linear (e.g. A), quadratic (e.g. A^2), when change in response is proportional to the square of the factor effects, or higher order
- interaction – appears when response to one factor changes with the level of the other factors; in two-factor factorial design (factors A and B) with two levels of factors this can calculated as the average difference between effect of A at a low level of B and the effect of A at a high level of B; interactions can be due to two linear effects, e.g. AB, the linear

and quadratic effects, e.g. A^2B, two quadratic effects, e.g. A^2B^2, or a combination of higher order effects

Results of design of experiment can be represented by a response curve or response surface. The response curve is the curve which relates the response to one quantitative factor, whereas the response surface is the surface which relates the response to two or more quantitative factors.

2^k factorial design is a special case of factorial design, which has the k number factors at only two levels – high and low. Complete replicate of 2^k factorial design requires 2^k observations. This design is very useful in the early stage of an experiment as it allows the experimenter to investigate large number of factors and requires the lowest number of runs compared to other factorial designs. A statistical model for 2^k factorial design will include:

- *k* main effects
- $\binom{k}{2}$ two factor interactions
- $\binom{k}{3}$ three factor interactions
- …
- one k factor interaction – with 1 degree of freedom

Therefore the complete model for 2^k factorial design will include the total of (2^k-1) effects.

A treatment is a combination of factor levels for which the response of the system is obtained. Treatment combinations are usually denoted by a lower-case letter. Each letter corresponds to one factor. If a letter exists in the treatment combination, this means that the upper level of the factor was used for this combination. If all factors are at a low level the treatment is denoted as (1). Treatment combinations can be written in standard order, e.g. for 2^4 design the standard order takes shape of: (1), a, b, ab, c, ac, bc , abc, d, ad, bd, cd, acd, bcd, abcd.

For the two-level factorial design a design matrix of -1 and +1 relating to upper and lower factor level can be constructed. In such a matrix the columns correspond to factor effects e.g. A, B, AB, C, …, whereas rows correspond to treatment combinations e.g. (1), a, b, ab, c… etc. The signs in columns of factors interactions are a product of the corresponding coefficients for two main effects. The design matrix has the following properties:

- each column has an equal number of “+1” and “-1“ entries

- the sum of products of the elements of any two columns is zero

By multiplying the elements in a column by the treatment combination, a contrast required to estimate any effect can be found quickly. For example the contrast for factor A in 2^2 design equals:

$$Contrast_{A} = -(1) + a - b + ab \quad \textbf{(4.1)}$$

Therefore the contrast for AB…K effect can be determined by the expansion of the following equation:

$$Contrast_{AB\cdots K} = (a \pm 1)(b \pm 1)\cdots(k \pm 1) \quad \textbf{(4.2)}$$

Where:

"+" is used if factor is not included

"-" is used if factor is included

Once the above equation has been expanded the number 1 is replaced with (1) which denotes a treatment combination consisting of only low levels of factors. After calculating the contrast, the effects can be found from the following equation:

$$AB\cdots K = \frac{2}{n2^{k}}(Contrast_{AB\cdots K}) \quad \textbf{(4.3)}$$

Calculated effects give a good indication of how each factor and factors' interactions influence the system's response.

Once the experiment has been performed and effects have been calculated, a regression model representation can be created. For a simple two-factor factorial experiment this takes the form of:

$$y = \beta_0 + \beta_1 x_1 + \beta_2 x_2 + \beta_{12} x_1 x_2 + \varepsilon \quad \textbf{(4.4)}$$

where:

β – coefficients that have been found

x_1 – coded variable representing factor A

x_2 – coded variable representing factor B

x_1x_2 – interaction between parameters A and B

ε – random error term

The parameters x_1 and x_2 in the above equation are defined on a scale from -1 to 1 corresponding to high and low levels of factors A and B. As they are unitless they are often referred to as coded variables. The reason for using coded variables instead of the actual levels of factor is that coded

variables help to compare the relative size of factor effects which otherwise would not be directly comparable, e.g. mass and stiffness. Therefore the parameters β used in the regression model can be found directly from the effects, e.g. in the case of two-factor factorial design β for main effect would equal $\beta_1 = \frac{A}{2}$ whereas β for two factor interaction would be $\beta_{12} = \frac{AB}{2}$. Alternatively coefficients β can be found by using least squares estimates.

The 2^k design uses only two levels of factors and therefore cannot capture non-linearities of single effects. The only non-linearity comes from the interactions of the factors. The technique which enables the experimenter to capture non-linearities of single effects consists of the addition of centre points to the 2^k design.

For such a design, a model considering second order (quadratic) effects can be fitted:

$$y = \beta_0 + \sum_{j=1}^{k} \beta_j x_j + \sum_{i<j} \sum \beta_{ij} x_i x_j + \sum_{j=1}^{k} \beta_{jj} x_j^2 + \varepsilon \qquad \textbf{(4.5)}$$

where β_{jj} represents pure quadratic effect

One disadvantage of the 2^k design is the high number of treatments for experiments with large number of factors. The fractional factorial design assumes that the chosen high order interactions are negligible and therefore the information about main effects and low order interactions can be found by completing only a fraction of the full factorial experiment. The fractional factorial design is denoted as 2^{k-p} where k is the number of factors and p is the number of design generators. A generator is a factorial effect (such as ABC) for which all the treatment combinations of fractional factorial design are at a high level and therefore have a plus sign in the design matrix. Sometimes the generator is referred to as a word. As the identity column in the design matrix also has a plus sign, the following equation can be written:

$$I = ABC \qquad \textbf{(4.6)}$$

This equation is often called the defining relation. The complete defining relation is made of the p chosen generators (as shown in the equation above) as well as their $2^p - p - 1$ generalised interactions. A 2^{k-p} fractional factorial design can be referred to as $1/2^p$ fraction of the 2^k full factorial design. For example the 2^{3-1} design contains only 4 runs instead of 8 in full factorial design therefore a 2^{3-1} design is a one-half fraction of a 2^3 design. Results of one fractional factorial design can be combined with results from subsequent experimentation to create a larger design.

Due to the reduced number of runs in fractional factorial design, when compared to full factorial design, some of the high order interactions are combined with low order ones or main effects. Such effects which cannot be estimated separately in fractional factorial design are called aliases. Only

sums of aliases can be estimated in the fractional factorial design. The aliased effects can be found using the defining relation. This is done by multiplying an effect, for which aliases are to be found, by the defining relation. For example for a design described by the defining relation of $I = ABC$ the aliases of effect A can be found as follows:

$$A \cdot I = A \cdot ABC = A^2BC = BC \qquad \textbf{(4.7)}$$

because $A^2 = I$

In order to obtain information hidden in aliased effects, the alternate fraction needs to be run. For example, if the principle fraction has a defining relation of $I = +ABC$ then the alternate or complementary fraction to this is $I = -ABC$. Together they form a complete factorial design.

Design resolution *R* of fractional factorial design describes which effects are aliased with each other. When no effect containing *p* factors is aliased with another effect containing less then $R - p$ factors then the design has a resolution *R*. For example, for resolution III design:

- no main effect is aliased with any other main effect
- main effects are aliased with two-factor interactions
- two-factor interactions are aliased with each other

Roman numeral subscript is used to denote the resolution, e.g. 2^{3-1}_{III}. It is easy to see that higher resolution designs are more desirable as the assumptions regarding which interactions are negligible can be less restrictive. It is important to choose the defining relation, so that no effects which are potentially important are aliased with each other, otherwise it will be impossible to distinguish between them without running another fraction of design. For a given design resolution it is desirable to use long words as this ensures low aberration. A minimum aberration design is characterised by the lowest possible number of main effects aliased with R-1 order interactions, the lowest possible number of two factor interactions aliased with R-2 order interactions, etc. Selection of 2^{k-p} fractional factorial designs for $k \leq 15$ factors and up to $n \leq 128$runs with generators resulting in the highest possible design resolutions with minimum aberration has been described by Montgomery [86].

Estimating an effect from the results of fractional factorial design is similar to estimating one from full factorial design and requires the experimenter to first find the contrast of the *i*th effect by multiplying the elements in the *i*th column by the treatment combination. The *i*th effect of a fractional factorial design can then be estimated by:

$$\ell_i = \frac{2 \cdot (Contrast_i)}{N} = \frac{(Contrast_i)}{\frac{N}{2}} \tag{4.8}$$

Where:

$N = 2^{k-p}$ – is the total number of observations

The 2^{k-p} design allows for estimation of $2^{k-p} - 1$ effects together with their aliases.

4.1.3. DoE Implementation in SIMPACK

The SIMPACK software used in this research does not come with any built-in DoE tool. Therefore such a tool had to be implemented before the experiment could take place. The initial investigation showed that an algorithm controlling the simulation could be written in two different ways:

- batch mode
- Qt script – which is a built-in scripting language in SIMPACK

Qt script offered access to a wider range of built-in functions than batch mode, hence it was decided that this option was better suited to the algorithm. Written DoE script can be split into two main parts:

- Generator of design of experiment
- Execution of design of experiment together with collection of results

The script implemented into SIMPACK can generate full factorial and fractional factorial designs, run the simulations, and generate the corresponding matrix of responses. The script takes into account the rollover metric chosen for this study which requires multiple simulations for each treatment combination. The rollover metric is described in more detail in the following chapters. Additionally the script is able to run any number of treatment combination specified directly by the user, thus opening doors to the running of more advanced designs not covered by the script. The algorithm for generating the design of experiment is shown in the Appendix A.

4.2. Stability Analysis

Rollover stability analysis has not been performed before on a high fidelity, non-linear vehicle model. This section describes the most commonly used stability analysis techniques and discusses their application to studying rollover in a high fidelity model.

Stability of the linear time invariant system represented by a transfer function has been defined by Franklin et al. [87] as:

"A linear time-invariant system is said to be stable if all the roots of the transfer function denominator polynomial have negative real parts (i.e. they are all in the left hand s-plane) and is unstable otherwise."

Therefore the system described by transfer function e.g.:

$$H(s) = \frac{1}{s + \sigma} \tag{4.9}$$

will be stable if the pole is located on the left hand of the s-plane origin i.e. $\sigma > 0$, and hence $s < 0$. The impulse response of a stable system will decay with time. If the pole is located in the right hand side of the s-plane, i.e. $s > 0$, then the system is unstable and its response to impulse will increase in time. The transfer function for a linear, time invariant system, before cancellation of any poles and zeros is performed, can be written as:

$$T(s) = \frac{Y(s)}{R(s)} = \frac{b_0 \cdot s^m + b_1 \cdot s^{m-1} + \ldots + b_m \cdot s^0}{s^n + a_1 \cdot s^{n-1} + \ldots + a_n} \tag{4.10}$$

where $m \leq n$

The solution of a system characteristic differential equation, i.e. the denominator of transfer function, can be written as a partial-fraction expansion:

$$y(t) = \sum_{i=1}^{n} K_i \cdot e^{p_i \cdot t} \tag{4.11}$$

where:

K_i - depends on initial conditions and location of zeros

p_i - roots of system characteristic equation

Therefore it is clear that if p have negative real parts then for an increasing time response y(t) will converge to 0. Hence a system's stability can be determined by finding the roots of the characteristic equation and checking if all of their real parts are negative i.e. if roots lay on the left

of the $j\omega$ axis on the s-plane. If this is not the case and one or more roots are located on the right hand of $j\omega$ axis then the system is unstable. A special case occurs when the roots of the characteristics equations lay exactly on the $j\omega$ axis – such a system can be described as neutrally stable and its response will neither increase nor decay.

4.2.1. Routh's stability criterion

Over the years several methods have been developed to determine stability without the need for solving roots of a characteristics equation polynomial. The characteristic polynomial can be written in form of:

$$s^n + a_1 \cdot s^{n-1} + a_2 \cdot s^{n-2} + ... + a_n = 0 \qquad \textbf{(4.12)}$$

The necessary, but not sufficient, condition for all roots being negative is that all coefficients a_1, a_2 … a_n of the characteristic polynomial must be positive. If one or more coefficients equal 0 or are negative then the polynomial will have roots with positive real parts. E. J. Routh developed a necessary and sufficient condition for a system being stable i.e. all roots of the characteristic polynomial being on the left of the $j\omega$ axis on the s-plane [87]. The method requires finding Routh's array and then checking if all elements in the first column of Routh's array are positive. If this criterion is satisfied, then the system is stable. To find Routh's array, the coefficients of the characteristic polynomial need to be arranged in two rows. The first row begins with 1 and contains even coefficients, whereas the second row contains odd-numbered coefficients. The next rows are found by computing determinants made of elements from the two previous rows. These determinants consist of two elements from the first column and two elements from the consecutive column [87]. All roots of the characteristic polynomial are on the left of the $j\omega$ axis and therefore the system is stable only if all coefficients in the first column are positive. If this is not the case, then the number of roots to the right of the $j\omega$ axis corresponds to the number of changes of sign of coefficients in the first column. An example of a Routh array is given below:

	1st column	**2nd column**	**3rd column**	**…**
N	1	a_2	a_4	…
n-1	a_1	a_3	a_5	…
n-2	b_1	b_2	b_3	…
n-3	c_1	c_2	c_3	…
…	…	…	…	…
1	*			
0	*			

where coefficients b_1, b_2,…,c_1 , c_2,… are computed as follows:

$$b_1 = -\frac{\det\begin{bmatrix} 1 & a_2 \\ a_1 & a_3 \end{bmatrix}}{a_1},\ b_2 = -\frac{\det\begin{bmatrix} 1 & a_4 \\ a_1 & a_5 \end{bmatrix}}{a_1},$$

$$c_1 = -\frac{\det\begin{bmatrix} a_1 & a_3 \\ b_1 & b_2 \end{bmatrix}}{b_1},\ c_2 = -\frac{\det\begin{bmatrix} a_1 & a_5 \\ b_1 & b_3 \end{bmatrix}}{b_1} \quad \textbf{(4.13)}$$

4.2.2. Nyquist stability

The Nyquist stability criterion has its foundations in the Argument Principle. Franklin et al. [87] defined the Argument Principle in the following way:

"A contour map of a complex function will encircle the origin Z – P times, where Z is the number of zeros inside contour and P is the number of poles inside contour."

This criterion provides a methodology for assessing the stability of a complex system from frequency response. Consider a contour C_1 on an s-plane representing the values of s for which transfer function H(s) is going to be evaluated. For a point s_0 lying on the contour the transfer function will result in a complex quantity:

$$H_1(s_0) = \vec{v} = |\vec{v}| \cdot e^{j\alpha} \quad \textbf{(4.14)}$$

Where α is the value of argument of $H_1(s_0)$ and it can be found as:

$$\alpha = \theta_1 + \theta_2 + \theta_3 + ... + \theta_m - (\phi_1 + \phi_2 + \phi_3 + ... + \phi_n) \quad \textbf{(4.15)}$$

If the s point travels around the contour in a clockwise direction the values of α will change accordingly. If all poles and zeros are outside the contour, then for s traveling around the contour the values of α will never go through the net change of 360º. This is due to the fact that the components of α, namely θ and ϕ, will only go through the net change of 360° if the corresponding pole or zero is placed within the contour. If this is not the case than values of θ and ϕ will rise and fall but never change by 360º. Therefore for a transfer function with poles and zeros placed outside

the contour C_1 a plot of corresponding function $H_1(s)$ on the s plane will not encircle the origin as $H_1(s_0) = |\vec{v}| \cdot e^{j\alpha}$ and α does not change by 360º.

However if a pole or zero is located within the contour then for an *s* value traveling around contour C_1 the value of α will go through the net change of 360° and therefore a plot of $H_1(s)$ will encircle the origin. As α is defined as the difference between the sum of angles from poles and the sum of angles from zeros, the number of origin encirclements indicates a difference between the number of poles and the number of zeros encircled by contour C_1, for example for 2 zeros located in the contour C_1, $H_1(s)$ will encircle the origin 2 times in a counter-clockwise direction. If a pole is added in the contour C_1, then $H_1(s)$ will encircle the origin only once in a counter-clockwise direction. If the number of poles and zeros in the contour C_1 is equal, then the angles will cancel each other and α will not go through a net change of 360º.

If the contour C_1 is enlarged so that it covers the entire right hand side of an s-plane then all poles and zeros located in the right hand side of the s-plane will be encircled by contour and therefore the plot of $H_1(s)$ will encircle the origin Z-P times where Z is the number of zeros and P is the number of poles in the right hand plane. The above statement is very useful when looking at the stability of closed loop systems. Consider the transfer function of the closed loop system written as:

$$\frac{Y(s)}{R(s)} = \frac{K \cdot G(s)}{1 + K \cdot G(s)} \qquad \textbf{(4.16)}$$

Where

G(s) – transfer function of plant

K – gain

The plot of $1 + K \cdot G(s)$ is simply of plot of $K \cdot G(s)$ shifted by 1 to the right hand side of the Im-Re plane. Therefore by analysing an open loop system $K \cdot G(s)$ and looking at the number of encirclements of -1, conclusions about the stability of a closed loop system $1 + K \cdot G(s)$ can be drawn. If a pole is located in the right hand plane then $K \cdot G(s)$ encircles -1 clockwise; if a zero is in the right hand plane then $K \cdot G(s)$ encircles -1 anti-clockwise. The total number of encirclements equals $Z - P$, where Z is right hand side zero of $1 + K \cdot G(s)$ and P right hand side pole of $1 + K \cdot G(s)$. The analysis can be simplified if the system analysed has more poles than zeros and hence has zero response at infinite frequency which is true for any physical system $K \cdot G(s)$. The contour stretched to cover the entire right hand side of the s-plane will have infinite

imaginary values for any real value greater than 0. Therefore it is sufficient to analyse the system for all s values lying on the imaginary axis i.e. s equal from $-j\cdot\infty$ to $j\cdot\infty$ (real part of s = 0).

4.2.3. Lyapunov stability criteria

Lyapunov in his doctoral thesis discussed stability problems of non-linear systems. He proposed two methods for dealing with such stability problems. A brief overview of Lyapunov's methods has been presented by Parks [88] whereas more detailed considerations have been presented by Khalil [89] and Murray [76]. Before the Lyapunov stability criteria are introduced here, the principle definitions need to be given a brief summary:

i) Local stability

A system is locally stable, in the sense of Lyapunov, if all solutions starting near equilibrium x*=0 will remain near equilibrium at all times. This can be written after [76] as:

$$\|x(t_0)\| < \delta \Rightarrow \|x(t)\| < \varepsilon \qquad \forall t \geq t_0 \tag{4.17}$$

where $\varepsilon > 0$ and there exist $\delta(t_0, \varepsilon) > 0$

This means that states of x will only increase up to ε but will never be greater than ε. If δ is not a function of t_0, i.e. δ only depends on ε, then such a system is uniformly stable

ii) Assymptotic Stability

Asymptotic stability (according to [76]) – a system is asymptotically stable at equilibrium x*=0 at given time $t = t_0$ if:

x* = 0 is stable

x* = 0 is locally attractive, which means that there exists $\delta(t_0)$ such that:

$$\|x(t_0)\| < \delta \Rightarrow \lim_{t\to\infty} x(t) = 0 \tag{4.18}$$

iii) Exponential stability

Exponential stability (according to [76]) – a system is exponentially stable at equilibrium point x*=0 if there exist constants m, $\alpha > 0$ and $\varepsilon > 0$ such that:

$$\|x(t)\| \leq m \cdot e^{-\alpha(t-t_0)} \cdot \|x(t_0)\| \tag{4.19}$$

$$\text{for all } \|x(t_0)\| \leq \varepsilon \text{ and } t \geq t_0$$

The greatest constant α which satisfies the above equation is called the rate of convergence.

4.2.4. Lyapunov's First Method

Lyapunov's First Method is often referred to as the indirect method of Lyapunov. It uses linearisation of a system to determine if a non-linear system is stable in a certain area around equilibrium. This method provides the theoretical background which validates linearisation. Consider a dynamic system described by a set of non-linear first order differential equations:

$$\dot{x}_i = f_i(x_1,...,x_n) \quad \text{for i = 1,..., n} \tag{4.20}$$

where f_i are functions which for $x_i = 0$ take value of 0

and an origin of system which is shifted so that $\boldsymbol{x} = 0$ is the point of equilibrium, then a set of linearised equations can be found. The linearised differential equations can be written in the form of:

$$\dot{x} = J \cdot x \tag{4.21}$$

where: x - is state matrix

$\dot{x}$ - is matrix of states first differential

J - is Jacobian matrix with respect to x and evaluated near the origin;

each entry (i,j) of this matrix can be found as:

$$J_{i,j} = \left[\frac{\partial f_i(x)}{\partial x_j} \right]_{x=0} \quad \text{for i, j = 1,..., n} \tag{4.22}$$

An alternative approach to obtaining a J matrix is to expand functions f_i as a power series and omit all terms apart from ones linear to $x_i s$. For a fixed time t the non-linear part of equation, i.e.

$$f_{nonlin}(x) = f(x) - J \cdot x \tag{4.23}$$

will be approaching 0 when x approaches 0.

Once the set of linear equations has been found, eigenvalues of J can be calculated to check stability. If all eigenvalues are negative or have negative real parts then the linear system is stable. Lyapunov has proved that if a linearised system is asymptotically stable then the original non-linear system will also have a region of stability in some neighbourhood of the origin.

4.2.5. Lyapunov's Second Method

Lyapunov's Second Method is sometimes referred to as Lyapunov's Direct Method. It provides a methodology for checking if a system is asymptotically stable without the need for solving non-linear differential equations. It uses so-called Lyapunov functions to draw conclusions about the system's stability. This is a generalisation from the fact that if there is a measure of energy in the system, then by analysing this measure, the stability of the system can be studied. If the origin of a system described by non-linear differential equations is moved, so that the origin coincides with the equilibrium which is examined (x = 0 is equilibrium), then a positive-define function V = V(x) which is always greater from 0 apart from x = 0 where V is equal to 0 can be found. Therefore in space of x, function V will surround origin x = 0 with closed surfaces which are defined by V(x)=const. In order to check the stability of the system, the rate of change in time of function V following the trajectory of a non-linear differential equation needs to be examined. This can be done by calculating:

$$\dot{V} = \sum_{i=0}^{n} \frac{\partial V}{\partial x_i} \frac{dx_i}{dt} = \sum_{i=0}^{n} \frac{\partial V}{\partial x_i} f_i(x) \qquad \textbf{(4.24)}$$

If $\dot{V}$ is a negative-define function i.e. is always negative apart from x =0 for which f(x) = 0) then this means that with time it will move towards point x=0 and therefore the system is asymptotically stable. Murray et al. [76] gives a wider and more exact definition covering also other cases:

"Let $V(x,t)$ be a non-negative function with derivative $\dot{V}$ along the trajectories of the system.

1. If $V(x,t)$ is locally positive definite and $\dot{V}(x,t) \leq 0$ locally in x and for all t, then the origin of the system is locally stable (in the sense of Lyapunov).

2. If $V(x,t)$ is locally positive definite and decrescent, and $\dot{V}(x,t) \leq 0$ locally in x and for all t, then the origin of the system is uniformly locally stable (in the sense of Lyapunov).

3. If $V(x,t)$ is locally positive definite and decrescent, and $-\dot{V}(x,t)$ is locally positive definite, then the origin of the system is uniformly locally asymptotically stable.

4. If $V(x,t)$ is positive definite and decrescent, and $-\dot{V}(x,t)$ is positive definite, then the origin of the system is globally uniformly asymptotically stable."

Interestingly Lyapunov's theory only defines sufficient conditions for the stability of the system's origin. What it does not do is to provide a technique for the derivation of the Lyapunov function V. Therefore finding the Lyapunov function can sometimes be a very laborious task.

4.2.6. Conclusions on the best suited method

The high fidelity vehicle model described in Chapter 3 contains non-linear differential equations (e.g. trigonometric terms), hence Nyquist and Routh's stability criteria cannot be directly applied to examine the stability of the vehicle in terms of rollover.

The MBS software used to create the vehicle model can provide a full set of linearised differential equations in the form of system matrixes which are derived from linearisation of the system at given point in time. Provided that these linearised equations are derived when the system is in equilibrium, then the Lyapunov Indirect Method is very well suited to examining the stability of the system. This has the additional benefit that it avoids the non-trivial derivation of function V required in the Lyapunov Direct Method.

4.2.7. Validation of results from SIMPACK model linearization

Before the non-linear full vehicle model could be linearised in order to determine its stability through the Lyapunov Indirect Method, the linearisation performed by SIMPACK was validated using a simple non-linear model. The results obtained from SIMPACK were compared with results obtained by the analytical solution of differential equations. For validation purposes a simple pendulum model with rotational spring and damper attached to its base was chosen as shown in Figure 4.1. The model contains non-linear trigonometric terms which makes it a good basis for validation of linearisation performed by SIMPACK.

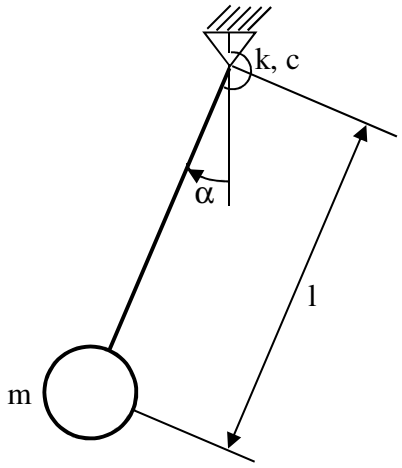

Figure 4.1 Simple pendulum consisting of mass m suspended on massless arm with length l and attached to the ground by rotational spring k and rotational damper c.

The differential equation describing the pendulum can be written as:

$$m \cdot g \cdot l \cdot \sin\alpha + k \cdot \alpha + c \cdot \dot{\alpha} + m \cdot l^2 \cdot \ddot{\alpha} = 0 \qquad \textbf{(4.25)}$$

In order to calculate the eigenvalues, the above equation is firstly converted from a single, second order differential equation into two, first order differential equations:

$$\omega = \dot{\alpha} \qquad \textbf{(4.26)}$$

$$\dot{\omega} = -\frac{g}{l} \cdot \sin\alpha - \frac{k}{m \cdot l^2} \cdot \alpha - \frac{c}{m \cdot l^2} \cdot \omega \qquad \textbf{(4.27)}$$

The above can be re-written in the matrix form:

$$\begin{bmatrix} \dot{\alpha} \\ \dot{\omega} \end{bmatrix} = \begin{bmatrix} 0 & \omega \\ -\frac{g}{l} \cdot \sin\alpha - \frac{k}{m \cdot l^2} \cdot \alpha & -\frac{c}{m \cdot l^2} \cdot \omega \end{bmatrix} \qquad \textbf{(4.28)}$$

In order to write the state space equations the *sin(*α*)* term needs to be linearised. This will be done for two equilibrium conditions corresponding to α equals 0 and α equals π.

Equations linearised at $\alpha = 0$

For $\alpha = 0$ the $\sin\alpha = \alpha$ and therefore the equation (4.28) takes the form:

$$\begin{bmatrix} \dot{\alpha} \\ \dot{\omega} \end{bmatrix} = \begin{bmatrix} 0 & \omega \\ -\frac{g}{l} \cdot \alpha - \frac{k}{m \cdot l^2} \cdot \alpha & -\frac{c}{m \cdot l^2} \cdot \omega \end{bmatrix} \tag{4.29}$$

This can be presented in the state space form of $\dot{x} = \mathrm{A} \cdot x$:

$$\begin{bmatrix} \dot{\alpha} \\ \dot{\omega} \end{bmatrix} = \begin{bmatrix} 0 & 1 \\ -\frac{g}{l} - \frac{k}{m \cdot l^2} & -\frac{c}{m \cdot l^2} \end{bmatrix} \cdot \begin{bmatrix} \alpha \\ \omega \end{bmatrix} \tag{4.30}$$

The eigenvalues of the system can then be found from the following equation:

$$\begin{bmatrix} 0 & 1 \\ -\frac{g}{l} - \frac{k}{m \cdot l^2} & -\frac{c}{m \cdot l^2} \end{bmatrix} \cdot \begin{bmatrix} \alpha \\ \omega \end{bmatrix} = \lambda \cdot \begin{bmatrix} \alpha \\ \omega \end{bmatrix} \tag{4.31}$$

Where

λ – is the eigenvalue sought (scalar)

The trivial solution of the above equation is when both α and ω equal 0. Other solutions can be found as follows:

$$\begin{bmatrix} -\lambda & 1 \\ -\frac{g}{l} - \frac{k}{m \cdot l^2} & -\frac{c}{m \cdot l^2} - \lambda \end{bmatrix} \cdot \begin{bmatrix} \alpha \\ \omega \end{bmatrix} = 0 \tag{4.32}$$

Hence the characteristic determinant must be equal to 0:

$$\begin{vmatrix} -\lambda & 1 \\ -\frac{g}{l} - \frac{k}{m \cdot l^2} & -\frac{c}{m \cdot l^2} - \lambda \end{vmatrix} = 0 \tag{4.33}$$

Assuming the following properties of the pendulum model:

m = 1 kg
l = 1 m
k = 100 Nm/rad
c = 1 Nms/rad

The equation (4.33) takes the form of:

$$\begin{vmatrix} -\lambda & 1 \\ -109.81 & -1-\lambda \end{vmatrix} = 0$$

From the above characteristic determinant, two roots of the characteristic equation can be found:

$$\lambda = -0.5 \pm 10.467i$$

Therefore the natural (damped) frequency of the pendulum is:

$$f = \frac{|\mathrm{Im}|}{2 \cdot \pi} = 1.66587\,[\mathrm{Hz}]$$

whereas the un-damped frequency can be calculated as:

$$f_{undamped} = \frac{|\lambda|}{2 \cdot \pi} = 1.66777\,[\mathrm{Hz}]$$

Equations linearised at $\alpha = \pi$ (inverse pendulum).

In order to achieve the equilibrium position for $\alpha = \pi$ the external force F_e had to be applied to balance the force from the spring rotational spring mounted at the base of pendulum.

$$F_e = k \cdot \pi \tag{4.34}$$

Next, let us describe the angular position of the pendulum using angle $\beta = \alpha - \pi$. Taking into account external force and the fact that $\sin\alpha = -\sin\beta$ the differential equation of motion takes the shape of:

$$-m \cdot g \cdot l \cdot \sin\beta + k \cdot \beta + c \cdot \dot{\beta} + m \cdot l^2 \cdot \ddot{\beta} = 0 \tag{4.35}$$

Which can be written in matrix form thus:

$$\begin{bmatrix} \dot{\beta} \\ \dot{\omega} \end{bmatrix} = \begin{bmatrix} 0 & \omega \\ \frac{g}{l} \cdot \sin\beta - \frac{k}{m \cdot l^2} \cdot \beta & -\frac{c}{m \cdot l^2} \cdot \omega \end{bmatrix} \tag{4.36}$$

Which after linearisation takes the state-space form of:

$$\begin{bmatrix} \dot{\beta} \\ \dot{\omega} \end{bmatrix} = \begin{bmatrix} 0 & 1 \\ \frac{g}{l} - \frac{k}{m \cdot l^2} & -\frac{c}{m \cdot l^2} \end{bmatrix} \cdot \begin{bmatrix} \beta \\ \omega \end{bmatrix} \tag{4.37}$$

The system eigenvalue can be found by solving the following equation:

$$\begin{bmatrix} 0 & 1 \\ \frac{g}{l} - \frac{k}{m \cdot l^2} & -\frac{c}{m \cdot l^2} \end{bmatrix} \cdot \begin{bmatrix} \beta \\ \omega \end{bmatrix} = \lambda \cdot \begin{bmatrix} \beta \\ \omega \end{bmatrix} \tag{4.38}$$

Where

λ is the eigenvalue sought

Hence the characteristic determinant must be equal to 0:

$$\begin{vmatrix} -\lambda & 1 \\ \frac{g}{l} - \frac{k}{m \cdot l^2} & -\frac{c}{m \cdot l^2} - \lambda \end{vmatrix} = 0 \qquad \textbf{(4.39)}$$

From the above characteristic determinant, two roots of the characteristic equation can be found:

$$\lambda = -0.5 \pm 9.48367i$$

Therefore the natural (damped) frequency of the pendulum is:

$$f = \frac{|\mathrm{Im}|}{2 \cdot \pi} = 1.50937 \text{ [Hz]}$$

Whereas the un-damped frequency can be calculated as:

$$f_{undamped} = \frac{|\lambda|}{2 \cdot \pi} = 1.511469 \text{ [Hz]}$$

Compared with the pendulum linearised at $\alpha = 0$ the natural frequency has decreased significantly as gravity is now acting against the spring stiffness.

SIMPACK test model

In order to check if the SIMPACK results agree with the ones calculated manually, a single pendulum model was set up. The same values for m, k, c and l were used as in the above calculations. The system was examined at two equilibrium positions corresponding to α equal 0 and π, with the former requiring constant external torque $k\pi$ to balance the spring torque. At each position the system was linearised and the system matrix A was found. Next the natural frequencies and critical damping were found. The graphical representation of the SIMPACK pendulum model is shown in Figure 4.2.

SIMPACK model linearisation results at $\alpha = 0$

First the pendulum angle α was set to 0 and linear system matrices were exported. The output from SIMPACK is shown in Figure 4.3.

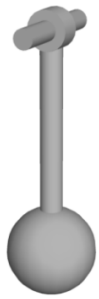

Figure 4.2 Single pendulum model in SIMPACK

```
************************************************************
** Starting SIMPACK Solver Version 8904, Build 87, 32 bit **
** For Task:                                              **
** GENERATING LINEAR SYSTEM MATRICES A B C D              **
************************************************************

**     Load globals list   : .../global_mbs_elements.sys
** Load MBS main structure
**     Load globals mapping
** Perform MBS data check and pre-processing

+-----------------------------------------------------+
|                                                     |
|  calculate linear system of the nonlinear system:   |
|                                                     |
|     +-----------------------------------------+     |
|     |      xp   = g( t, x, u(t), f^e )        |     |
|     |             with : f^e  = g(t,x,u,mess) |     |
|     |             with : mess = mess(t,x,u(t)) |     |
|     +-----------------------------------------+     |
|                                                     |
|  linearised system:                                 |
|                                                     |
|   +-----------------------------------------------+ |
|   | dxp = A * delta_x + B * delta_u + BF * delta_f | |
|   +-----------------------------------------------+ |
|                                                     |
|    with : A       = d(g)/d(x)                       |
|           B       = d(g)/d(u)                       |
|           BU      = d(g)/d(f)                       |
|                                                     |
|           mess    = mess_lin + Cx * delta_x         |
|                              + Cu * delta_u         |
|           Cx      = d(mess)/d(x)                    |
|           Cu      = d(mess)/d(u)                    |
|                                                     |
|           x       = x_lin + delta_x                 |
|           delta_u = u(t)   - u_lin                  |
|           delta_f = f^e(t) - f_lin                  |
|                                                     |
|           u_lin   = 0.                              |
|           mess_lin= mess( t_lin, x_lin, u_lin )     |
|           f_lin   = f^e(t_lin,x_lin,u_lin,mess_lin) |
|                                                     |
+-----------------------------------------------------+

Excitation vector at linearisation point:
-----------------------------------------
   - set/store u_l     = 0

Calculate:
----------
   - store     x_l     = x(t_lin)
    - calculate A,B,C,D ..........

CPU time for calculating linear system matrices =  0.0000000E+00 [s]

*** A-Matrix

   1           2
 0.0000E+00  0.1000E+01
-0.1098E+03 -0.1000E+01

** SIMPACK module executed

ATTENTION :Enter <RETURN> to exit :
===================================
```

Figure 4.3 A-Matrix outputted by SIMPACK for single pendulum with $\alpha = 0$

It can be seen that the A-Matrix calculated by SIMPACK is exactly the same as that found by hand calculations, i.e.:

$$\begin{bmatrix} \dot{\alpha} \\ \dot{\omega} \end{bmatrix} = \begin{bmatrix} 0 & 1 \\ -109.81 & -1 \end{bmatrix} \cdot \begin{bmatrix} \alpha \\ \omega \end{bmatrix}$$

Additionally the calculation of eigenvalues was performed within SIMPACK. The results shown in Figure 4.4 are the same as calculated in the first part of this section.

```
 * Linearisation of equations of motion and
   calculation of eigenvalues and eigenvectors

 * Info: Maximum state derivative:
   zgpp(      1): $J_Pendulum =  0.0000000E+00

 * Calculate linear system matrix A ..........
 * Calculate eigenvalues and eigenvectors
 * End of linearisation and eigenvalue calculation
   CPU-time for
   - Linearisation:   1.9998550E-03 [s]
   - Eigenvalues  :   1.0001659E-03 [s]

****************************** E I G E N V A L U E S ******************************

   No.     |  Real-Part      Imag.-Part | Nat.Damping  Frequency | Undamped Frequ.
           |    [1/s]         [rad/s]   |      [-]         [Hz]  |       [Hz]
-----------+----------------------------+-------------------------+----------------
   1/   2 | -5.0000E-01 +/- 1.0467E+01 |    0.0477       1.6659 |      1.6678
********************************************************************************
```

Figure 4.4 Eigenvalues, natural frequencies and natural damping calculated by SIMPACK for single pendulum model with $\alpha = 0$

SIMPACK model linearisation results at $\alpha = \pi$

The same test was performed on the model with $\alpha = \pi$ and external moment of $k\pi$ applied to balance the torque generated by the rotational spring mounted at the base of the pendulum. The linear system matrixes and eigenvalues were calculated. The results shown in Figure 4.5 and Figure 4.6 show that both the linear system A-Matrix and system eigenvalues agree with the values calculated earlier.

The results of deriving system matrices and calculating eigenvalues in an equilibrium position in SIMPACK are accurate and therefore can be used to assess the stability of the non-linear system by applying Lyapunov's second method.

```
************************************************************
** Starting SIMPACK Solver Version 8904, Build 87, 32 bit **
** For Task:                                              **
** GENERATING LINEAR SYSTEM MATRICES A B C D              **
************************************************************

**     Load globals list   : .../global_mbs_elements.sys
** Load MBS main structure
**     Load globals mapping
** Perform MBS data check and pre-processing

+-----------------------------------------------------+
|                                                     |
|  calculate linear system of the nonlinear system:   |
|                                                     |
|     +-----------------------------------------+     |
|     |      xp   = g( t, x, u(t), f^e )        |     |
|     |             with : f^e  = g(t,x,u,mess) |     |
|     |             with : mess = mess(t,x,u(t)) |     |
|     +-----------------------------------------+     |
|                                                     |
|  linearised system:                                 |
|                                                     |
|   +---------------------------------------------+   |
|   | dxp = A * delta_x + B * delta_u + BF * delta_f |
|   +---------------------------------------------+   |
|                                                     |
|    with : A       = d(g)/d(x)                       |
|           B       = d(g)/d(u)                       |
|           BU      = d(g)/d(f)                       |
|                                                     |
|           mess    = mess_lin + Cx * delta_x         |
|                              + Cu * delta_u         |
|           Cx      = d(mess)/d(x)                    |
|           Cu      = d(mess)/d(u)                    |
|                                                     |
|           x       = x_lin + delta_x                 |
|           delta_u = u(t)   - u_lin                  |
|           delta_f = f^e(t) - f_lin                  |
|                                                     |
|           u_lin   = 0.                              |
|           mess_lin= mess( t_lin, x_lin, u_lin )     |
|           f_lin   = f^e(t_lin,x_lin,u_lin,mess_lin) |
|                                                     |
+-----------------------------------------------------+

Excitation vector at linearisation point:
-----------------------------------------
   - set/store u_l     = 0

Calculate:
----------
   - store     x_l     = x(t_lin)
    - calculate A,B,C,D ..........

CPU time for calculating linear system matrices =  9.9992752E-04 [s]

*** A-Matrix

   1           2
 0.0000E+00  0.1000E+01
-0.9019E+02 -0.9988E+00

** SIMPACK module executed

ATTENTION :Enter <RETURN> to exit :
===================================
```

Figure 4.5 A-Matrix outputted by SIMPACK for single pendulum with $\alpha = \pi$

```
**     Load globals list   : .../global_mbs_elements.sys
** Load MBS main structure
**     Load globals mapping
** Perform MBS data check and pre-processing

 * Linearisation of equations of motion and
   calculation of eigenvalues and eigenvectors

 * Info: Maximum state derivative:
   zgpp(      1): $J_Pendulum =  1.0206792E-09

 * Calculate linear system matrix A ..........
 * Calculate eigenvalues and eigenvectors
 * End of linearisation and eigenvalue calculation
   CPU-time for
   - Linearisation:   2.0000935E-03 [s]
   - Eigenvalues  :   0.0000000E+00 [s]


****************************** E I G E N V A L U E S ******************************

   No.     |  Real-Part      Imag.-Part | Nat.Damping  Frequency | Undamped Frequ.
           |    [1/s]         [rad/s]   |     [-]         [Hz]   |      [Hz]
-----------+---------------------------+-----------------------+-----------------
   1/   2 | -5.0000E-01 +/- 9.4837E+00 |    0.0526       1.5094 |      1.5115

*******************************************************************************
```

Figure 4.6 Eigenvalues, natural frequencies and natural damping calculated by SIMPACK for single pendulum model with $\alpha = \pi$

5. Simulation results

5.1. Justification of rollover criteria

Prior to starting the experiment, a reliable method for measuring vehicle rollover resistance had to be selected. The selection of a method includes the selection of a vehicle manoeuvre used to excite vehicle rollover, as well as the corresponding metric quantifying rollover resistance.

As vehicle rollover is binary in nature, i.e. the vehicle has rolled over or it has not, the intermediate state not existing, the roll angle itself cannot be used as a direct measure of rollover resistance. It can however be used to establish whether the vehicle has rolled over. Therefore another variable, describing the vehicle condition or manoeuvre at which rollover occurs, needs to be employed as the direct measure of rollover resistance.

As will be discussed later in section 5.4, loss of contact between the inside tyres in a turn and the ground is a critical point from a stability point of view. The roll angle is undoubtedly related to the tendency of the inside tyres to leave the ground. It can be used to estimate if, for a given vehicle setup, wheel lift off has occurred. However as the wheel lift off depends not only on the steady state vehicle characteristics but also on its transient behaviour and the type of manoeuvre employed in the test, this method of estimating wheel lift off is inaccurate. Moreover as is shown in section 2.2.2, wheel lift off is not a good indicator of whether the vehicle is going to rollover as based on results presented by Eger et al. [23], Ghike et al. [22] or Tammy [43] the time between tyre lift-off and actual rollover can be relatively long even if no corrective action is taken. If in that time a corrective action is taken by either the driver or control system the vehicle can return to its stable condition.

For the purpose of this study vehicle rollover is defined as a geometrical position of the vehicle at which the roll angle is equal to or greater than 90º. Also, the following assumption is made; for a given type of manoeuvre there exists a roll angle at which, if reached, the vehicle is certain to rollover, i.e. to achieve at least 90º of roll. Such a roll angle is specific to the test performed on the vehicle hence it can be established only once the type of manoeuvre is chosen and its conditions are well defined.

Firstly let us consider the advantages and disadvantages of potential methods for quantifying rollover resistance. These methods can be divided into two main groups:

1. Quasi-steady state methods
    a. Critical steering wheel angle during constant speed cornering:

Manoeuvre:

- Constant velocity cornering with steadily increasing steering wheel angle

Measure of rollover resistance:

- Steering wheel angle at which vehicle rolls over

Advantages:

- Single simulation required to establish rollover resistance

Disadvantages:

- Steady state measurement – vehicles can resist rollover in steady state much better than during transient manoeuvres [35]
- Velocity control is problematic to achieve

b. Critical vehicle velocity at constant steering wheel angle

Manoeuvre:

- Constant steering wheel angle cornering with steadily increasing vehicle velocity

Measure of rollover resistance:

- Vehicle velocity at which the vehicle rolls over

Advantages:

- Single simulation required to establish rollover resistance

Disadvantages:

- Steady state measurement – vehicles can resist rollover in steady state much better than during transient manoeuvres [35]
- Velocity control is problematic to achieve

2. Transient methods

a. Critical steering wheel angle amplitude at constant vehicle velocity

Manoeuvre:

- Sinusoidal steering input with steadily increasing amplitude at constant vehicle velocity

Measure of rollover resistance:

- Steering angle amplitude at which the vehicle rolls over.

Advantages:

- Single simulation required to establish rollover resistance

Disadvantages:

- vehicles with the roll natural frequency close to the excitation frequency would be penalised
- Velocity control is problematic to achieve

b. Critical vehicle velocity at constant amplitude sinusoidal steering

Manoeuvre:

- Constant amplitude sinusoidal steering input with steadily increasing vehicle velocity

Measure of rollover resistance:

- Velocity at which the vehicle rolls over.

Advantages:

- Single simulation required to establish rollover resistance

Disadvantages:

- vehicles with the roll natural frequency close to the excitation would be penalised
- Velocity control problematic to achieve

Two approaches from the above list were chosen for the initial investigation:

- Critical vehicle velocity at constant steering wheel angle
- Critical vehicle velocity at constant amplitude sinusoidal steering

Unfortunately, the first simulations showed that increasing vehicle velocity until the vehicle rolls over is not a straightforward task, particularly for the latter test. The problem comes from the simple fact that once the inner wheels lift off, the torque applied to the outer wheels needs to be increased to maintain forward acceleration. This on the other hand reduces the maximum lateral forces that the outer tyres can transmit, which mitigates rollover. Therefore very high friction scaling would need to be applied to achieve rollover. Moreover, for the simulation with sinusoidal input, the rolling resistance is changing as the vehicle's slip angle oscillates. This in turn requires a

very stiff forward velocity controller. Apart from the above-listed disadvantages of the first two approaches, these metrics can also be regarded as unrealistic as one would expect that most drivers would rather try to reduce vehicle velocity during a near rollover event rather than try to increase it.

An alternative method consisting of removal of a longitudinal degree of freedom and specifying fixed forward velocity could be applied. However this approach has been disregarded in this study as it bears no resemblance to the physical world. Similar issues with velocity control were found when investigating the remaining two approaches:

- Critical steering wheel angle during constant speed cornering
- Critical steering wheel angle amplitude at constant vehicle velocity

One can therefore conclude that for a typical SUV on a road with a typical friction coefficient, it is not possible to maintain the forward vehicle velocity over an extended length of time at near rollover condition, i.e. with two wheels just off the ground, without modifying the system parameters e.g. friction coefficient, or altering the model's DoFs.

Due to the issue associated with closed loop velocity control, alternative approaches with open loop velocity control were investigated. The manoeuvres are based on various steering inputs at vehicle coast down.

3. Transient methods with vehicle coasting down

    a. Critical friction scaling factor during given steering manoeuvre at coast down

        Manoeuvre:

        - Fixed (open loop) steering wheel input during vehicle coast down

        Measure of rollover resistance:

        - Critical friction scaling factor at which the vehicle rolls over

        Advantages:

        - No closed loop speed control or artificial removal of longitudinal degree of freedom is needed
        - Open loop steering input

        Disadvantages:

        - Multiple runs required to establish the critical friction scaling factor

b. Critical velocity during given manoeuvre at coast down

   Manoeuvre:

   - Fixed (open loop) steering wheel input during vehicle coast down

   Measure of rollover resistance:

   - Critical vehicle initial velocity at which the vehicle rolls over

   Advantages:

   - No closed loop speed control or artificial removal of longitudinal degree of freedom is needed
   - Open loop steering input

   Disadvantages:

- Multiple runs required to establish the critical friction scaling factor

Both of the above approaches avoid the problem of maintaining vehicle velocity past two wheel lift off by finding a critical rollover measure from coast down runs. The first of them assumes a scaling friction coefficient to determine the vehicle's rollover propensity. This however influences other tyre properties, which could mean that the validity of the conclusion on tyre parameters affecting rollover could be compromised. Therefore the latter approach to measuring rollover resistance was chosen. This is the only method considered so far, which does not affect the system's dynamics by the introduction of a controller, removal of degrees of freedom or varying the friction coefficient.

Once the appropriate type of manoeuvre had been found, the exact steering wheel input needed to be established. Testing physical vehicles for rollover often involves sudden steering wheel inputs performed at a given vehicle velocity, such as the double lane change test performed by Teknikens Värld [3] or the ISO 3888 Part 2 standard. Other types of manoeuvres used for assessing rollover propensity are the J-turn or fishhook. The evaluation of various open and closed loop manoeuvres in the context of assessing vehicle rollover propensity has been summarised in the NHTSA report DOT HS 809 513 [90]. Two manoeuvres were regarded as most suited to this task; Roll Rate Feedback Fishhook and J-turn. During the evaluation, rollover propensity was characterised by monitoring the vehicle's entry velocity at which two wheel lift off occurred. For the purpose of this study an open loop J-turn manoeuvre was chosen over the Roll Rate Feedback Fishhook due to its simplicity. However, simulations show that loss of contact in combination with a roll velocity residue do not necessarily lead to rollover, even without corrective intervention from the driver.

Non-linearities in tyre forces and suspension and further loss of forward speed in case of a coast-down test-case mean that the vehicle might return to a stable state, even if the loss of contact is reached with a roll velocity residue.

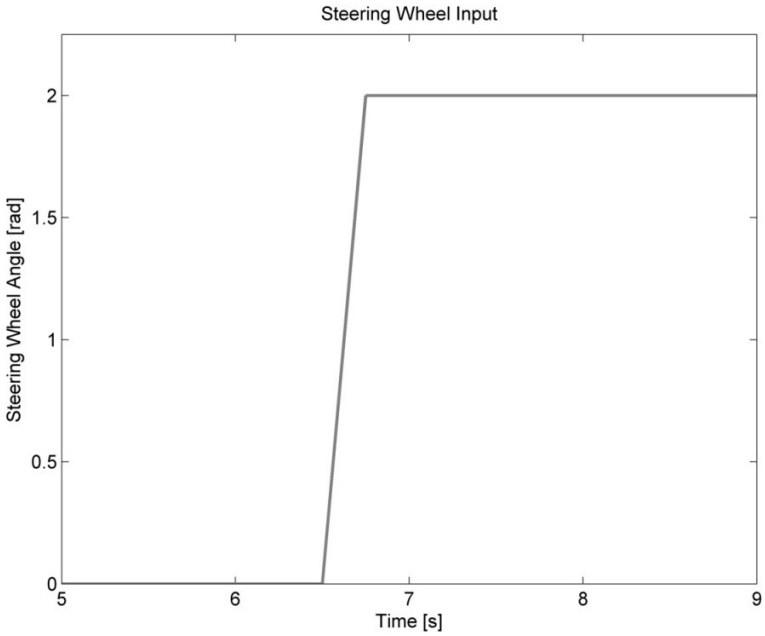

Figure 5.1 Steering wheel input used for the DoE study.

As the occurrence of two wheel lift off is not a reliable indicator of impending rollover, hence a more reliable indicator is necessary. Based on a large number of simulations, it was concluded that a rollover is certain if the roll angle exceeds 57.3º. It is important to note that this angle is specific to the J-turn manoeuvre performed on the nominal vehicle under investigation. For the purpose of this study the rollover propensity characterisation simulations were carried out by launching the vehicle at a low velocity and after a short initial period of time when the vehicle is rolling freely, applying a fixed steering input in the form of a step (steep ramp) steer (see Figure 5.1). Next the vehicle is launched at high velocity. If the vehicle does not roll during the first run but rolls during the second, then the critical rollover velocity $V_{Critical}$ is considered to be somewhere between these two boundaries. The following run is performed at a launch velocity equal to the average of two velocity boundaries. Vehicle rollover or its absence is detected, which defines a new velocity boundary, and a new launch velocity is chosen. The process is repeated until critical rollover velocity $V_{Critical}$ is found. The number of runs required to achieve a given accuracy can be found from the formula:

$$\text{number of runs} = 2 + \text{round}\left(\log_2\left(\frac{\text{range}}{\text{error}}\right) + 0.5\right) \quad \textbf{(5.1)}$$

Therefore if the range of velocities equals 40km/h, and the required accuracy is 1km/h, one would need 8 runs to achieve it. Actually using 8 runs would give an accuracy of 0.625km/h.

In order to achieve a good spread of critical rollover velocity for the chosen method during the DoE, a range of friction scaling factors resulting in high critical velocity sensitivity had to be found. This was necessary as vehicle rollover is very sensitive to the level of available friction. Hence for high values of the friction scaling factor the spread of critical velocities would be very low, whereas for low values, vehicle rollover is likely not to occur at all. In order to further amplify rollover sensitivity, an additional mass of 180 kg was placed above the vehicle's roof line.

In line with the above considerations, a relationship between vehicle critical rollover velocity and friction scaling factor was found. Firstly the friction scaling factor was varied from 1.1 to 1.9 in steps of 0.025. For each factor a critical rollover velocity was found from values between 15 m/s and 55 m/s with a tolerance of 0.078125 m/s resulting from the iterative nature of the search algorithm used to find the critical rollover velocity. The search algorithm limits the number of simulations necessary to find the critical rollover velocity and is described in more detail as part of the DoE script in the Appendix A Figure 9.5. In the second step the friction factor was varied between 1.35 and 1.45 in steps of 0.005 in order to improve the resolution of the results. The relationship between critical velocity and friction scaling factor is shown in Figure 5.2. A friction scaling factor of 1.375 was chosen for further investigation as it offered good critical rollover velocity sensitivity.

It is worth mentioning that the friction scaling factor multiplies the maximum friction measured at the nominal tyre load. This should not be mistaken for the actual friction coefficient used by the tyre which is defined as the ratio of horizontal and vertical force and depends on other factors such as vertical force, tyre slip, camber angle, etc.

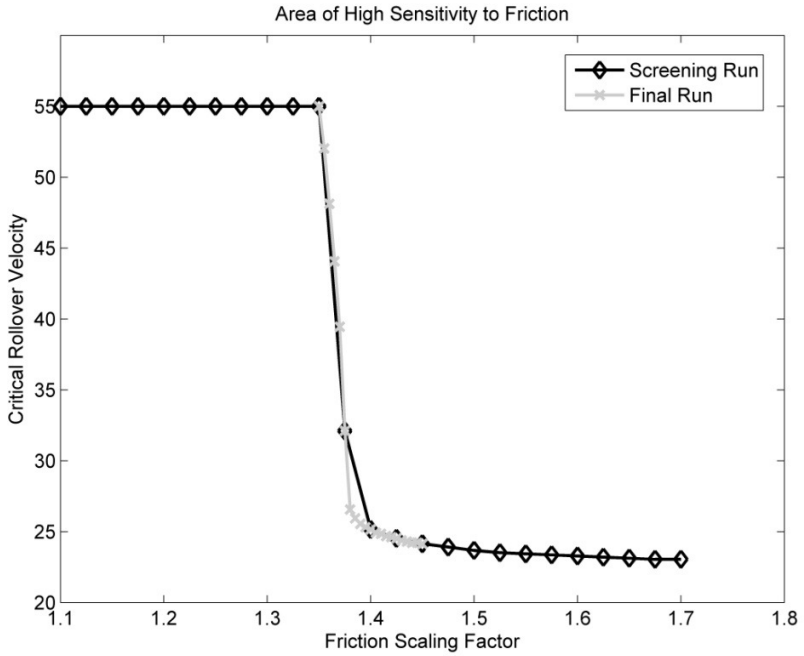

Figure 5.2 Relation between critical rollover velocity and friction scaling factor.

5.2. Tyre - Analysis of experimental design

A DoE investigation was first performed to study the influence of tyre properties on vehicle rollover. Due to its empirical nature MF tyre 6.1 offers a good way of modifying tyre properties by changing tyre factors. From the list of all factors used to define tyre properties the following seven were of particular interest:

$\lambda_{Ky\alpha}$ - Scale factor of cornering stiffness

λ_{Mx} - Scale factor of overturning moment

$\lambda_{\mu x}$ - Scale factor of longitudinal peak friction coefficient

$\lambda_{\mu y}$ - Scale factor of lateral peak friction coefficient

$\lambda_{y\gamma}$ - Scale factor of camber stiffness

K_z - Tyre vertical stiffness

p_{Dy2} - Variation of lateral friction with load

In order to keep the responses linear it was decided to set the upper and lower limits of factors at only +/-1% from their nominal values. This applies to all factors apart from $\lambda_{\mu x}$ and $\lambda_{y\gamma}$ which were varied by +/-0.2% due to the high sensitivity of the vehicle to tyre friction. In order to reduce the number of runs, fractional factorial design was chosen with design generators E=ABC, F=BCD and G=ACD. The design matrix obtained is given in Table 5.1.

Treatment	Factorial Effect						
	A	B	C	D	E	F	G
(1)	-1	-1	-1	-1	-1	-1	-1
aeg	1	-1	-1	-1	1	-1	1
bef	-1	1	-1	-1	1	1	-1
abfg	1	1	-1	-1	-1	1	1
cefg	-1	-1	1	-1	1	1	1
acf	1	-1	1	-1	-1	1	-1
bcg	-1	1	1	-1	-1	-1	1
abce	1	1	1	-1	1	-1	-1
dfg	-1	-1	-1	1	-1	1	1
adef	1	-1	-1	1	1	1	-1
bdeg	-1	1	-1	1	1	-1	1
abd	1	1	-1	1	-1	-1	-1
cde	-1	-1	1	1	1	-1	-1
acdg	1	-1	1	1	-1	-1	1
bcdf	-1	1	1	1	-1	1	-1
abcdefg	1	1	1	1	1	1	1

Table 5.1 Design matrix – geometric notation.

This design ensures that no main factor is aliased to any two-factor interaction and only factors E, F and G are aliased with three-factor interactions. The following two-factor interactions are aliased with each other:

$$\begin{aligned} AB &= CE = FG \\ AC &= BE = DG \\ AD &= CG = EF \\ AE &= BC = DF \end{aligned} \qquad \textbf{(5.2)}$$

$$AF = BG = DE$$

$$AG = BF = CD$$

$$BD = CF = EG$$

$$BE = AC = DG$$

The results of all the runs are given in Table 5.2. Based on these results statistical analysis was used to determine the influence of each factor. Firstly, contrasts (i.e. the total effects) for each factor were calculated using the geometric notation from Table 5.1.

Treatment	Critical Rollover velocity [m/s]
(1)	36.953125
aeg	38.28125
bef	42.34375
abfg	26.796875
cefg	36.40625
acf	34.453125
bcg	27.578125
abce	43.28125
dfg	25.9375
adef	35.625
bdeg	28.59375
abd	27.265625
cde	37.8125
acdg	26.015625
bcdf	26.796875
abcdefg	27.1875

Table 5.2 Vehicle model response to all studied treatments.

The contrasts were found by using the plus and minus signs in the factorial effects column and placing them in front of the response for each treatment they refer to. For example a contrast for the factor A equals:

$$Contrast_A = (-(1) + aeg - bef + abcfg - cefg + acf - bcg + abce - dfg + adef - bdeg + abd - cde + acdg - bcdf + abcdefg) \quad \textbf{(5.3)}$$

Therefore the total effect of factor A which is "Scale factor of cornering stiffness" equals -3.515625 for all runs. In order to determine the effect of factor A, the value of the total effect of factor A needs to be divided by $n2^{k-p}$ where n – number of repetitions, k – number of investigated factors, p – size of fraction. The values of effects for each factor are given in Table 5.3.

Factor code	Factor name	Effect	Variation +/-	Comment
A	$\lambda_{Ky\alpha}$	-0.4395	1.0%	Scale factor of cornering stiffness
B	λ_{Mx}	-2.7051	1.0%	Scale factor of overturning moment
C	$\lambda_{\mu x}$	-0.2832	0.2%	Scale factor of long. peak friction coefficient
D	$\lambda_{\mu y}$	-6.3574	0.2%	Scale factor of lat. peak friction coefficient
E	$\lambda_{y\gamma}$	7.2168	1.0%	Scale factor of camber stiffness
F	K_z	-1.2793	1.0%	Tyre vertical stiffness
G	p_{Dy2}	-5.9668	1.0%	Variation of lat. friction μ_y with load

Table 5.3 Effect of tyre properties on critical vehicle rollover velocity.

The study shows that the most influential tyre properties on vehicle rollover are:

peak friction coeff. (D) – note that this factor was varied by +/- 0.2%

camber stiffness (E)

friction variation with load (G)

overturning moment (B)

tyre vertical stiffness (F)

The influence of tyre cornering stiffness and friction coefficient in the longitudinal direction was found to be relatively small. The influence of most factor interactions was also relatively weak compared to the influence of the main factors themselves. However an aliased interaction of $AF = BG = DE$ is significant and should be investigated in further studies. This interaction reveals synergy between independent tyre parameters in the way in which they affect rollover.

Based on values of effects a response surface model was created. The comparison of responses generated using the response surface model and multi-body model are shown in Table 5.4. It can be seen that this simplified model fits the results from the multi-body model very well.

	Critical rollover velocity $V_{Critical}$		
Treatment	Actual value [m/s]	Predicted value [m/s]	Residual [m/s]
(1)	36.953	37.490	-0.537
aeg	38.281	38.301	-0.020
bef	42.344	40.723	1.621
abfg	26.797	27.100	-0.303
cefg	36.406	37.178	-0.771
acf	34.453	35.488	-1.035
bcg	27.578	28.535	-0.957
abce	43.281	41.279	2.002
dfg	25.938	23.887	2.051
adef	35.625	36.631	-1.006
bdeg	28.594	29.678	-1.084
abd	27.266	27.988	-0.723
cde	37.813	38.066	-0.254
acdg	26.016	24.443	1.572
bcdf	26.797	26.865	-0.068
abcdefg	27.188	27.676	-0.488

Table 5.4 Comparison between simulation and response surface results generated from the main effects only.

5.3. Kinematics and Compliance - Analysis of experimental design

Kinematic and compliance (K&C) characteristics can usually be linked to vehicle steering and handling properties by experienced development engineers; therefore they should also be influential on vehicle rollover. In order to establish the link between K&C properties and rollover propensity using design of experiment methodology, direct control over the input to the experiment, in this case K&C metrics, is required. However, as these metrics are a function of suspension geometry and component stiffnesses, they cannot be changed independently in a simple manner, as a single geometrical or compliance change influences all characteristics simultaneously. Attempts to change just one characteristic while keeping others unchanged have been made successfully in the past; however, they usually involve a large number of iterations of geometry and stiffnesses before such change is achieved. As the purpose of this study is to find the most influential K&C characteristics and establish the link between them and rollover resistance, such an approach was regarded as ineffective and too time consuming. Therefore, a novel approach based on statistical tools is proposed here. The method can be split into four separate stages. Firstly a large number of iterations with different suspension geometries and component stiffnesses are generated using a space filling method such as a Latin Hypercube. In the second stage, each of the above-mentioned iterations is characterised using a number of K&C metrics. In the third stage, for each of the above iterations a rollover propensity characterised by rollover critical velocity is found. Finally a regression model is fitted using the set of K&C characteristics as an input, and rollover propensity as the response. Such a process creates a link between K&C characteristics of the suspension and rollover propensity, despite not having direct control over the previously generated characteristics.

Before starting the experiment, the factors influencing the K&C characteristics had to be defined. The factors chosen as the most influential were:

- suspension arm and links hardpoint positions (x,y,z) – primarily affecting kinematics
- suspension bushes and ball joint stiffness – primarily affecting compliance; in order to reduce the number of inputs in the first stage of the experiment, stiffness at only one end of each link was varied
- spring stiffness, spring aid non-linear characteristic and clearance, rebound spring stiffness and clearance – primarily affecting wheel rate characteristic and roll stiffness
- anti-roll bar stiffness – primarily affecting roll stiffness

As factors at both front and rear suspensions were chosen as an input, the total number of factors equalled 98 input parameters to the design of experiment – for details see Table 5.5 and Table 5.6.

Front Suspension Element Name	Number of			Range		Unit
	Sub-elements	Direct.	DoE Factors	Low	High	
Upper Control Arm Mounting Points	3	3	**9**	-10	10	[mm]
Lower Front Link Mounting Points	2	3	**6**	-10	10	[mm]
Lower Rear Link Mounting Points	2	3	**6**	-10	10	[mm]
Track Road Mounting Points	2	3	**6**	-10	10	[mm]
Road Spring Stiffness	1	1	**1**	-20	20	[%]
Jounce Bumper Contact	1	1	**1**	-20	50	[mm]
Jounce Bumper Linear Rate	1	1	**1**	-74	163	[%]
Jounce Bumper Linear Rate Range	1	1	**1**	-18	27	[mm]
Jounce Bumper Cubic Rate	1	1	**1**	-74	163	[%]
Rebound Spring Contact	1	1	**1**	-2	58	[mm]
Rebound Spring Rate	1	1	**1**	-85	52	[%]
Upper Control Arm Inboard Bush Stiffness	2	2	**4**	-50	50	[%]
Lower Front Link Inboard Bush Stiffness	1	1	**1**	-50	50	[%]
Lower Rear Link Inboard Bush Stiffness	1	1	**1**	-50	50	[%]
Track Rod Outer Ball Joint Stiffness	1	1	**1**	-50	50	[%]
Bearing and Hub Camber Stiffness	1	1	**1**	-50	50	[%]
Bearing and Hub Toe Stiffness	1	1	**1**	-50	50	[%]
Anti-Roll Bar Stiffness	1	1	**1**	-50	50	[%]
Total number of factors			**44**			

Table 5.5 Front suspension factors with their ranges used to generate Latin Hypercube matrix

As the number of inputs to the first stage of the experiment is large, a Latin Hypercube was chosen to arrange them in an input matrix. Matlab was used to generate a Latin Hypercube with coded variables varying between 0 and 1. The Latin Hypercube generated values of 98 independent variables at 100 different value ranges, in 1000 runs. Initially the number of necessary runs required to draw reliable conclusions was unknown. Therefore the experiment was built from batches of 100 runs. After simulating K&C response and vehicle rollover resistance to each factor combination described in 100 runs from the first batch of runs, a regression model linking rollover resistance and all K&C characteristics was fitted and the value of R^2 adjusted was calculated. Next a response from another batch of 100 runs was generated and the response surface fitted to the results from both previous batches and the value of R^2 adjusted was calculated. Once the R^2 adjusted of the regression model was not affected by the latest Latin Hypercube the process was stopped. In stage two of the experiment, a number of K&C characteristics had to be captured.

Rear Suspension Element Name	Number of			Range		Unit
	Sub-elements	Direct.	DoE Factors	Low	High	
Upper Link Mounting Points	2	3	6	-10	10	[mm]
Toe Link Mounting Points	2	3	6	-10	10	[mm]
Lower Control Arm Mounting Points	3	3	9	-10	10	[mm]
Lower Link Mounting Points	2	3	6	-10	10	[mm]
Subframe Mounting Points	2	3	6	-10	10	[mm]
Road Spring Stiffness	1	1	1	-20	20	[%]
Jounce Bumper Contact	1	1	1	-8	62	[mm]
Jounce Bumper Linear Rate	1	1	1	-78	117	[%]
Jounce Bumper Linear Rate Range	1	1	1	-17	28	[mm]
Jounce Bumper Cubic Rate	1	1	1	-99	1150	[%]
Rebound Spring Contact	1	1	1	-15	45	[mm]
Rebound Spring Rate	1	1	1	-75	150	[%]
Upper Link Inboard Bush Stiffness	1	1	1	-50	50	[%]
Lower Control Arm Inboard Bush Stiffness	2	2	4	-50	50	[%]
Toe Link Inboard Bush Stiffness	1	1	1	-50	50	[%]
Internal Link Lower Bush Stiffness	1	1	1	-50	50	[%]
Bearing and Hub Camber Stiffness	1	1	1	-50	50	[%]
Bearing and Hub Toe Stiffness	1	1	1	-50	50	[%]
Subframe Bush Stiffness	2	2	4	-50	50	[%]
Anti-Roll Bar Stiffness	1	1	1	-50	50	[%]
	Total number of factors		**54**			

Table 5.6 Rear suspension factors with their ranges used to generate Latin Hypercube matrix

Four K&C simulations were chosen to generate these characteristics; a vertical simulation, a roll simulation with anti-roll bars, a roll simulation without anti-roll bars, and a lateral compliance simulation. A number of key characteristics were chosen from each simulation:

- Kinematics:
    - Camber vs. wheel centre vertical displacement
    - Toe vs. wheel centre vertical displacement
    - Contact patch force vs. wheel centre vertical displacement
    - Wheel centre lateral displacement vs. wheel centre vertical displacement
    - Kinematic roll centre height vs. wheel centre vertical displacement
- Lateral in phase compliance simulation:
    - Camber vs. lateral force

    - Toe vs. lateral force
    - Jacking i.e. vertical vs. lateral force
    - Wheel centre lateral displacement vs. lateral force
- Roll simulation with and without anti-roll bars (maintaining constant front to rear load distribution);
    - On-centre wheel rate in roll
    - Anti-roll bar contribution to roll stiffness (combined result from simulation with and without anti-roll bar)

In order to be able to capture the K&C characteristics in an easy-to-process way, a number of metrics were developed. For most metrics, 3 points on the characteristics, start, middle and end, were recorded and the second order polynomial was fitted. This resulted in two key coefficients, the first describing the linear gradient, the second describing the non-linearity.

For more complex characteristics such as suspension stiffness in bump (effects of the main spring, rebound spring and non-linear spring aid), 5 equally spaced points were captured. Based on these points, 4 linear instantaneous stiffnesses were derived, resulting in 4 metrics from this simulation. Additionally, the contribution of the anti-roll bar to roll stiffness was described by a single number reflecting the additional roll stiffness due to the anti-roll bar. Based on the results of these 4 simulations, the vehicle's K&C from front and rear axles is characterised using 36 different metrics, 18 per each axle. The list of all metrics is given in Table 5.7.

Suspension geometry can directly affect steering wheel ratio. In Section 5.2 of this thesis, focusing on finding the area of high sensitivity to tyre parameters and studying their effect on rollover, the steering wheel angle input in the step steer manoeuvre was fixed to 114.6°. Changing the steering ratio whilst keeping a fixed steering wheel angle would lead to the vehicle following a different path to the base model. This in turn has a direct influence on the vehicle's lateral acceleration and rollover critical speed. In order to compensate for this, a procedure for normalising the steering wheel input was implemented. The procedure is briefly described below.

After reading in factor levels corresponding to the given treatment, the vehicle model is set to travel on an initially straight road at 10 m/s. Vehicle speed remains constant thanks to a closed loop driveline controller driving all 4 wheels with an equal torque reacted at the vehicle body for the front wheels and rear subframe for the rear wheels. Similarly the vehicle model is also equipped with a simple closed loop steering controller which follows the road by reducing lateral path deviation at the front axle by controlling the steering wheel angle.

Symbol	Simulation	Metric
γ_V	Vertical Kinematics	Linear dependency of camber angle γ on wheel travel
γ_{V^2}	Vertical Kinematics	Quadratic dependency of camber angle γ on wheel travel
K_{V2r}	Vertical Kinematics	Suspension rate in second half of rebound travel
K_{V1r}	Vertical Kinematics	Suspension rate in first half of rebound travel
K_{V1b}	Vertical Kinematics	Suspension rate in first half of bump travel
K_{V2b}	Vertical Kinematics	Suspension rate in second half of bump travel
α_V	Vertical Kinematics	Linear dependency of toe angle α on wheel travel
α_{V^2}	Vertical Kinematics	Quadratic dependency of toe angle α on wheel travel
ρ_V	Vertical Kinematics	Kinematic roll centre height
ρ_{V2}	Vertical Kinematics	Rate of change of kinematic roll centre height due to wheel travel
ψ_V	Vertical Kinematics	Linear dependency of wheel centre lateral position on wheel travel
ψ_{V^2}	Vertical Kinematics	Quadratic dependency of wheel centre lateral position on wheel travel
γ_L	Lateral Compliance	Linear dependency of camber angle γ on lateral force at contact patch
φ_L	Lateral Compliance	Normalised jacking force due to lateral force at contact patch
α_L	Lateral Compliance	Linear dependency of toe angle α on lateral force at contact patch
ψ_L	Lateral Compliance	Linear dependency of wheel centre lateral position on lateral force at contact patch
K_R	Roll Test with Anti-Roll Bars	Wheel rate in roll
ζ_R	Roll Tests with and without Anti-Roll Bars	Anti-roll bar contribution to wheel rate

Table 5.7 K&C metrics employed in the experiment.

After an initial 65m straight, the road on which the vehicle travels begins to turn right, and after 15m the transition becomes a constant radius corner with the radius set to 29.317m. This radius corresponds to the radius at which a baseline vehicle would travel with a forward velocity of 10m/s

and a steering wheel angle of 114.6º. The vehicle equipped with both driveline and steering controllers will, after settling down, reach a steady state constant radius condition. The steering wheel angle corresponding to this condition becomes the reference steering wheel angle and is later used to find the rollover critical speed.

This method of setting the reference steering wheel angle ensures that changes in steering wheel ratio due to modified suspension geometry are not influencing the rollover results. However, the method has a potential down side, in the fact that it also cancels out part of the influence of the understeer gradient as the reference steering wheel angle is obtained at a lateral acceleration far from $0m/s^2$. In fact the lateral acceleration is $3.41m/s^2$, which corresponds to average cornering conditions. The reason why the reference steering wheel angle is set at such a condition is that, in reality, a driver is able to "map" [91] the required steering wheel angle to vehicle speed and corner radius, and is therefore accounting for the steering ratio and understeer gradient of a vehicle which he or she is driving.

Once the reference steering wheel angle has been found, it is then used as the final value of the step steer input used to determine rollover critical speed. The process of finding the rollover critical speed is the same as in the tyre DoE described in section 5.2. It consists of 11 runs at various vehicle start velocities varying between 15m/s and 55m/s. The result of the process is the highest vehicle velocity at which it does not rollover.

Once both K&C metrics and corresponding rollover critical velocities have been found, outputs from both tests are linked using a response surface. This allows the effects to be statistically separated from each other, and rated in order of statistical significance. The large number of inputs to the regression model meant that only the main factors could be assessed initially. Once all the insignificant factors had been excluded from the model, the effect of the interaction and second order terms were studied. An additional complication when fitting the regression model results from the fact that some of the metrics are dependent on each other, e.g.:

- suspension rate in bump and roll stiffness
- roll stiffness and anti-roll bar contribution to roll stiffness
- jacking force and kinematic roll centre height.

The fact that some variables are co-dependent makes the choice of terms in a statistical model somewhat more difficult. This is because inclusion of one parameter will affect the regression coefficient of another parameter. To find the best set of parameters in the statistical model a step wise regression algorithm was used. The original step wise regression Matlab function was modified to base the decision on inclusion or exclusion of parameters not on p-values but on t-

statistics. In order to check how well a given set of potential K&C metrics can be assembled together into a statistical model, a step wise regression was performed for different values of t-statistics and the plot of adjusted R-square vs. number of terms in the statistical model was generated. Such a graph can help to decide where the best compromise between model complexity and model accuracy is.

The results of stepwise regression using the K&C metrics as an input and rollover critical velocity as an output are shown in Table 5.8 and Figure 5.3. The stepwise regression has been performed for different values of t-statistics used to determine which metrics should be excluded or included in the statistical model. It is worth pointing out that stepwise regression was based on the initial model with all terms included. This resulted in better model fit than stepwise regression with no terms in the initial model.

TSTAT	0.001	1	2	3	4	5	6	7	8
Metric	Included in statistical model?								
${}^{F}\gamma_{V^2}$	True	True	True	False	False	False	False	False	False
${}^{F}\gamma_{V}$	True	True	True	True	True	True	True	True	True
${}^{F}K_{V2r}$	True	True	False	False	False	False	False	False	False
${}^{F}K_{V1r}$	True	True	True	True	True	True	True	True	True
${}^{F}K_{V1b}$	True	True	True	True	True	True	False	False	False
${}^{F}K_{V2b}$	True	True	True	True	True	False	False	False	False
${}^{F}\alpha_{V^2}$	True	True	True	True	True	True	False	False	False
${}^{F}\alpha_{V}$	True	False	False	False	False	False	False	False	False
${}^{F}\rho_{V2}$	True	False	False	False	False	False	False	False	False
${}^{F}\rho_{V}$	True	False	False	False	False	False	False	False	False
${}^{F}\psi_{V^2}$	True	False	False	False	False	False	False	False	False
${}^{F}\psi_{V}$	True	True	True	True	True	True	True	True	False
${}^{R}\gamma_{V^2}$	True	True	True	True	True	True	True	False	False
${}^{R}\gamma_{V}$	True	True	True	True	True	True	True	False	False
${}^{R}K_{V2r}$	True	False	False	False	False	False	False	False	False

${}^{R}K_{V1r}$	True	True	True	True	False	False	False	False	False
${}^{R}K_{V1b}$	True	True	True	True	True	True	True	True	True
${}^{R}K_{V2b}$	True	False	False	False	False	False	False	False	False
${}^{R}\alpha_{V^2}$	True	True	True	False	False	False	False	False	False
${}^{R}\alpha_{V}$	True	True	True	True	False	False	False	True	False
${}^{R}\psi_{V^2}$	True	False	False	False	False	False	False	False	False
${}^{R}\psi_{V}$	True	True	True	True	True	True	True	True	False
${}^{R}\rho_{V2}$	True	False	False	False	False	False	False	False	False
${}^{R}\rho_{V}$	True	True	True	True	True	True	True	False	False
${}^{F}\gamma_{L}$	True	True	True	True	True	True	True	True	True
${}^{F}\varphi_{L}$	True	False	False	False	False	False	False	False	False
${}^{F}\alpha_{L}$	True	False	False	False	False	False	False	False	False
${}^{F}\psi_{L}$	True	True	True	True	True	True	False	False	False
${}^{R}\gamma_{L}$	True	True	True	True	True	True	True	True	True
${}^{R}\varphi_{L}$	True	True	True	True	True	True	True	True	True
${}^{R}\alpha_{L}$	True	True	False	False	False	False	False	False	False
${}^{R}\psi_{L}$	True	True	False	False	False	False	False	False	False
${}^{F}K_{R}$	True	True	True	True	True	True	True	True	True
${}^{R}K_{R}$	True	False	False	False	False	False	False	False	False
${}^{F}\zeta_{R}$	True	True	True	False	False	False	False	False	False
${}^{R}\zeta_{R}$	True	True	False	False	False	False	False	False	False
R^2	0.8613	0.8605	0.8595	0.8569	0.8531	0.8506	0.8408	0.8360	0.8083
$R^2_{Adjusted}$	0.8561	0.8569	0.8564	0.8543	0.8507	0.8483	0.8389	0.8343	0.8070
No of terms	36	25	21	18	16	15	12	10	7

Table 5.8 Summary of statistical models generated using stepwise regression; note that letter F in the left superscript denotes front axle and letter R denotes rear axle.

The simplest model was obtained by stepwise regression with limit t-statistics set to 8. It consisted of 7 main terms:

- Front suspension rate on centre rebound
- Rear suspension rate on centre bump
- Front bump camber
- Front and rear camber compliance
- Rear jacking force
- Front roll stiffness on centre

However the quality of fit of this model measured by calculating R^2 adjusted was only 0.807. A plot of R^2 adjusted as a function of the number of model terms was used to find a compromise between model accuracy and complexity (Figure 5.3). A 16-term statistical model seems to fulfil this requirement fairly well. Apart from all metrics included in the 7-term model it additionally includes:

- Front suspension on centre bump rate and full bump rate
- Front bump toe non-linearity

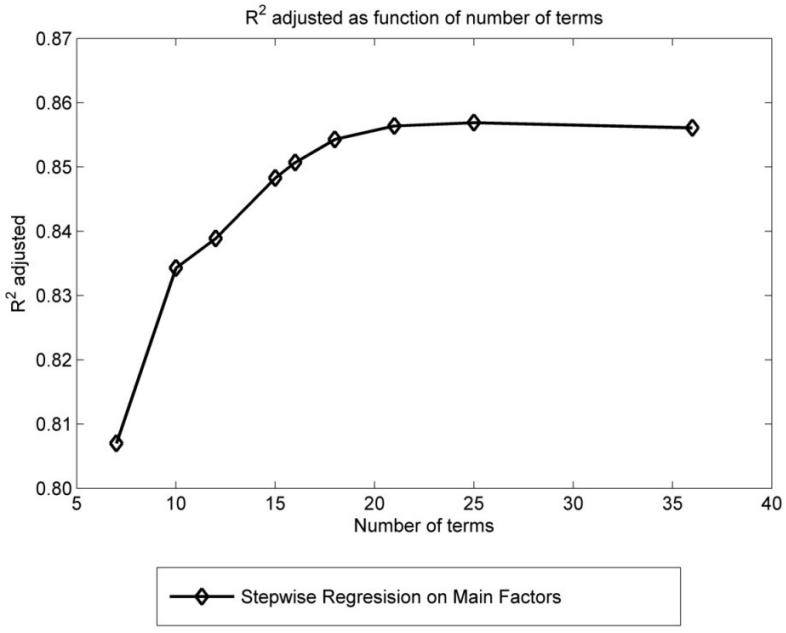

Figure 5.3 Relation between critical number of model terms and quality of fit.

- Front wheel centre lateral travel with bump
- Rear camber compliance linearity and non-linearity

- Rear wheel centre lateral travel with bump
- Rear kinematic roll centre height
- Front wheel centre compliance

In order to check the quality of the model constructed using stepwise regression based on the t-statistic, an algorithm testing all possible combinations of the 16 factor model was used. The number of 16 factor combinations available from 36 possible factors is 7.31E+09. Calculating the adjusted R^2 for all these models would take too long, so the number of factors in the initial pool had to be reduced. To do that both forward and backward regression with t-statistics set to two was performed and if a factor was included in at least one of the two resulting models, it was included in the pool of potential factors. The result was 25 potential factors, which gives 2042975 combinations of 16-term models to test. The results of this study are shown in Table 5.9 and Figure 5.4.

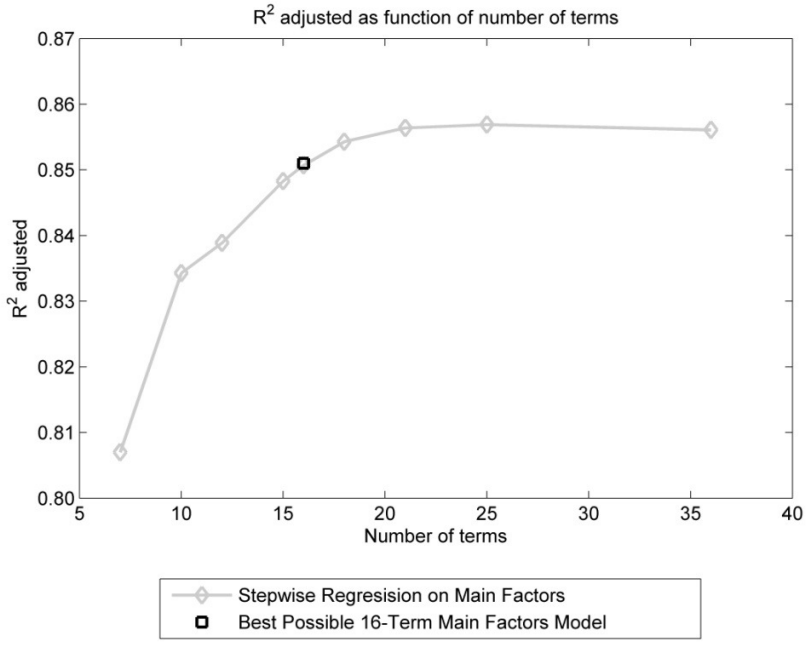

Figure 5.4 Comparison of models generated using stepwise regression and best possible model.

	Model from stepwise regression	Best possible model
Metric	Included in statistical model?	
${}^{F}\gamma_{V^2}$	False	False
${}^{F}\gamma_{V}$	True	True
${}^{F}K_{V2r}$	False	False
${}^{F}K_{V1r}$	True	True
${}^{F}K_{V1b}$	True	True
${}^{F}K_{V2b}$	True	True
${}^{F}\alpha_{V^2}$	True	True
${}^{F}\psi_{V}$	True	True
${}^{F}\rho_{V}$	False	False
${}^{R}\gamma_{V^2}$	True	False
${}^{R}\gamma_{V}$	True	True
${}^{R}K_{V1r}$	False	False
${}^{R}K_{V1b}$	True	True
${}^{R}K_{V2b}$	False	False
${}^{R}\alpha_{V^2}$	False	False
${}^{R}\alpha_{V}$	False	True
${}^{R}\psi_{V^2}$	False	False
${}^{R}\psi_{V}$	True	True
${}^{R}\rho_{V}$	True	True
${}^{F}\gamma_{L}$	True	True
${}^{F}\psi_{L}$	True	True
${}^{R}\gamma_{L}$	True	True
${}^{R}\varphi_{L}$	True	True
${}^{F}K_{R}$	True	True
${}^{F}\zeta_{R}$	False	False
R^2	0.8531	0.8534
$R^2_{Adjusted}$	0.8507	0.8510
No of terms	16	16

Table 5.9 Comparison of model generated using stepwise regression and best possible model.

The best possible model found by testing all possible combinations was only marginally better than the one chosen by stepwise regression with all terms included in the initial model. Moreover the

only difference between the model generated by stepwise regression and the best possible model was one factor. This showed that stepwise regression with all terms included in the initial model is a very efficient way of finding well-fitting statistical models. Therefore in subsequent studies the stepwise regression starting with a full model was used.

So far all statistical models generated in this study have been constructed of only main factors. In complex systems the interactions between the factors are a significant part of the observed process. Therefore in the next part of the study a number of models with interactions and squared terms were generated. As a basis for this, a best possible 16 term model was chosen. Based on the 16 terms included in the model, all possible 1st order interactions and squared terms were generated resulting in a total of 152 potential model terms. To find the best model, the stepwise regression starting with a full model was employed, with an additional constraint ensuring that all 16 main effects are always included in the model. The achieved model fit has been shown in Table 5.10 and Figure 5.5.

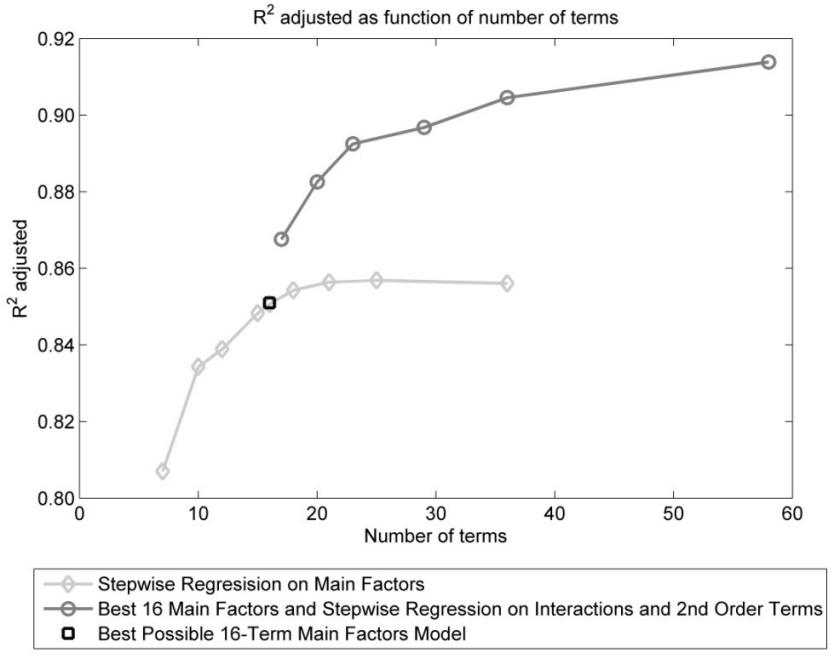

Figure 5.5 Addition of interactions and 2nd order terms in the statistical model.

The results show that including interactions can significantly improve the model fit. Based on the above diagram, a model with 23 terms was chosen as it gives a good compromise between complexity and the quality of fit. For comparison a 20 term model is also included in Table 5.10.

TSTAT:	5		6	
Metric	TSTAT	coefficient	TSTAT	coefficient

${}^{F}\gamma_{V}$	12.08284	4524.174	12.27968	4779.185
${}^{F}K_{V1r}$	-4.13178	-0.84496	13.98935	0.250867
${}^{F}K_{V1b}$	1.427189	0.072421	-0.02648	-0.00137
${}^{F}K_{V2b}$	-8.93141	-0.07417	-8.08901	-0.07003
${}^{F}\alpha_{V^2}$	-4.50119	-32422.9	-4.42448	-33270.6
${}^{F}\psi_{V}$	7.947827	83.03506	7.452588	81.34546
${}^{R}\gamma_{V}$	-1.00784	-334.532	-7.41488	-1769.59
${}^{R}K_{V1b}$	-9.78957	-0.30481	-22.3506	-0.14861
${}^{R}\alpha_{V}$	7.713683	121.3813	7.368396	120.9666
${}^{R}\psi_{V}$	-9.86778	-397.396	-9.81768	-412.568
${}^{R}\rho_{V}$	-8.65296	-0.4563	-8.80496	-0.48388
${}^{F}\gamma_{L}$	-6.99715	-154181	-30.1908	-260712
${}^{F}\psi_{L}$	5.517819	34239.66	4.980048	32216.93
${}^{R}\gamma_{L}$	0.055234	2613.999	-17.5857	-242492
${}^{R}\varphi_{L}$	8.014139	280.8634	8.132765	297.3028
${}^{F}K_{R}$	-27.8578	-0.05478	-26.2715	-0.05389
${}^{F}\gamma_{V}\cdot{}^{F}K_{V1b}$	-10.621	-14.2986	-10.4611	-14.7018
${}^{F}\gamma_{V}\cdot{}^{R}\rho_{V}$	-6.1707	-13.1821	-6.55134	-14.5432
${}^{F}K_{V1r}\cdot{}^{R}\gamma_{L}$	-5.37013	-5219.07	-	-
${}^{F}K_{V1b}\cdot{}^{R}\gamma_{L}$	7.891618	1562.256	6.219507	1230.818
${}^{F}K_{V2b}\cdot{}^{F}K_{R}$	8.24E+00	7.18E-05	7.49269	6.81E-05
${}^{R}K_{V1b}\cdot{}^{F}\gamma_{L}$	-5.12347	-1453.61	-	-
${}^{R}\gamma_{V}\cdot{}^{R}\gamma_{V}$	5.745221	27036.67	-	-
R^2	0.895		0.8849	
R^2 adj	0.8925		0.8826	
No of terms	23		20	

Table 5.10 Summary of models including interactions and 2nd order terms.

For convenience it is worth stating here the full meaning of the significant interactions in the 23 term model:

- front linear camber gain and front suspension rate in bump on centre
- front linear camber gain and rear roll centre height
- front suspension rate in rebound on centre and rear linear camber compliance
- front suspension rate in bump on centre and rear linear camber compliance

- front suspension rate in full bump and front suspension roll stiffness
- rear suspension rate in bump on centre and front linear camber compliance
- additionally rear suspension linear camber gain squared is also significant.

It is noticable that the introduction of interactions has pushed the t-statistics of some of the main factors below the originally specified value of 5 used to derive the 23 term model. The factors affected the most are:

- rear linear camber gain
- rear linear camber compliance

However, as interactions include these factors, they are left in the model despite having low t-statistics values. In order to better understand the strength of each of the main factors, a conversion table has been constructed (Table 5.11).

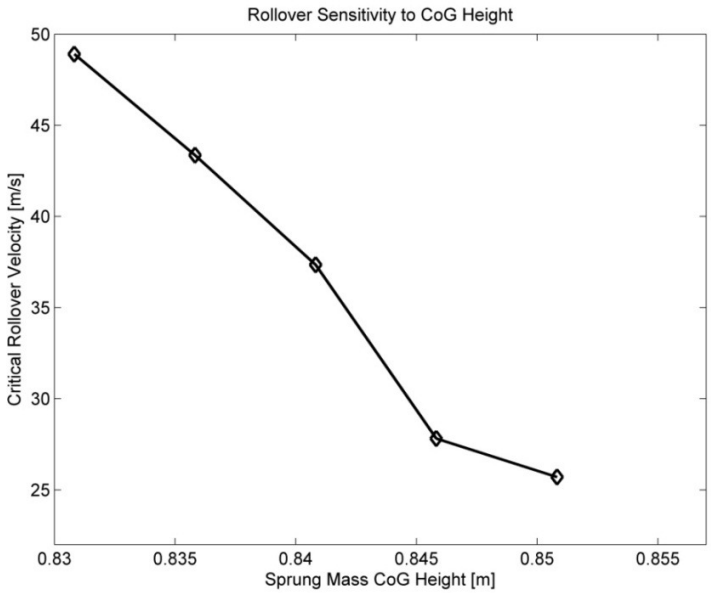

Figure 5.6 Rollover sensitivity to sprung mass CoG.

	Desired change to increase $V_{Critical}$	Change of	Unit	Effect on $V_{Critical}$
${}^{F}\gamma_{V}$	less negative camber gain with bump	0.002	°/mm	9.048
${}^{F}K_{V1r}$	softer	-10	N/mm	8.450
${}^{F}K_{V1b}$	stiffer	10	N/mm	0.724

${}^{F}K_{V2b}$	softer	-10	N/mm	0.742
${}^{F}\alpha_{V^2}$	more toe out change with bump and rebound	-0.00002	º/mm^2	0.648
${}^{F}\psi_{V}$	less WC track change	0.01	mm/mm	0.830
${}^{R}\gamma_{V}$	more negative camber in bump	-0.002	º/mm	0.669
${}^{R}K_{V1b}$	softer	-10	N/mm	3.048
${}^{R}\alpha_{V}$	more toe in with bump	0.005	º/mm	0.607
${}^{R}\psi_{V}$	more WC track change	-0.01	mm/mm	3.974
${}^{R}\rho_{V}$	lower roll centre	-10	mm	4.563
${}^{F}\gamma_{L}$	higher camber compliance	-0.00001	º/N	1.542
${}^{F}\psi_{L}$	lower WC compliance	0.00002	mm/N	0.685
${}^{R}\gamma_{L}$	lower camber compliance	0.00001	º/N	0.026
${}^{R}\varphi_{L}$	less jacking force	0.02	N/N	5.617
${}^{F}K_{R}$	softer in roll	-150	N/º	8.217

Table 5.11 Summary of most influential K&C metrics on rollover propensity.

For comparison, on average, a 1mm change in the vehicle sprung mass CoG results in 1.24m/s change in critical rollover velocity, as seen on Figure 5.6.

5.4. Stability investigations

In an effort to gain additional insight into rollover dynamics and evaluate the use of two wheel lift off as an indicator of imminent rollover, a brief study of stability was carried out. From a purely qualitative point of view, the phase plane trajectory (PPT) of the roll velocity versus roll displacement was employed. The J-turn manoeuvre provided a suitable starting point. The upper half of Figure 5.7 illustrates the roll velocity plotted against roll displacement for one of the manoeuvres that did result in rollover. In the lower part of the same figure, the vertical tyre forces are presented as a function of time. The resulting PPT diagram resembles closely that of a pendulum [92]. Starting from the origin of the reference frame, both the roll angle and roll velocity increase as a result of the steering excitation. The roll velocity reaches a peak after which it reduces to almost generate a critical saddle point at approximately 6.3° of roll angle. For an appropriately

smaller forward velocity, a mathematically perfect saddle point would have been achieved whereby the roll speed would have reached zero and at that point the PPT diagram would have been non-differentiable. This point would have been a point of unstable equilibrium, directly equivalent to the case of a pendulum resting in the inverted position. By establishing the point in time when the approximate saddle point is reached, it becomes evident that this is also the point when both inside tyres lose their contact with the ground. This point is clearly depicted in the lower part of Figure 5.7.

Further understanding of stability can be gained by observing the eigeinvalues of the linearised system as it progresses slowly through an approximately steady-state manoeuvre, where the lateral acceleration increases gradually. The steady-state condition is required so that it is possible to isolate a number of trim points, about which the system can be linearised and its eigenvalues obtained to establish stability, based on Lyapunov's Indirect Method [92]. In this context, the previously used transient test case is inappropriate. Instead, the case of a vehicle travelling forward with a constant velocity and a steering controller tracking the required roll angle is used. To avoid traction problems and the need for a locked or active differential as well as reduction in available tyre lateral force due to longitudinal tyre slip due in turn to driving torque, a PID controller calculates the necessary thrust which is applied in the form of a force at the centre of mass of the vehicle. Thus a constant forward speed is maintained without altering the behaviour of the tyres and with minimal influence on the overall dynamics of the vehicle. The PID steering controller is used to find equilibrium conditions for a range of discrete roll angles. Once equilibrium is achieved, the steering controller is deactivated and eigenvalues are calculated. For this test the forward speed was set to 30m/s. As mentioned already, it is much more difficult to induce rollover by a quasi-steady state manoeuvre, therefore for the purpose of this simulation the coefficient of friction was set equal to 1.6.

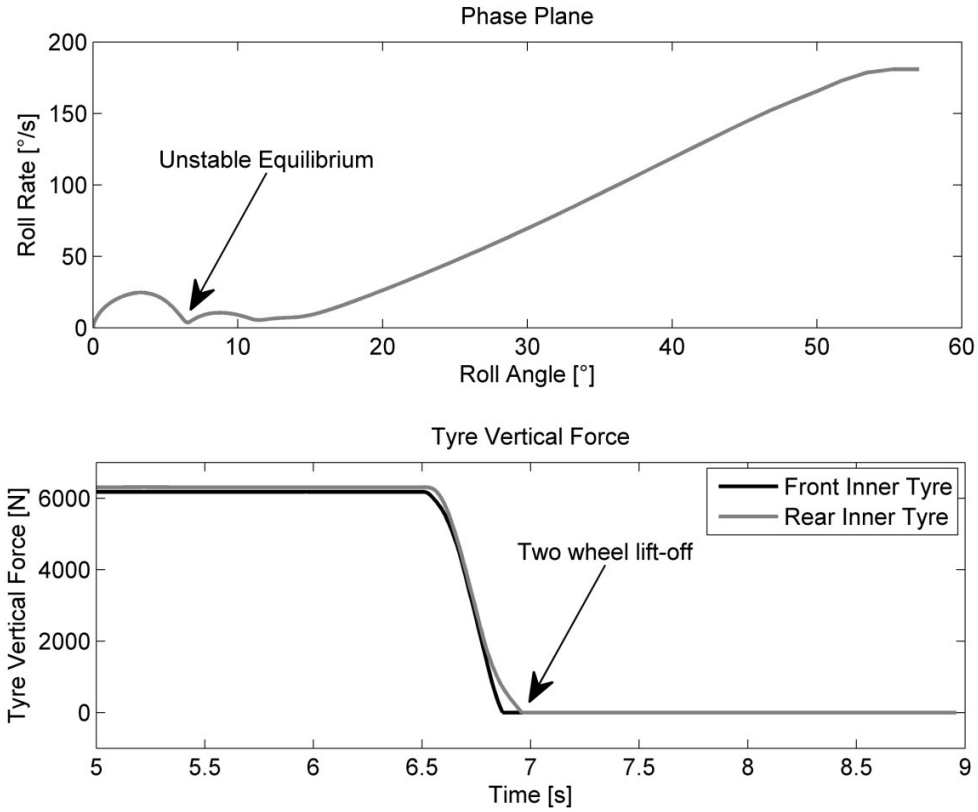

Figure 5.7 Roll angle – roll velocity phase plane and tyre vertical forces plotted in the time domain.

The migration of eigenvalues as a result of increasing the roll-angle is shown in Figure 5.8. As the vehicle contains 165 degrees of freedom and an additional 15 internal states for each tyre, the total number of eigenvalues is substantial. Therefore only real values of roll mode are shown in Figure 5.8. The eigenvalue results were compared with the number of tyres in contact with the road. It is evident that the transition to unstable behaviour coincides with the lift off of both inside tyres.

Therefore, it can be concluded that tyre loss of contact represents a reliable metric of rollover. In theory, it would be expected that if the point of loss of contact is reached and if there is the slightest roll velocity residue at that point, the manoeuvre would definitely result in a rollover situation.

However, simulations show that loss of contact in combination with a roll velocity residue do not necessarily lead to rollover, even without corrective intervention from the driver. Non-linearities in tyre forces and suspension and further loss of forward speed in case of a coast-down test-case mean that the vehicle might return to a stable state, even if the loss of contact is reached with a roll velocity residue.

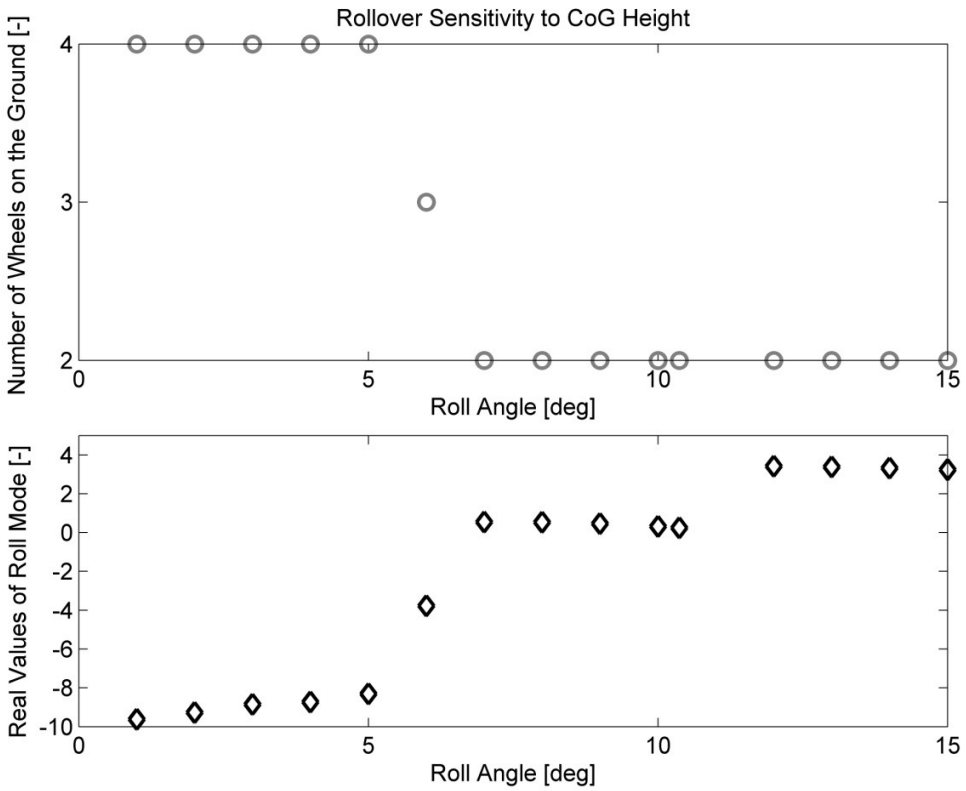

Figure 5.8 Number of tyres in contact with road and roll mode stability during steady state manoeuvre.

6. Suggested controller

6.1. Introduction

Currently existing control schemes try to prevent rollover at the cost of maintaining the vehicle path chosen by the driver. However such intervention into vehicle path can itself potentially be the source of an accident. The ideal rollover prevention control scheme should be able to mitigate rollover without influencing the vehicle path. Such a scheme, rather than reducing the indirect cause of the rollover i.e. the tyre lateral forces which influence lateral acceleration and therefore indirectly reduce the roll moment, would have to alleviate the direct cause, reducing the roll moment itself, allowing the lateral forces to be used for an obstacle avoidance manoeuvre. The ideal rollover control scheme therefore requires the application of external stabilising moment to the vehicle. The practical implementation of such a scheme is not trivial; introduction of a fifth wheel or a roof mounted jet engine could be seen as unreasonable. However, there exists an actuator which seems to be perfectly suited to this application. The torque reaction wheel (RW), commonly employed for altitude control of satellites, uses the principle of conservation of momentum to apply external moments to a satellite. There exists a wide literature concerning the use of torque reaction wheels in aeronautical applications e.g. [93-97]. The designs vary from three [97] to six [93] reaction wheels which are usually configured so that any three of them can provide controllability around all three axes of rotation, although alternative spherical rotors are also investigated [94]. The inertia properties of RW are a small fraction of the inertia of the object they are controlling, e.g. 0.107 kg*m^2 for RW compared to a 9000 kg*m^2 object [95]. From a brief examination of the literature one can also conclude that even rapid manoeuvres of satellites or spacecraft take in the region of 30s [96] and the maximum torques generated by the RW are relatively small. All of this means that even though the principles of operations in both spacecraft applications and vehicle rollover prevention are the same, the inertia, torque, power and energy requirements will be vastly different and they will determine whether such a system is feasible for rollover prevention. One potential implementation of the system is to become a secondary application of a kinetic energy recovery system (KERS) as such a system is likely to store enough momentum to be used in rollover prevention. This chapter will investigate the likely advantages as well as limitations of such an application. No existing literature has been found on the application of RW as a rollover prevention actuator.

6.2. Pendulum based controller

For the purpose of this study a simple controller was constructed based on the state space formulation of an inverted pendulum. The schematic of how the pendulum can be used to represent the vehicle in a near rollover situation is shown in Figure 6.1.

The pendulum properties calculated from the parameters of the vehicle in test condition (vehicle with 180kg roof load) are presented in Table 6.1.

Parameter	Description	Value	Unit
z_{CoG}	CoG above the ground	781.97	mm
tr_{fr}	Front track at contact patch	1641.9	mm
tr_{re}	Rear track at contact patch	1668.3	mm
m	Total vehicle mass	2556.0	kg
I	Total vehicle roll inertia	1374.9	kg m^2

Table 6.1 Vehicle parameters required to find properties of equivalent pendulum

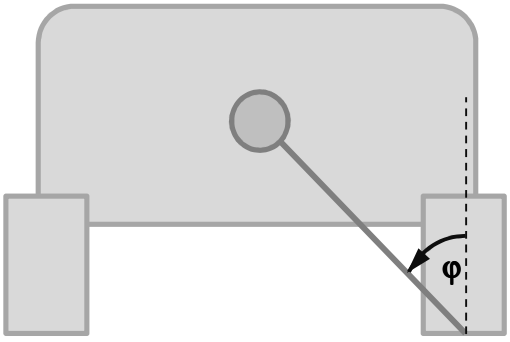

Figure 6.1 Pendulum representation of a vehicle during rollover.

Therefore the pendulum parameters can be calculated as follows:

$$tr_{av} = \frac{\left(tr_{fr} + tr_{re}\right)}{2} = 1655.1 \text{ mm} \quad \textbf{(6.1)}$$

$$l = \sqrt{{z_{CoG}}^2 + \left(\frac{tr_{av}}{2}\right)^2} = 1138.6 \text{ mm} \quad \textbf{(6.2)}$$

$$\varphi_{stat} = atan\left(\frac{tr_{av}}{2 \cdot z_{CoG}}\right) = 46.62° \quad \textbf{(6.3)}$$

Where:

l – length of the pendulum

tr_{av} – average track

φ_{stat} – angle of pendulum with vehicle in static condition

It is assumed that the vehicle is able to achieve 1g steady state lateral acceleration a_y, hence the steady state rollover critical pendulum angle φ_{crit} equals 45°. The effect of lateral acceleration and gravity can be substituted by effective gravity g_{eff} to linearise the pendulum's state space equations at φ_{crit} and calculate the natural frequency of the pendulum under these conditions:

$$g_{eff} = \sqrt{a_y^2 + g^2} = 13.873 \text{ m} \cdot \text{s}^{-1} \quad \textbf{(6.4)}$$

Angle α is defined as

$$\alpha = \varphi - \varphi_{crit} \quad \textbf{(6.5)}$$

The pendulum equations can now be written as:

$$m \cdot g_{eff} \cdot l \cdot \sin\alpha - (m \cdot l^2 + I) \cdot \ddot{\alpha} = 0 \quad \textbf{(6.6)}$$

$$\ddot{\alpha} = \frac{m \cdot g_{eff} \cdot l}{m \cdot l^2 + I} \cdot \sin\alpha \tag{6.7}$$

Linearisation for small angle change yields:

$$\sin\alpha = \alpha \tag{6.8}$$

Hence:

$$\ddot{\alpha} = \frac{m \cdot g_{eff} \cdot l}{m \cdot l^2 + I} \cdot \alpha \tag{6.9}$$

If

$$\omega = \dot{\alpha} \tag{6.10}$$

then

$$\begin{bmatrix} \dot{\alpha} \\ \dot{\omega} \end{bmatrix} = \begin{bmatrix} 0 & \omega \\ \frac{m \cdot g_{eff} \cdot l}{m \cdot l^2 + I} \cdot \alpha & 0 \end{bmatrix}$$

$$\begin{bmatrix} \dot{\alpha} \\ \dot{\omega} \end{bmatrix} = \begin{bmatrix} 0 & 1 \\ \frac{m \cdot g_{eff} \cdot l}{m \cdot l^2 + I} & 0 \end{bmatrix} \begin{bmatrix} \alpha \\ \omega \end{bmatrix} \tag{6.11}$$

Eigenvalues are calculated by:

$$\begin{bmatrix} 0 & 1 \\ \frac{m \cdot g_{eff} \cdot l}{m \cdot l^2 + I} & 0 \end{bmatrix} \begin{bmatrix} \alpha \\ \omega \end{bmatrix} = \lambda \begin{bmatrix} \alpha \\ \omega \end{bmatrix}$$

$$\begin{bmatrix} -\lambda & 1 \\ \frac{m \cdot g_{eff} \cdot l}{m \cdot l^2 + I} & -\lambda \end{bmatrix} \begin{bmatrix} \alpha \\ \omega \end{bmatrix} = 0 \tag{6.12}$$

Find determinant of:

$$\begin{vmatrix} -\lambda & 1 \\ \frac{m \cdot g_{eff} \cdot l}{m \cdot l^2 + I} & -\lambda \end{vmatrix} = \lambda^2 - \frac{m \cdot g_{eff} \cdot l}{m \cdot l^2 + I} = 0 \tag{6.13}$$

$$\lambda = \pm\sqrt{\frac{m \cdot g_{eff} \cdot l}{m \cdot l^2 + I}} = \pm 2.9345 \tag{6.14}$$

As expected the eigenvalue of the inverted pendulum has positive real values. In order to stabilise the pendulum a closed loop control system is necessary. To find the controller gains a state space formulation is employed. The closed loop system response poles and zeros are chosen to achieve damped frequency of 10Hz and 0.6 fraction of critical damping (i.e. poles at $s = -47.1 \pm 62.8i$). The frequency of the closed loop system is over 4 times higher than the plant dynamics; the damped frequency of roll for a full vehicle model traveling in a straight line equals 2.34Hz. Such a high frequency is chosen because the operation of the system is safety critical and therefore the system's response in an emergency situation needs to be rapid. However due to these high dynamic system requirements, a high level of power and torque demand is expected.

Therefore the state space controller takes the form of:

$$\dot{\mathbf{x}} = \mathbf{A}\mathbf{x} + \mathbf{B}\mathrm{u} \tag{6.15}$$

$$\mathrm{u} = -\mathbf{K}\mathbf{x} \tag{6.16}$$

$$\mathbf{A} = \begin{bmatrix} 0 & 1 \\ \dfrac{m \cdot g_{eff} \cdot l}{m \cdot l^2 + I} & 0 \end{bmatrix} \tag{6.17}$$

$$\mathbf{B} = \begin{bmatrix} 0 \\ \dfrac{1}{m \cdot l^2 + I} \end{bmatrix} \tag{6.18}$$

The next step is to find gains:

$$\mathbf{K} = [\boldsymbol{K_1} \quad \boldsymbol{K_2}] \tag{6.19}$$

which will give a closed loop system damped frequency of 10Hz and 0.6 fraction of critical damping. This can be achieved by expanding (6.15) into

$$\begin{bmatrix}\dot{\alpha}\\ \dot{\omega}\end{bmatrix} = \begin{bmatrix}0 & 1\\ \dfrac{m\cdot g_{eff}\cdot l - K_1}{m\cdot l^2 + I} & \dfrac{-K_2}{m\cdot l^2 + I}\end{bmatrix}\begin{bmatrix}\alpha\\ \omega\end{bmatrix} \tag{6.20}$$

The characteristic equation of a closed loop system is

$$\begin{aligned}\det(s\mathbf{I} - (\mathbf{A} - \mathbf{BK})) &= \det\left(\begin{bmatrix}s & 0\\ 0 & s\end{bmatrix} - \begin{bmatrix}0 & 1\\ \dfrac{m\cdot g_{eff}\cdot l - K_1}{m\cdot l^2 + I} & \dfrac{-K_2}{m\cdot l^2 + I}\end{bmatrix}\right)\\ &= \det\left(\begin{bmatrix}s & -1\\ -\dfrac{m\cdot g_{eff}\cdot l - K_1}{m\cdot l^2 + I} & s - \dfrac{K_2}{m\cdot l^2 + I}\end{bmatrix}\right)\\ &= s^2 - \frac{sK_2}{m\cdot l^2 + I} - \frac{m\cdot g_{eff}\cdot l - K_1}{m\cdot l^2 + I}\end{aligned} \tag{6.21}$$

Hence, taking into account the desired closed loop system damped frequency of 10Hz and 0.6 fraction of critical damping (i.e. poles at $s = -47.1 \pm 62.8i$) the desired characteristic equation is:

$$\big(s - (-47.1 - 62.8i)\big)\big(s - (-47.1 + 62.8i)\big) = s^2 + 94.2s + 6162.25 = 0$$

Therefore the gains can be found as:

$$s^2 + \frac{sK_2}{m\cdot l^2 + I} - \frac{m\cdot g_{eff}\cdot l - K_1}{m\cdot l^2 + I} = s^2 + 94.2s + 6162.25$$

$$K_1 = 6162.25\cdot(m\cdot l^2 + I) + m\cdot g_{eff}\cdot l$$

$$K_2 = 94.2\cdot(m\cdot l^2 + I)$$

The control system derived above was incorporated into the full vehicle model equipped with a torque reaction wheel. Before the simulation was performed, the activation condition was set so that the controller is only active when the pendulum angle is smaller than 40º (note that 0º is a purely vertical pendulum) whilst aiming to maintain 40º pendulum angle.

The first simulation results look promising. The controller is able to prevent the vehicle from rolling over (Figure 6.2). Moreover the vehicle path is tighter than for the vehicle without the controller (Figure 6.3). This means that in principle the control scheme is able to achieve the two main requirements characterising ideal rollover control.

However the torque and power requirements generated are unrealistically high as shown in Figure 6.4. Due to this very high demand the pendulum controller has very little practical significance. As a rollover situation is always a safety critical event, the control system should always aim to apply

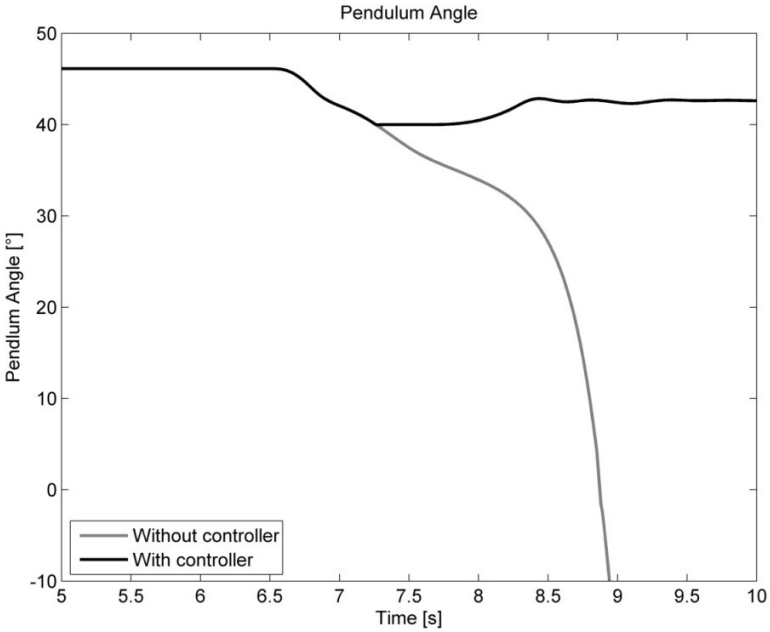

Figure 6.2 Pendulum angle with and without the controller

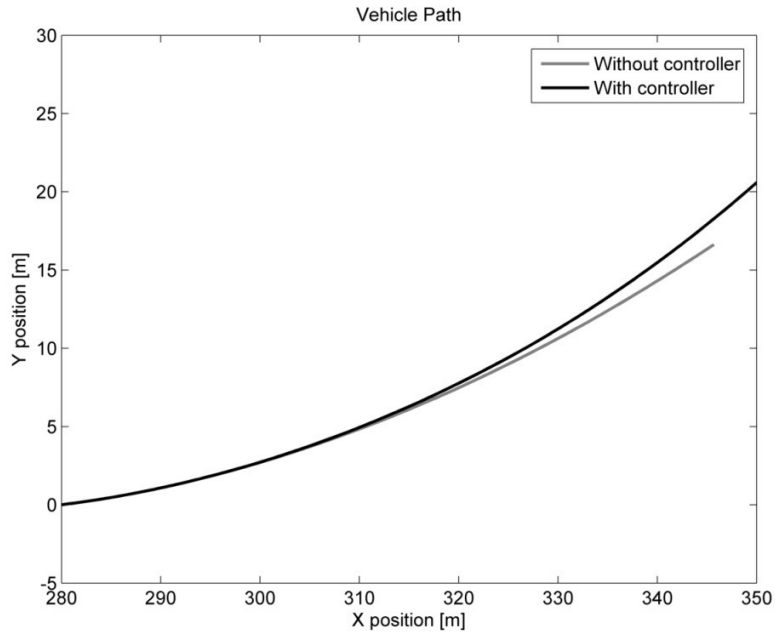

Figure 6.3 Vehicle path with and without the controller

all available power in order to restore the vehicle roll stability. Therefore, the main focus of the next investigation should be on maximising the effectiveness of the actuator to reduce its torque, power and energy consumption. For this stage of the study the controller itself can be as simple as a

pendulum angle-based on-off trigger, hence the structure of the controller will not be investigated any further at this point.

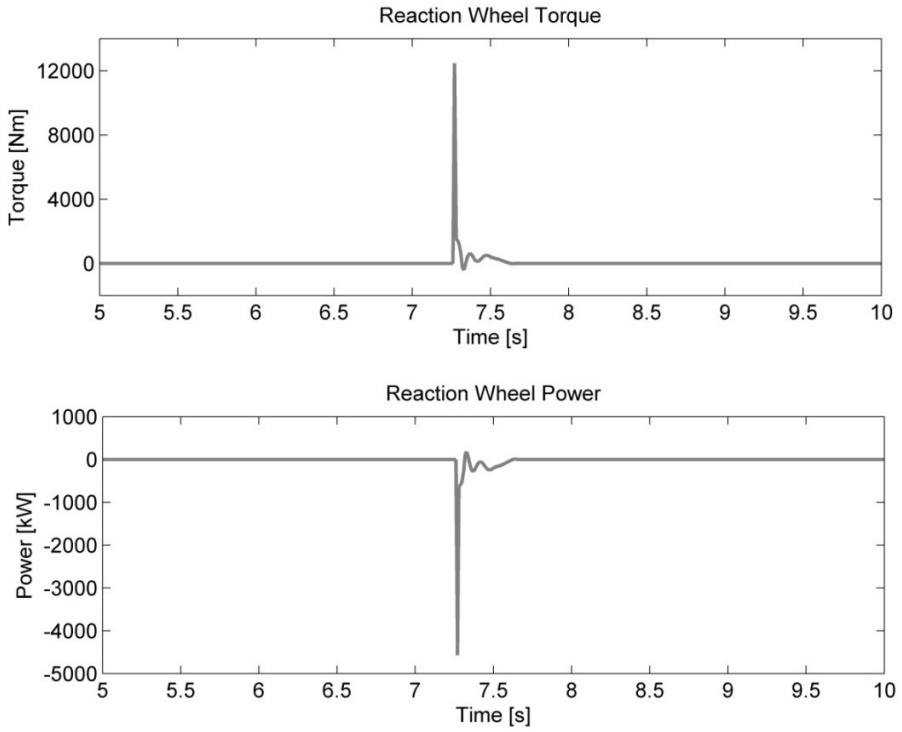

Figure 6.4 Torque and power requirements

6.3. Actuator limitations

As initial runs with RW showed that the demands which the simple controller places on the actuator are rather extreme, the actuator limitations are investigated first of all. The potential actuator limitations are:

- Maximum stabilising torque
- Maximum power - As torque acts over time the rotational velocity of the RW increases, and therefore the actuator power limit may be reached. The limit is determined by the maximum rotational velocity, electrical power supply (in the case of accelerating RW), brake power (in the case of braking of RW) etc.
- Maximum energy consumed in one instance – as power acts over a period of time the overall energy consumption increases

The relationship between the torque, power and energy is governed by the inertia of the reaction wheel. Reaction wheel torque and acceleration is described by the following equation:

$$\ddot{\beta} = \frac{T}{I_{RW}} \tag{6.22}$$

The power of the reaction wheel is described by the following equation:

$$P = T \cdot \dot{\beta} \tag{6.23}$$

And finally the total energy consumption between the controller activation time t_{start} and controller deactivation time t_{end} is described by:

$$E_{total} = \int_{t_{start}}^{t_{end}} T \cdot \dot{\beta} \cdot dt \tag{6.24}$$

For the case where the reaction wheel is able to instantaneously generate the maximum torque, the power can be calculated from:

$$P_{max} = T \cdot \dot{\beta}_{end} = T \cdot \ddot{\beta} \cdot (t_{end} - t_{start}) = \frac{T^2}{I_{RW}} \cdot (t_{end} - t_{start}) \tag{6.25}$$

The energy can be found as follows:

$$dE = P \cdot dt = \frac{T^2}{I_{RW}} \cdot t \cdot dt \tag{6.26}$$

$$\int_{t_{start}}^{t_{end}} dE = \frac{T^2}{I_{RW}} \cdot \int_{t_{start}}^{t_{end}} t \cdot dt \tag{6.27}$$

$$E_{total} = \frac{T^2}{I_{RW}} \cdot \frac{(t_{end} - t_{start})^2}{2} \tag{6.28}$$

From a brief investigation of the equations one can conclude that the higher the inertia of the reaction wheel, the lower the power and energy consumption. For the extreme example of a reaction wheel with infinite inertia, the power and energy consumption would equal:

$$\lim_{I_{RW} \to \infty} P = 0 \tag{6.29}$$

$$\lim_{I_{RW}\to\infty} E_{total} = 0 \tag{6.30}$$

For the purpose of this study a fairly large, but not unreasonable, reaction wheel inertia of 1 kg m^2 has been assumed.

Firstly let us consider the torque limitation of the actuator. The vehicle model is in its test condition (180kg roof load, tyre friction scaling factor set to 1.375, standard steering input). The critical pendulum angle, below which the actuator is triggered, is always set to 40º unless a study on optimum critical angle is performed.

A torque limit influence on rollover propensity is investigated by finding a rollover critical velocity, using the process described in section 5.1, for a range of maximum torque limits of 0Nm to 400Nm. The result of the study, shown in Figure 6.5, suggests that there is a linear relationship between maximum available torque and rollover critical velocity. Interestingly, even applying a 100Nm of torque can increase the rollover critical velocity to 41.09m/s from 37.34m/s for the vehicle with no controller – a not insignificant 10% increase.

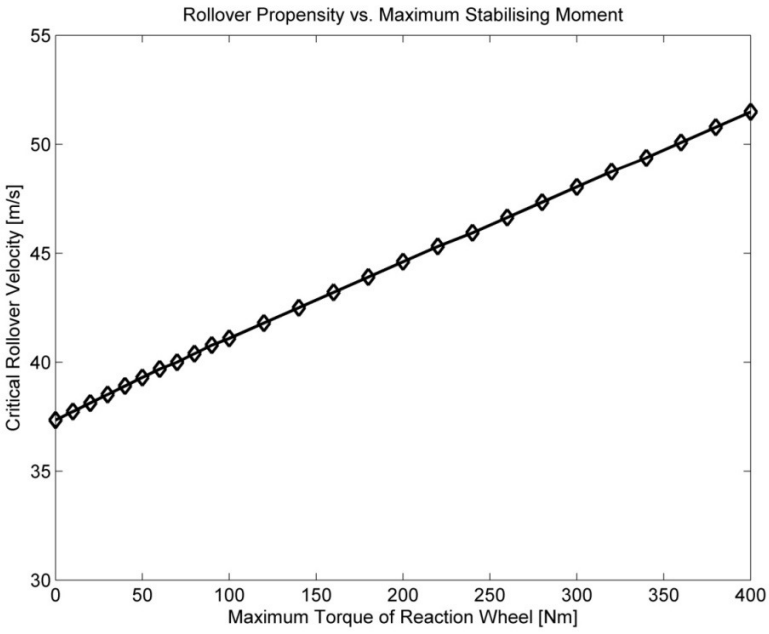

Figure 6.5 Influence of maximum torque on vehicle rollover propensity

An interesting point of investigation is how the pendulum trigger angle influences the rollover propensity. A brief investigation regarding this has been carried out under a maximum torque limitation of 100Nm. The results show that there exists an optimum pendulum angle at which the actuator is triggered (Figure 6.6). Below this angle the relationship is approximately linear. However, this optimum angle of 43.5º is relatively close to the angle corresponding to the vehicle running straight (46.6º) and larger than the angle at which lift off of both wheels usually occurs i.e. ~42.2º. Therefore using the optimum pendulum angle to trigger the actuator may lead to the control system intervening when rollover is not imminent. From the driver's perspective such unnecessary interruption from the safety system is always unwelcome, therefore a pendulum angle lower than optimum would have to be used to initiate control action.

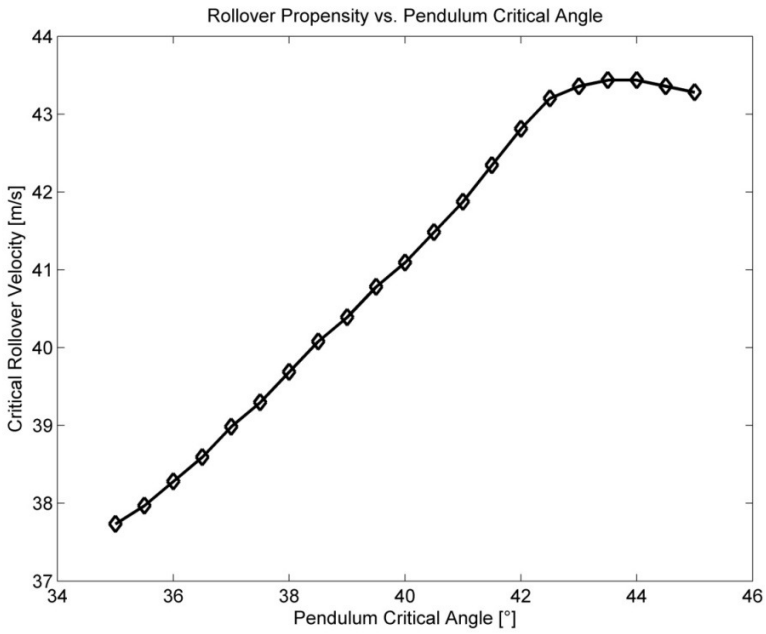

Figure 6.6 Rollover propensity as a function of pendulum critical angle under maximum torque limitation of 100Nm

If the maximum torque is maintained for a prolonged period of time (as in this case) the actuator rotational velocity increases which in turn leads to increased power consumption. Therefore in the next step the actuator power limitation has been investigated under the assumption of a maximum actuator torque of 100Nm. The actuator model applies the maximum torque until the maximum power is reached, and past that point torque equal to

$$T = \frac{P_{limit}}{\dot{\beta}} \tag{6.31}$$

is applied. The result of this study is shown in Figure 6.7.

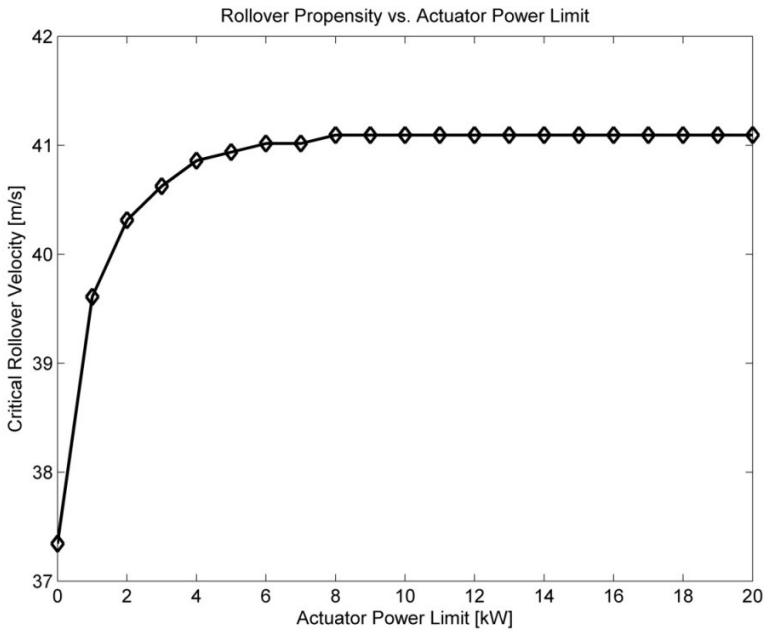

Figure 6.7 Rollover propensity vs. maximum actuator power under maximum torque limitation of 100Nm.

The result shows that power constraints most affect the ability to influence vehicle rollover propensity in the lower region of the investigated power levels. This is despite the fact that the imposed power limit influences the available actuator torque even for the 20kW simulation (the peak power in unrestricted simulation is 24.57kW). This is because the actuator is applying the torque all the time whilst the pendulum angle is below the critical level. However in the final stage of the actuation the pendulum angle is already increasing which means that the vehicle is returning to its stable condition. This highlights the fact that the actuator deployment strategy would be more effective if it were based on other rollover predictors (e.g. momentum, stability etc.) rather than the pendulum angle (which in turn is closely related to roll angle). As the power limit did not affect rollover resistance above 8kW, the study was repeated with the maximum torque set to 200Nm. The results shown in Figure 6.8 confirm that there is a non-linear relationship between the maximum power and rollover critical velocity.

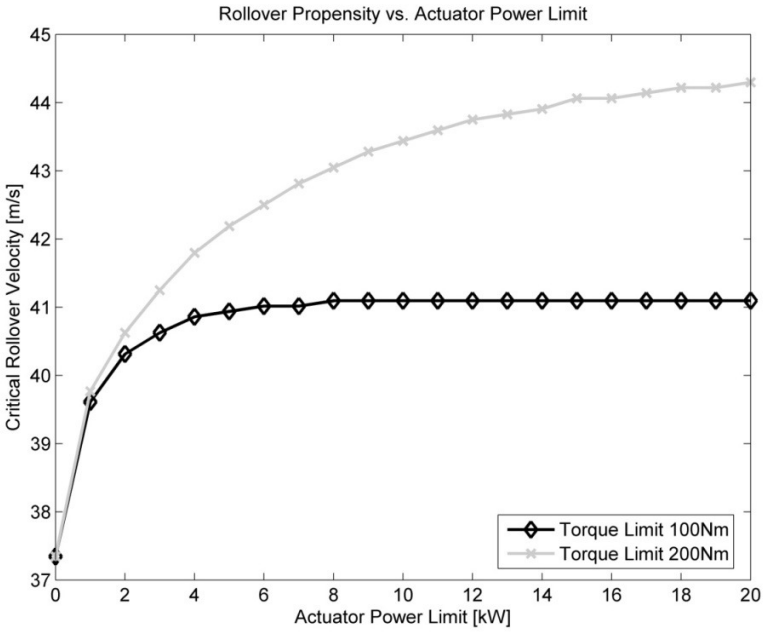

Figure 6.8 Rollover propensity vs. maximum actuator power under maximum torque limitations of 100Nm and 200Nm.

As in the case of maximum torque, a brief investigation was carried out into the influence of pendulum critical (trigger) angle on rollover resistance under the maximum torque limitation of 100Nm and maximum power limitation of 5kW. The results, shown in Figure 6.9, demonstrate a linear relationship between pendulum critical angle and rollover resistance in lower values of pendulum critical (trigger) angle. However this relationship turns into a highly non-linear one with a clearly defined optimum for the higher pendulum angles. Under given constraints the actuator is most effective when the pendulum critical (trigger) angle is set to 43º. The investigation into power limitations was repeated for maximum powers of 3kW and 1kW. The combined result is shown in Figure 6.10, and demonstrates that the optimum pendulum critical (trigger) angle is dependent on the power limitations. The lower the power limit, the lower the optimum critical angle.

At the next stage energy limitations were investigated. A relationship between rollover propensity and the total energy consumed is shown in Figure 6.11. This relationship is highly non-linear up to an energy limit of 4kJ. Above this value the energy limit is not reached hence rollover propensity is not sensitive to an energy limit when constrained with a maximum torque of 100Nm and maximum

power of 5kW. If the maximum torque is increased to 200Nm with maximum power limit still set to 5kW, the energy limit above which the propensity is not affected is in the region of 5.5kJ (Figure 6.12).

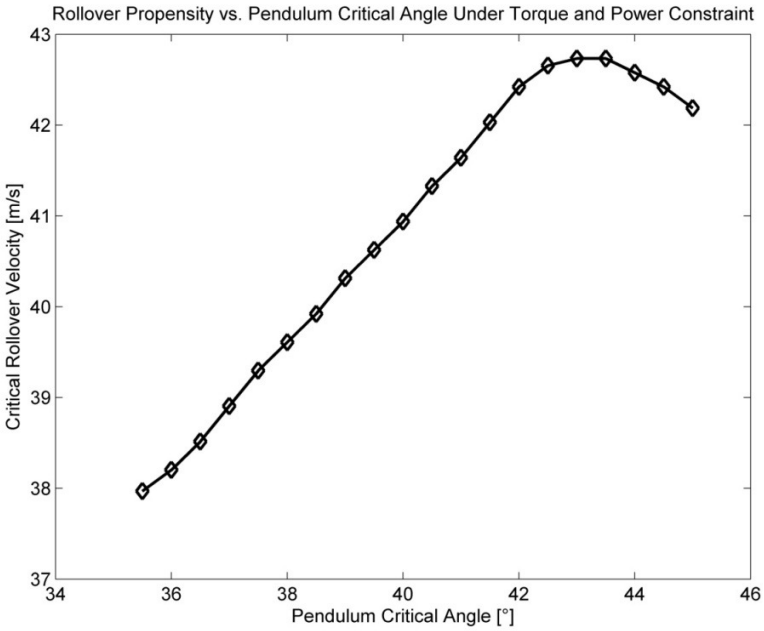

Figure 6.9 Rollover propensity vs. pendulum critical angle under torque and power constraint

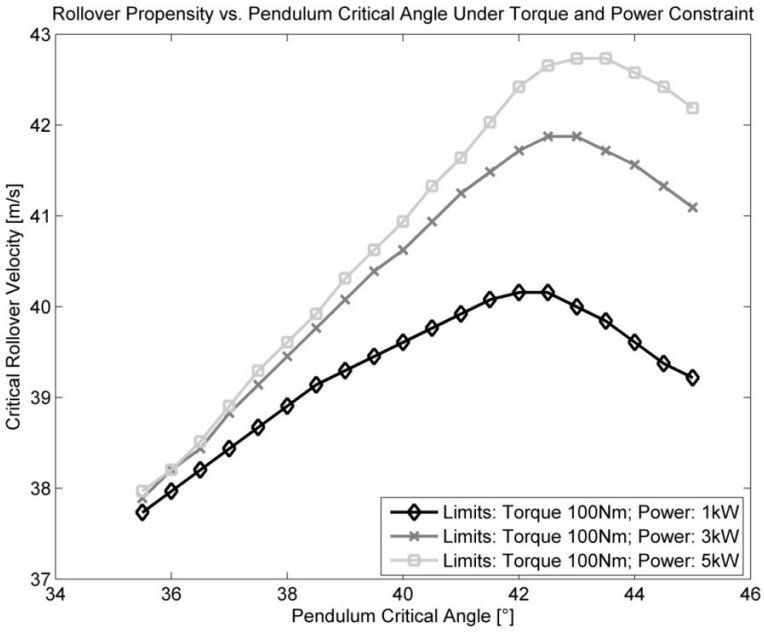

Figure 6.10 Rollover propensity vs. pendulum critical angle under maximum torque of 100Nm and power constraints of 1kW, 3kW and 5kW

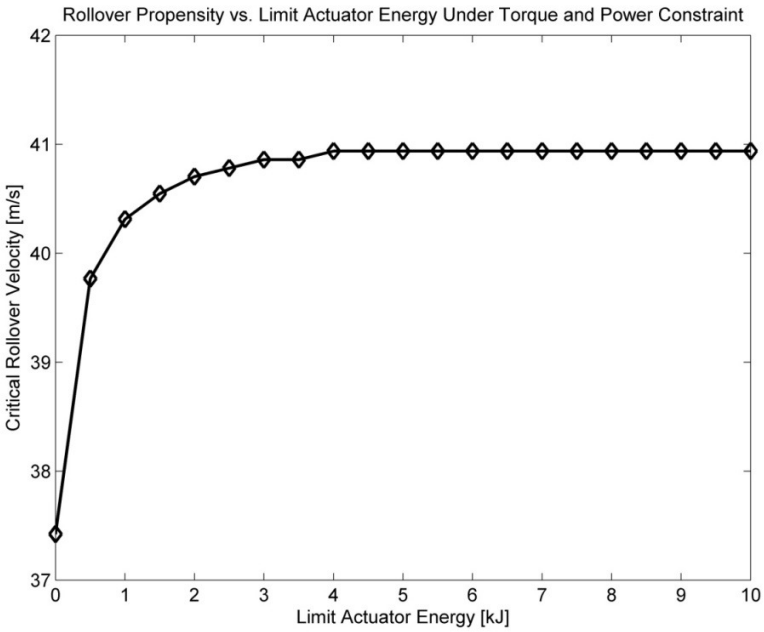

Figure 6.11 Rollover propensity vs. actuator energy under torque and power constraints (note: for unrestricted energy run total energy consumption equals 11.12kJ)

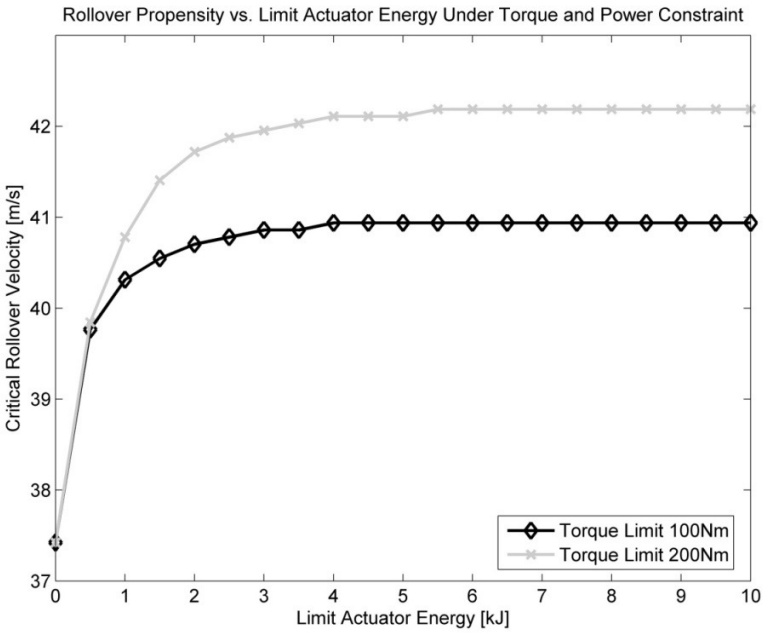

Figure 6.12 Rollover propensity vs. actuator energy under torque constraint of 100Nm and 200Nm and power constraint of 5kW

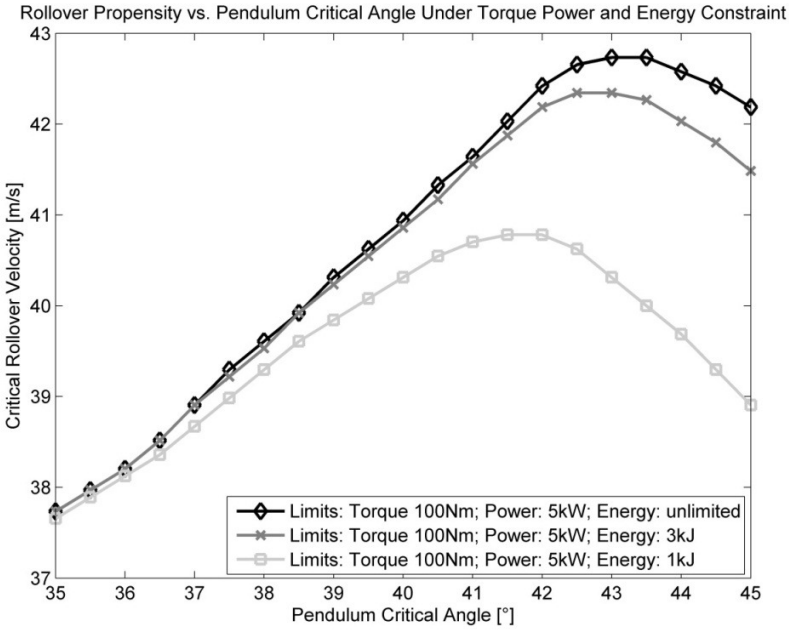

Figure 6.13 Rollover propensity vs. pendulum critical angle under torque constraint of 100Nm and power constraint of 5kW and various energy constraints.

Finally, the optimum pendulum critical angle is found under a 100Nm torque limit, a 5kW power limit and unlimited energy or energy limited to 1kJ, 3kJ. From the results shown in Figure 6.13 it is clear that the lower the energy limit, the lower the optimum pendulum critical angle at which the actuator is deployed.

Even though the actuator is able to prevent rollover with a high but realistic torque, power and energy requirements, the practical application of such a system brings cost, weight and packaging challenges. Especially as the actuator is potentially going to be used very rarely, if ever, during the life of a vehicle. Therefore the proposed control scheme could potentially be implemented as a secondary function of the KERS system in vehicles with a low rollover threshold. Such a solution makes much more economic sense. To enable the generation of stabilising torque based on the energy stored in KERS without affecting its efficiency, a potential system could take the form of:

- Clutch connecting to KERS in the event of emergency
- Braking system

The requirements from KERS used as an anti-rollover actuator are examined based on information concerning the KERS system developed for Formula 1[98]. The parameters of Flybrid KERS are shown in Table 6.2:

Parameter	Description	Value	Unit
E_{kin}	Total kinetic energy	400	kJ
P	Power	60	kW
$\dot{\beta}_{max}$	Maximum angular velocity	60000	rpm

Table 6.2 Parameters of Flybrid KERS system [98]

Based on available data a number of other parameters can be found. Time to store or recover the energy equals:

$$t = \frac{E_{kin}}{P} = 6.667s \tag{6.32}$$

The flywheel inertia is calculated from:

$$I_{flywheel} = \frac{2 \cdot E_{kin}}{\dot{\beta}_{max}^{\ 2}} = 0.02026\text{kg} \cdot \text{m}^2 \tag{6.33}$$

The torque at the flywheel at highest flywheel velocity can be found as:

$$T_{flywheel} = \frac{P}{\dot{\beta}_{max}} = 9.549\text{Nm} \tag{6.34}$$

However to maintain constant power, the torque must increase in an inversely proportional manner to the flywheel velocity. Therefore the torque found from equation (6.34) is not the maximum torque that can be applied directly to the flywheel. Assuming that the system is still able to extract the 60kW of energy at 6000rpm, the braking torque applied directly to the flywheel is 95.49Nm – much closer to 100Nm reaction wheel case examined earlier in this chapter. If a constant torque of 95.49Nm is applied to dissipate the entire energy stored in the flywheel then the total time of such an operation can be found from:

$$t_{operation} = \frac{\sqrt{E_{total} \cdot I_{RW} \cdot 2}}{T} = 1.333\text{s} \tag{6.35}$$

In order to apply 100Nm at the flywheel a brake with a radius of $r = 0.1\text{m}$ and friction coefficient $\mu = 0.4$ would require clamping force of

$$F_{clamping} = \frac{T}{r \cdot \mu} = 2500\text{N} \tag{6.36}$$

Such a level of clamping force is not unknown in conventional braking systems. The calculations shown here prove that an anti-rollover control scheme using a KERS flywheel as a torque reaction wheel is possible although not without challenges.

6.4. Conclusions

Based on this brief investigation into reaction wheel based rollover control, one can conclude that the torque power and energy requirements of such a control system are not unreasonable. In fact, based on a 1kg m^{-2} inertia of the reaction wheel, 100Nm maximum torque, 5kW maximum power and 3kJ of total energy one can potentially increase the rollover critical velocity to 42.35m/s compared to 37.42m/s for a vehicle with no actuator. This however would require activating the actuator reasonably early which could potentially lead to unnecessary interventions. If the actuator were activated at a more realistic 40º of pendulum angle, the rollover velocity could still be significantly increased (to 40.86m/s) over the case with no controller – results shown in Figure 6.14, Figure 6.15 and Figure 6.16. Additionally such a control scheme allows the driver to maintain the desired vehicle path as presented in Figure 6.15. This leads to the conclusion that this rollover control scheme is worth investigating further. A control scheme such as that presented by Eger et al. [23] or Choi [46], able to recognise a near rollover situation, would allow us to further increase the effectiveness of the actuator by triggering it at greater pendulum angles, potentially even before wheel lift off.

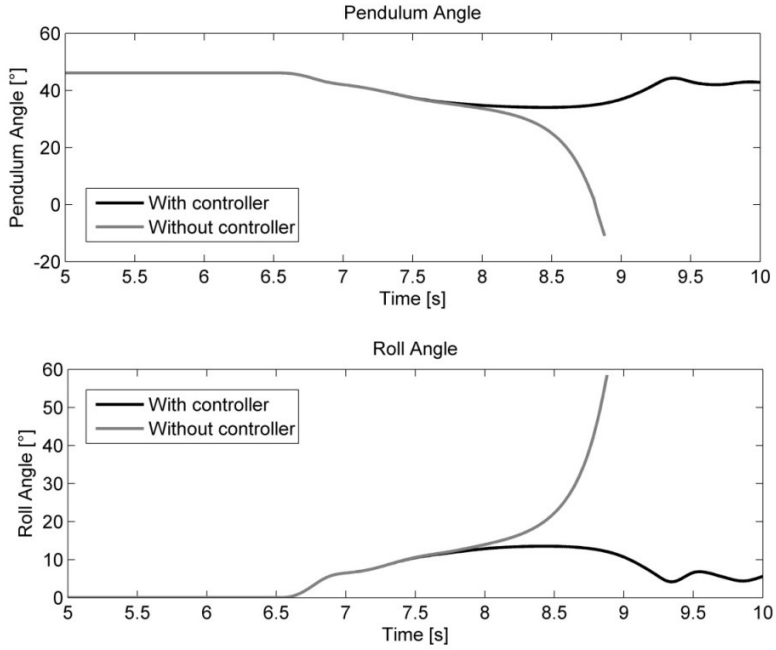

Figure 6.14 Vehicle roll and pendulum angles for simulation without and with controller; the latter is limited to 100Nm of torque, 5kW of power and 3kJ of energy

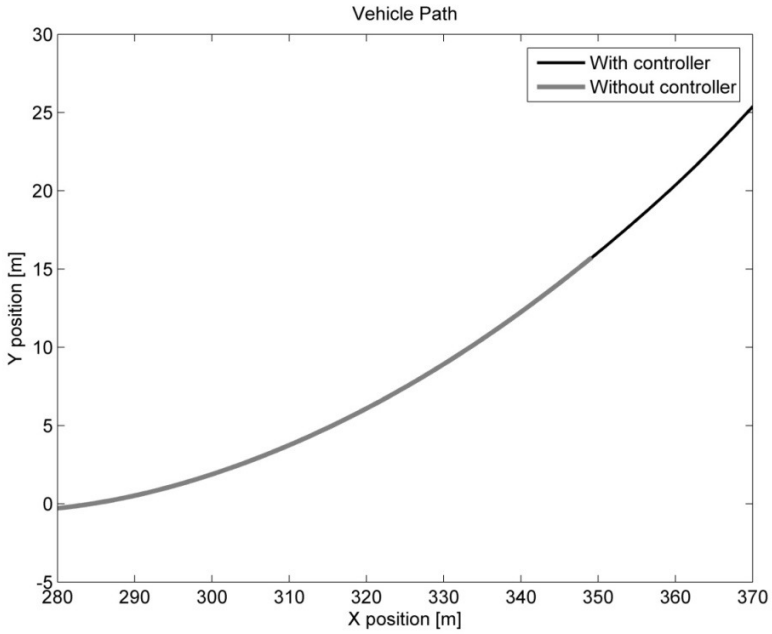

Figure 6.15 Vehicle CoG path for simulation without and with controller; the latter is limited to 100Nm of torque, 5kW of power and 3kJ of energy

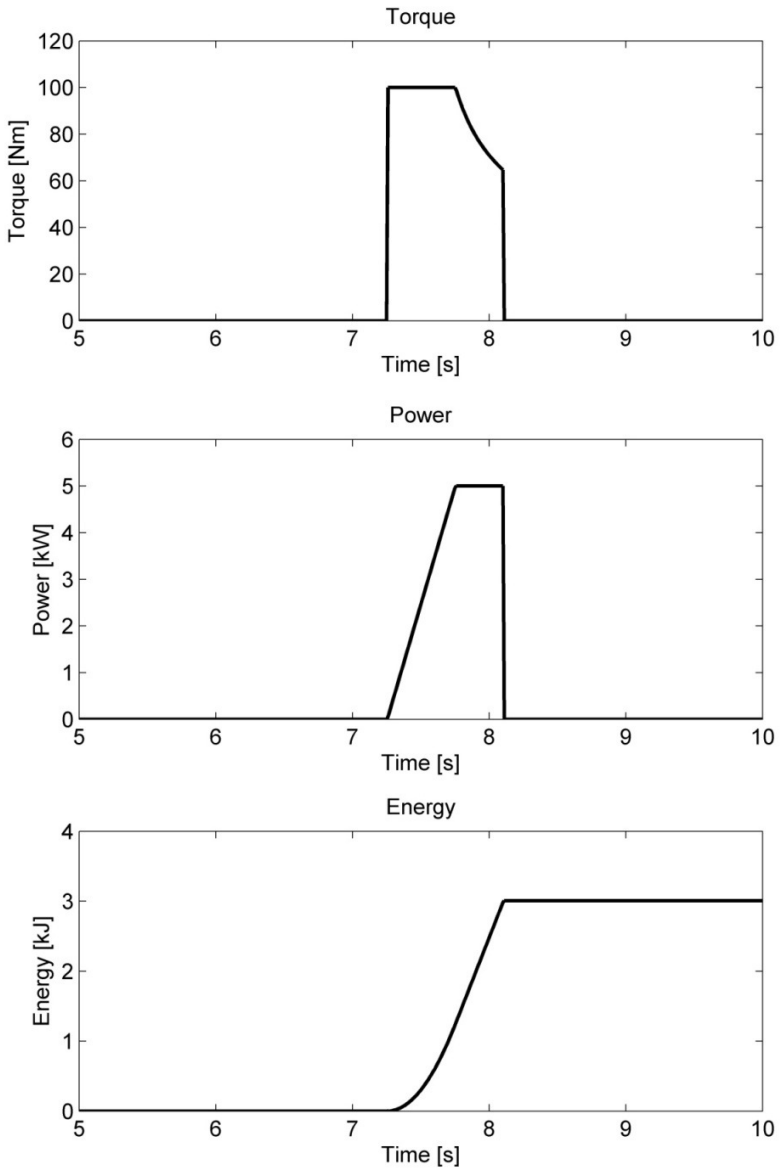

Figure 6.16 Reaction wheel torque, power and energy consumption for simulation without and with controller; the latter is limited to 100Nm of torque, 5kW of power and 3kJ of energy

7. Conclusions and recommendations for further work

This chapter summarises research aimed at understanding the untripped rollover dynamics of an SUV. Section 7.1 provides principal conclusions from the program of research, and section 7.2 discusses recommendations for future work.

7.1. Principal conclusions and fulfilment of research objectives

The research objectives outlined in Chapter 2 have largely been met.

Firstly the high fidelity non-linear model has been built. The chosen level of model complexity meant that the limitations of simpler models used commonly in rollover research could be overcome. Furthermore the high fidelity model has been correlated against physical data. The validated model provided a very good representation of the physical vehicle. This ensured that the results of all the studies performed using this model have a high level of confidence.

Secondly, a rollover propensity measurement has been thoroughly considered and developed. The proposed rollover metric bears a close resemblance to the real world situation. Moreover, as presented in Chapter 5, the metric is very sensitive to changes in vehicle parameters which allows an evaluation of the influence of vehicle characteristics on rollover with greater precision. Therefore the rollover propensity measurement developed here provides a reliable platform for measuring the influence of vehicle properties on rollover.

Thirdly, the influence of tyre properties on rollover has been systematically examined and the properties ranked in order of importance. The design of experiment technique employed in the study ensured that the conclusions were drawn from the experiment in an efficient and robust manner. The result of the study showed that the most influential tyre parameters on vehicle rollover are:

- peak friction coefficient
- camber stiffness
- friction variation with load
- overturning moment

- tyre vertical stiffness

The next research objective, understanding the influence of suspension system characteristics on rollover propensity, has been studied using a novel approach based on statistical methods. The approach consists of generating a large number of results with low level suspension parameters, such as hardpoints and stiffnesses, varied using a Latin Hypercube. For each result, the suspension properties are characterised using a number of metrics and the corresponding vehicle rollover propensity is found. The former information becomes a new input to the experiment whereas the latter is an output. The two pieces of information are then linked together using step wise regression. The resulting equation describing the critical rollover velocity response surface provides valuable information on the suspension properties which are most important in rollover prevention. This two-level approach allowed the study of the influence of suspension characteristics on vehicle rollover by changing low level suspension parameters. A high level of realism was therefore maintained throughout this study. Research revealed that the most influential properties are:

- front and rear suspension rate
- front roll stiffness
- front camber gain
- front and rear camber compliance
- rear jacking force.

Finally a novel control scheme based on a reaction wheel actuator was proposed. The control system allows vehicle rollover to be mitigated without affecting the path of the vehicle. Conclusions from the conducted investigation are:

- the actuator prevents rollover without altering vehicle path
- the torque, power and energy required to make significant improvement in rollover resistance are not unrealistic. Namely, up to 100Nm of torque, 5kW of power and 3kJ of energy is required to increase the critical rollover velocity by over 9%.

The calculations of torque, power and energy demands required to make a significant improvement in rollover resistance showed that although these requirements are high, the system could potentially become a secondary function of the KERS system on vehicles with a low rollover threshold.

The above developments in the field have the potential to positively contribute to the reduction of rollover accidents on the road and improve the statistical data cited in Chapter 1 for years to come.

7.2. Recommendations for further work

The research has highlighted several areas that could benefit from further investigation.

Firstly the study on suspension and tyre properties highlighted that tyre camber stiffness and suspension camber stiffness are significant factors with regard to rollover. The exact mechanism behind these phenomena has not been fully investigated. Additionally the study on suspension properties affecting rollover could be expanded by inclusion of damper characteristics. Generally speaking, the higher the damping the higher the vehicle rollover resistance [13], however the magnitude of this effect needs to be quantified and compared to other tyre and suspension properties.

The stability analysis revealed that after the lift off of the second wheel, the roll mode becomes unstable. However another effect has been observed, namely there exists a step change in roll stability at high roll angles, when the vehicle is already traveling on only two wheels. An in-depth study of this phenomenon would be beneficial for understanding how vehicle stability can be recovered at these high roll angles.

Finally the suggested innovative control scheme based on a torque reaction wheel uses a simple method based on pendulum angle for determining when the actuator should be engaged. In order to maximise the effectiveness of the actuator a more advanced predictive rollover algorithm such as that presented by Eger et al. [23] or Choi [46] could be employed.

8. References

[1] Nader, R., 1965, *Unsafe at any speed. The Designed-In Dangers of The American Automobile*, Grossman Publishers

[2] National Highway Traffic Society Administration, 1972, *Evaluation of the 1960-1963 Corvair Handling and Stability*, Technical Report

[3] Teknikens Värld, 1997, *Mercedes-volten*, 23/1997

[4] ADAC, 2010, *Der ADAC-Ausweichtest: Nie ohne ESP* [Online] Available from: http://www.adac.de/_mmm/pdf/tuz_fas_iftk_nie_ohne_esp_26397_51200.pdf [Accessed: 28th September 2014]

[5] Teknikens Värld, 2007, *Livsfarligt Toyota!* 23/2007

[6] Teknikens Värld, 2012, *Jeep Grand Cherokee moose test failure – the full story on film* [Online] Available from: http://teknikensvarld.se/jeep-grand-cherokee-moose-test-failure-the-full-story-on-film-120535. [Accessed: 28th September 2014]

[7] National Highway Traffic Society Administration, 2007, *Traffic Safety Facts 2005: A Compilation of Motor Vehicle Crash Data from the Fatality Analysis Reporting System and the General Estimates System*, Technical Report

[8] Altman, S., Santistevan, D., Hitchings, C., 2002, *A Comparison of Rollover Characteristics for Passenger Cars, Light Duty Trucks and Sport Utility Vehicles*, SAE Technical Paper 2002-01-0942

[9] Solmaz, S., Corless, M., Shorten, R., 2007, *A methodology for the design of robust rollover prevention controllers for automotive vehicles with active steering*, International Journal of Control, Vol. 80, No. 11, 1763-1779

[10] Parenteau, C., S., Viano D., C., Shah, M., Gopal, M., Davies, J., Nichols, D., Broden, J. 2003, *Field relevance of a suite of rollover test to real-world crashes and injuries*, Accident Analysis and Prevention, Vol 35, 103-110

[11] Acarman, T., Özgüner, Ü., 2006, *Rollover Prevention for Heavy Trucks Using Frequency Shaped Sliding Mode Control*, Vehicle System Dynamics, 44:10, 737-762

[12] Baumann, F., W., Lutz, E., 2004, *Effects Causing Untripped Rollover of Light Passenger Vehicles in Evasive Maneuvers*, SAE Technical Paper 2004-01-1057

[13] Dahlberg, E., 2000, *A Method Determining the Dynamic Rollover Threshold of Commercial Vehicles*, SAE Technical Paper 2000-01-3492

[14] Hac, A., Brown, T., Martens, J., 2004, *Detection of Vehicle Rollover*, SAE Technical Paper 2004-1-1757

[15] Jazar, R., N.,2008, *Vehicle Dynamics: Theory and Application*, Springer

[16] Hyun, D., Langari, R., 2003, *Modeling to Predict Rollover Threat of Tractor-Semitrailers*, Vehicle System Dynamics, 39:6, 401-414

[17] Kim, H., -J., Park, Y., -P., 2004, *Investigation of robust roll motion control considering varying speed and actuators dynamics*, Mechatronics 14, 35-54

[18] Rahnejat, H., 1998, *Multi-Body Dynamics: Vehicles, Machines and Mechanisms*, John Wiley & Sons, Inc., London

[19] Shabana, A., A., 2005, *Dynamics of Multibody Systems, Edition 3*, John Wiley & Sons, Inc.

[20] Wallrapp, O., 2004, *Review of Past Developments in Multibody System Dynamics at DLR - From FADYNA to SIMPACK*, Vehicle System Dynamics, 41:5, 339-348

[21] Shim, Taehyun and Ghike, Chinar, 2007, *Understanding the limitations of different vehicle models for roll dynamic studies*, Vehicle System Dynamics, 45:3, 191-216

[22] Ghike, Ch., Shim, T., 2006, *14 Degree-of-Freedom Vehicle Model for Roll Dynamics Study*, SAE Technical Paper 2006-01-1277

[23] Eger, R., Kiencke, U., 2003, *Modeling of rollover sequences*, Control Engineering Practice, 11, 209-216

[24] Hussain, K., Stein, W., Day, A.J., 2005, *Modeling commercial vehicle handling and rolling stability*, Proc. IMechE Vol. 219, Part K: Journal of Multi-body Dynamics

[25] Jones, R., A., 1999, *Understanding Vehicle Roll Using Mechanism Simulation Software*, SAE Technical Paper 1999-01-0030

[26] Durali, M., Kassaiezadeh, A., R., 2002, *Design and Software Base Modelling of Anit-Roll System*, SAE Technical Paper 2002-01-2217

[27] Wielenga, T., J., 1999, *A Method for Reducing On-Road Rollovers – Anti-Rollover Braking*, SAE Technical Paper 1999-01-0123

[28] Wielenga, T., J., 2000, *A Study in Rollover Prevention Using Anti-Rollover Braking*, SAE Technical Paper 2000-01-1642

[29] Vaculin, O., Krüger, R., W., Valasek, M., 2004, *Overview of Coupling of Multibody and Control Engineering Tools*, Vehicle System Dynamics, 41:5, 415-429

[30] Marimuthu, R., P., Jang, B. –C., Hong, S., J., 2006, *A Study on SUV Parameters Sensitivity on Rollover Propensity*, SAE paper 2006-01-0795

[31] Solmaz, S., Corless, M., Shorten, R., *A methodology for the desing of robust rollover prevention controllers for automotive vehicles: Part 1-Differential Braking*, 2006, Proceedings of the 45th IEEE Conference on Decision & Control

[32] Chen, L., -K., Hsu, S., -Y., 2006*, Investigation of Driver-Controller Interaction in Vehicle Rollover Prevention*, 2006 IEEE International Conference on Systems, Man and Cybernetics, Taiwan

[33] Takano, S., Nagai, M., *Dynamics Control of Large Vehicles for Rollover Prevention*, 2001, Proceedings of the IEEE International Vehicle Electronics Conference

[34] Gillespie, T., *Fundamentals of Vehicle Dynamics*, 1992, SAE PA 15096-0001

[35] Jin, Z., L., Weng, J., S., Hu, H., Y., *Rollover stability of a vehicle during critical driving manouvres*, Proc. IMechE Vol. 221 Part D: Journal of Automobile Engineering

[36] Lozia, Z., 1998, *Rollover thresholds of the biaxial truck during motion on an even road*, Vehicle System Dynamics, 29:1, 735-740

[37] Zhang, N., Dong, G., M., Du, H., P., *Investigation into untripped rollover of light vehicle in the modified fishhook and the sine maneuvers. Part I: Vehicle modelling, roll and yaw instability*, 2008, Vehicle System Dynamics, 46:4

[38] Wielenga, T., J., 1999, *Tire Properties Affecting Vehicle Rollover*, SAE Technical Paper 1999-01-0126

[39] Cole, D. J., 2001, *Fundamental Issues in Suspension Design for Heavy Road Vehicles*, Vehicle System Dynamics, 35:4, 319-360

[40] Gertsch, J., Shim, T., 2006, *Insightful Representations of Roll Plane Model Stability Limits*, SAE Technical Paper 2006-01-1284

[41] Yu, H., Güvenç, L., Özgüner, Ü., *Heavy duty vehicle rollover detection and active roll control*, 2008, Vehicle System Dynamics, 46:6, 451–470

[42] Barak, P., Tianbing, S., 2003, *On Body Roll Angle During Transient Response Maneuver of 3-D Model*, SAE Technical Paper 2003-1-0963

[43] Tammy, S., 2000, *Friction Induced Rollover from Lift-Off to Launch*, SAE Technical Paper 2000-01-1649

[44] Hecker, F., Schramm, H., Beyer, C., Holler, G., Bennet, M., 2000, *Heavy Vehicle Stability Notification and Assistance*, SAE Technical Paper 2000-01-3481

[45] Solmaz, S., *Topics in Automotive Rollover Prevention: Robust and Adaptive Switching Strategies for Estimation and Control*, 2007, PhD Thesis, National University of Ireland, Maynooth

[46] Seibum, B., Choi, 2008, *Practical vehicle rollover avoidance control using energy method*, Vehicle System Dynamics, 46:4, 323-337

[47] Johansson, B., Gäfvert, M., 2004, *Untripped SUV Rollover Detection and Prevention*, Decision and Control, 2004. CDC. 43rd IEEE Conference (Volume:5), IEEE paper

[48] Yoon, J., Kim, D., Yi, K., 2007, *Design of a rollover index-based vehicle stability control scheme*, Vehicle System Dynamics, 45:5, 459-475

[49] Tseng, H., E., Xu, L., Hrovat, D., 2007, *Estimation of Land Vehicle Roll and Pitch Angles*, Vehicle System Dynamics, 45:5, 433 – 443

[50] Hamblin, B., C., Martini, R., D., Cameron, J., T., Brennan, S., N., 2006, *Low-Order Modeling of Vehicle Roll Dynamics*, Proceedings of the 2006 American Control Conference, IEEE paper

[51] Mammar S., Baghdassarian, V., B., Nouveliere, L., 1999, *Speed Scheduled Vehicle Lateral Control*, Proceedings of the 1999 IEEE/IEEJ/JSAI International Conference on Intelligent Transportations Systems.

[52] Carlson, C., R., Brennan, S., 2003*, Optimal Rollover Prevention with Steer-by-Wire and Differential Braking*, presented at 2003 ASME IMECE, Washington, USA, 15th– 21st November 2003

[53] Dixon, J. C., 1996, *Tyres, Suspensions and Handling*, Second Edition, Society of Automotive Engineers, Warrendale

[54] Blundell, M., Harty, D., 2007, *The Multibody Systems Approach to Vehicle Dynamics*, Elsevier Ltd., Oxford

[55] Hac, A., 2005, *Influence of Chassis Characteristics on Sustained Roll, Heave and Yaw Oscillations in Dynamic Rollover Testing*, SAE Technical Paper 2005-01-0398

[56] Hac, A., 2002, *Influence of Active Chassis Systems on Vehicle Propensity to Maneuver-Induced Rollover*, SAE Technical Paper 2002-01-0967

[57] Pacejka, H., B., 2005, *Spin: camber and turning*, Vehicle System Dynamics, 43:1, 3-17

[58] Pacejka, H., 2002, *Tyre and Vehicle Dynamics*, First Edition, Society of Automotive Engineers, Oxford

[59] Malcher, D., Eskandarian, A., Delaigue, P., 2007, *Dynamic models for vehicle roll motion in prerollover manouvres*, Proc. IMechE Vol. 221, Part K: Journal of Multi-body Dynamics

[60] Takahashi, Toshimichi, Hada, Masatoshi, Oyama, Kozo and Sakai, Hideki, 2004, *New Model of Tire Overturning Moment Characteristics and Analysis of Their Influence on Vehicle Rollover Behaviour*, Vehicle System Dynamics, 42:1, 109 - 118

[61] Gilbert, M., G., 2003, *Effects of Tire Shoulder Wear on Vehicle Rollover Limit Testing*, SAE Technical Paper 2003-01-2865

[62] Schofield, B., Hägglund, T., Rantzer, A., 2006, *Vehicle Dynamics Control and Controller Allocation for Rollover Prevention*, Proceedings of the 2006 IEEE International Conference on Control Applications

[63] Holler, G., Macnamara, J., 2001, *Roll Over Prevention Based on State-of-the-Art ABS Systems*, SAE Technical Paper 2001-01-2727

[64] Miege, A., J., P., Cebon, D., 2005, *Optimal Roll Control of an Articulated Vehicle: Theory and Model Validation*, Vehicle System Dynamics, 43:12, 867-884

[65] Samson, D., J., M., Cebon, D., 2003, *Active Roll Control of Single Unit Heavy Road Vehicles*, Vehicle System Dynamics, 40:4, 229-270

[66] Everett, N., R., Brown, M., D., Crolla, D., A., 2000, *Investigation of a Roll Control System for an Off-road Vehicle*, SAE Technical Paper 2000-01-1646

[67] Cimba, D., Wagner, J., Baviskar, A., 2006, *Investigation of Active Torsion Bar Actuator Configurations to Reduce Vehicle Body Roll*, Vehicle System Dynamics, 44:9, 719-736

[68] Gordon, T., Howell, M., Brandao, F., 2003, *Integrated Control Methodologies for Road Vehicles*, Vehicle System Dynamics, 40:1, 157-190

[69] Gordon, T., J., 1996, *An Integrated Strategy for the Control of a Full Vehicle Active Suspension System*, Vehicle System Dynamics, 25:1, 229-242

[70] Jurecki, R., Staczyk, T., L., 2009, *Driver Model for the Analysis of Pre-Accident Situations*, Vehicle System Dynamics, 47:5, 589-612

[71] Smid, G., E., Cheok, K., C., 2001, *Virtual Proving Ground Environment For Designing a Roll-Over Detection and Warning System*, SAE Technical Paper 2001-01-3210

[72] Chen, B., C., Peng, H., 2001, *Differential-Braking-Based Rollover Prevention for Sport Utility Vehicles with Human-in-the-loop Evaluations*, Vehicle System Dynamics, 36:4, 359-389

[73] Mavros, G., 2010, *Enhanced Motorcycle Roll Stability by use of a Reaction Wheel Actuator*, 10th International Symposium on Advanced Vehicle Control, Loughborough

[74] Shabana, A., A., *Computational Dynamics*, 2001, John Wiley & Sons

[75] Moon, F., C., *Applied Dynamics: With Applications to Multibody and Mechatronic Systems*, 1998, John Wiley & Sons

[76] Murray, R. M., Li, Z., Sastry, S., S., A *Mathematical Introduction to Robotic Manipulation*, CRC Press 1994

[77] Hippmann, G., *Introduction to SIMPACK's MBS–Formalism*, SIMPACK Academy, 14th September 2010, Andechs

[78] TNO Automotive, *MF-Tyre/MF-Swift 6.1.2 Help Manual*, The Netherlands, 2010

[79] Eichberger, A., Schittenhelm, M., 2005, *Implementations, applications and limits of tyre models in multibody simulation*, Vehicle System Dynamics 43:sup1, 18-29

[80] Rauh, J., Mössner-Beigel, M., 2009, *Tyre simulation challenges*, Vehicle System Dynamics, 46:S1, 49-62

[81] Lugner, P., Plöchl, M., 2005, *Tyre model performance test: First experiences and results*, Vehicle System Dynamics 43:sup1, 48-62

[82] Bakker, E., Pacejka, H. B., 1987, *Tyre Modelling for Use in Vehicle Dynamics Studies*, SAE Paper No. 8700421

[83] Lugner, P., Plöchl, M., 2008, *Specifications of the test procedures*, Vehicle System Dynamics 45:S1, 21-28

[84] ISO, *Passenger cars -- Steady-state circular driving behaviour -- Open-loop test methods*, ISO-4138

[85] Antony, Jiju, 2004, *Design of Experiments for Engineers and Scientist*s, First Edition, Elsevier Publishing

[86] Montgomery, D., C., 2001, *Design and Analysis of Experiments*, Fifth Edition, John Wiley & Sons, Inc.

[87] Franklin, G., F., Powel, J. D., Emami-Naeini, A., *Feedback Control of Dynamic Systems*, 5th Edition, Pearson Prentice Hall 2006

[88] Parks, P. C., A. M. *Lyapunov's stability theory – 100 years on*, IMA Journal of Mathematical Control & Information 9: 275–303, 1992

[89] Khalil, H. K.,1996, *Nonlinear Systems*, 2nd Edition, Prentice-Hall

[90] Garrick J. Forkenbrock, W. Riley Garrot, Matk Heitz, Bryan C. O'Harra, *A Comprehensive Experimental Evaluation of Test Maneuvers That May Induce On-Road, Untripped, Light Vehicel Rollover. Phase IV of NHTSA's Light Vehicle Rollover Research Program*, 2002, NHTSA Report No DOT HS 809 513

[91] Hoult W., *A neuromuscular model for simulating driver steering torque*, PhD Dissertation, University of Cambridge, 2008

[92] Dutton, K., Thompson, S., Barraclough, B., *The Art of Control Engineering*, Prentice-Hall 1997

[93] Markley, F., L., Reynolds, R., G., Liu, F., X., Lebsock, K., L., 2010, *Maximum Torque and Momentum Envelopes for Reaction-Wheel*, Journal of Guidance, Control and Dynamics, Vol. 33, No. 5, 1606-1614

[94] Masuda, K., Uchiyama, K., 2012, *Development of Three-Dimensional Reaction Wheel Using Spherical Rotor*, AIAA Guidance, Navigation and Control Conference, Minneapolis, Minnesota, USA

[95] Rigger, R., 2010, *On stiction, limit and constraint avoidance for reaction wheel control*, SpaceOps 2010 Conference Delivering on the Dream, Hunstville, Alabama, USA

[96] Verbin, D., Lappas, V., J., 2013*, Rapid Rotational Maneuvering of Rigid Satellites with Reaction Wheels*, Journal of Guidance, Control and Dynamics, Vol. 36, No. 5, 1538-1544

[97] Verbin, D., Lappas, V., J., 2010*, Spacecraft Maneuver Control with Power Limited Reaction Wheels*, AIAA Guidance, Navigation and Control Conference, Toronto, Ontario, Canada

[98] Flybrid Systems, 2014, *Original F1 System*. [Online] Available from: http://www.flybridsystems.com/F1System.html. [Accessed: 28th September 2014]

9. Appendix A – DOE Script in SIMPACK

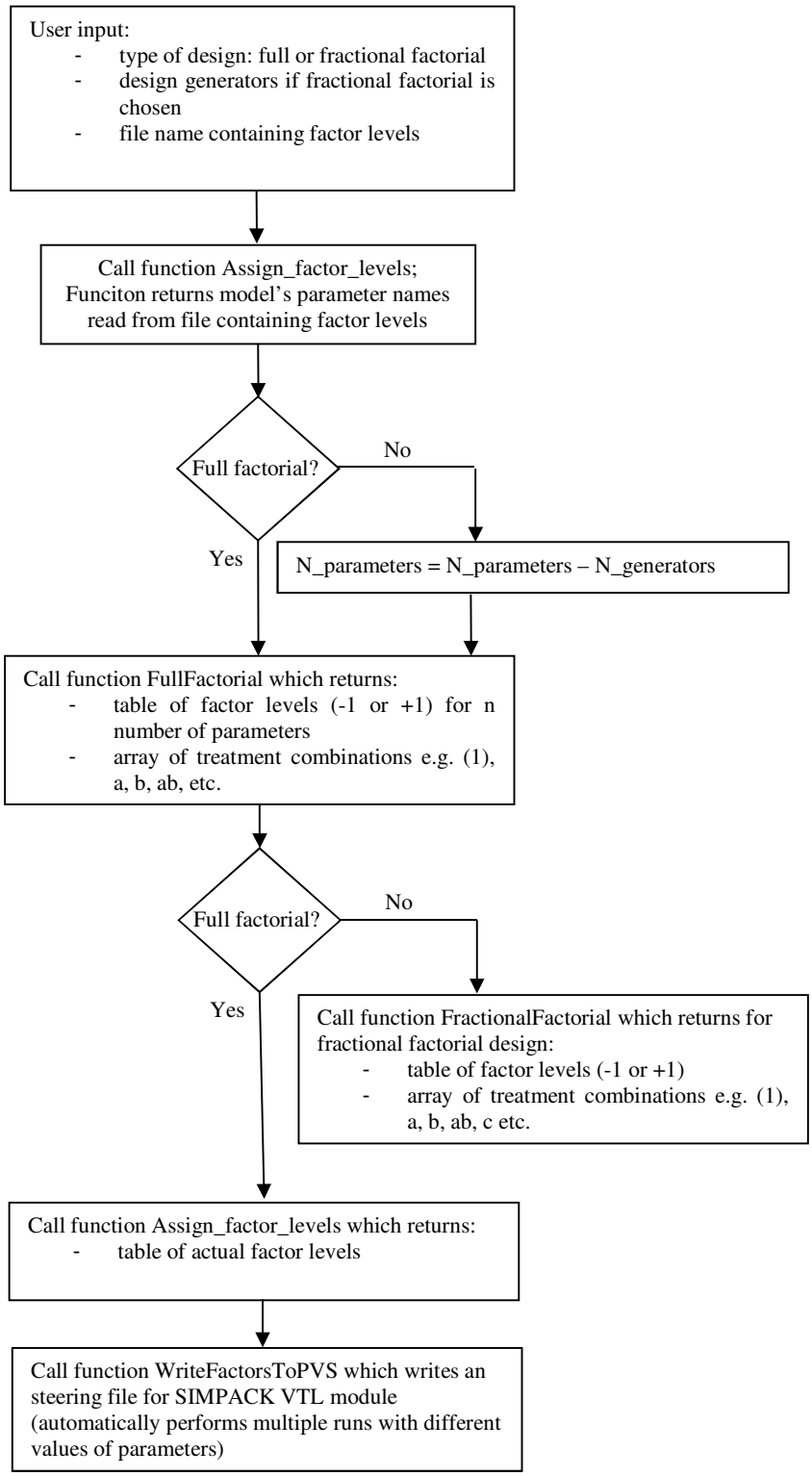

Figure 9.1 Main body of script

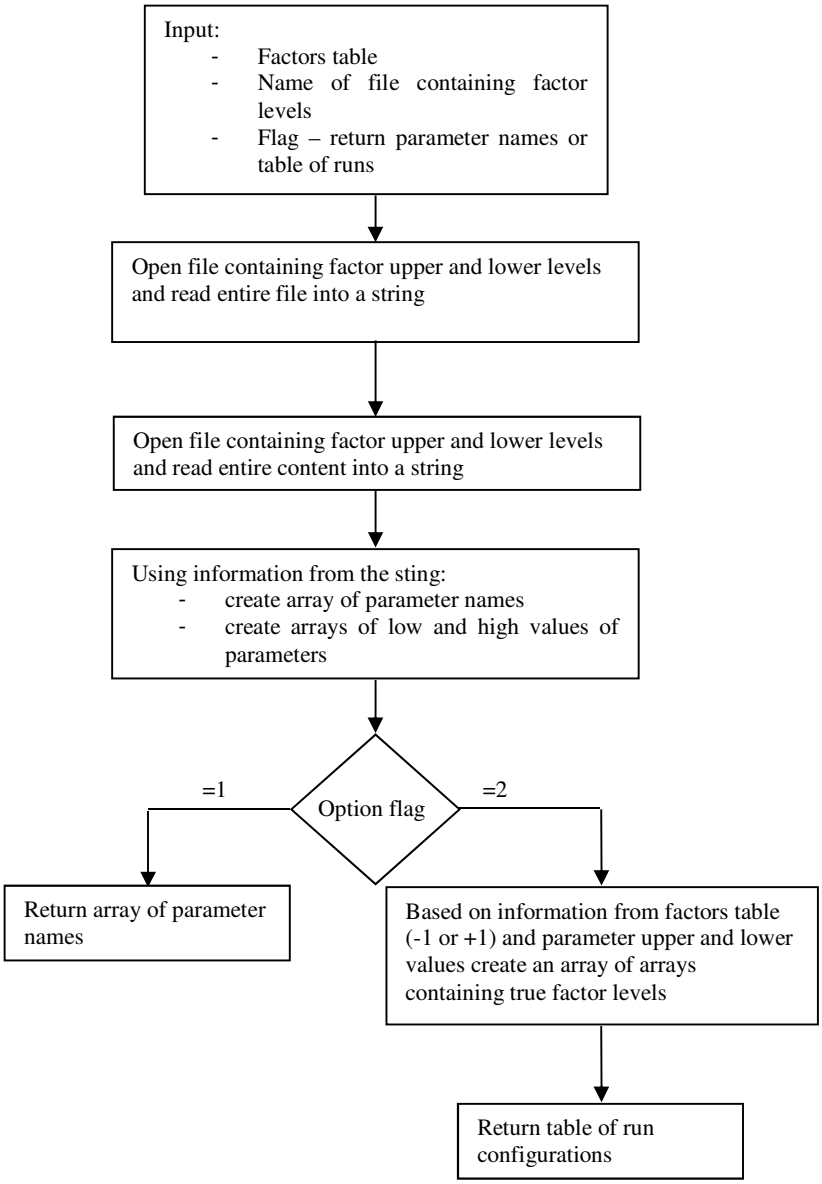

Figure 9.2 Function Assign_Factors_levels

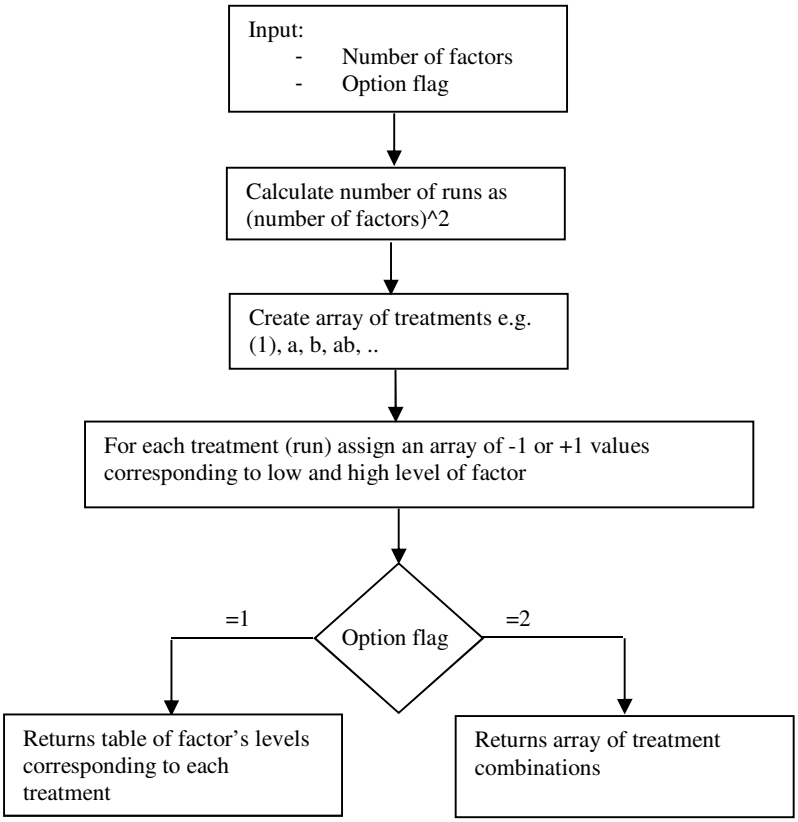

Figure 9.3 Function: full factorial

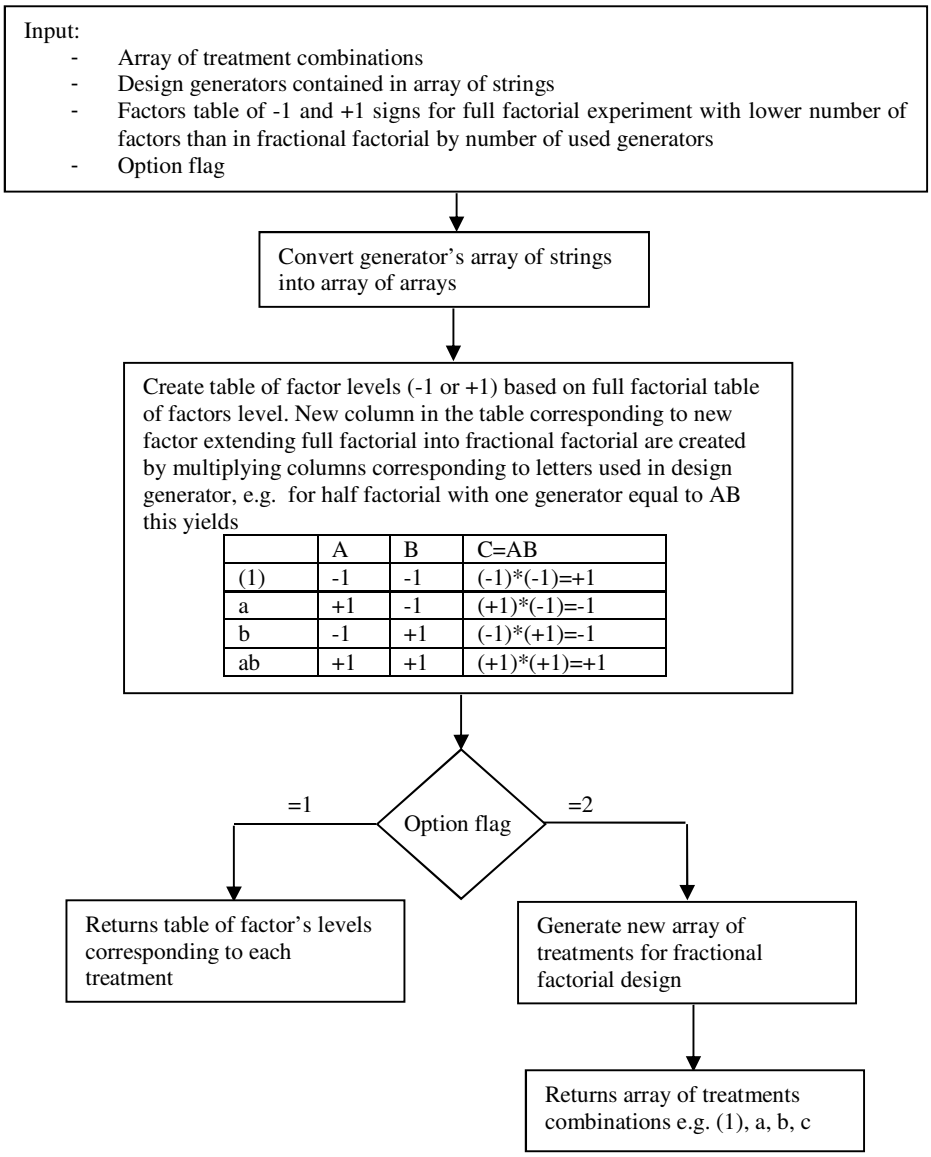

Figure 9.4 Function fractional factorial

2nd Part of SIMPACK script performs the runs and writes a result file. The operation of this script is shown in figures below:

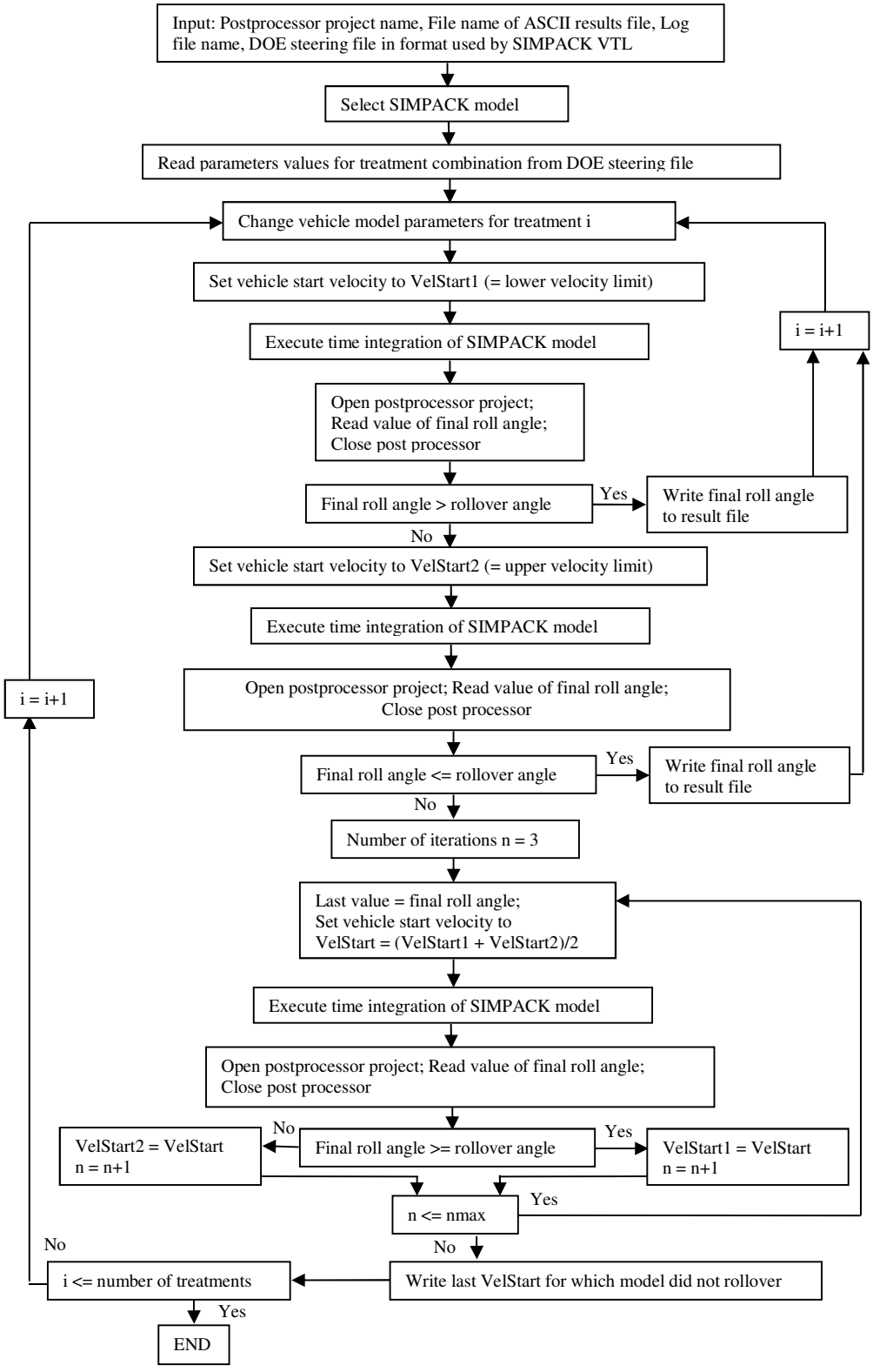

Figure 9.5 Script performing runs and writing out results to ASCII file